NOLTR 69-219
12135 FRI

SIMULATION OF THE DYNAMICAL LOADING OF PMMA IN THE NOL REGULAR CARD GAP TEST

2 APRIL 1970

NOL

UNITED STATES NAVAL ORDNANCE LABORATORY, WHITE OAK, MARYLAND

NOLTR 69-219
12135 FRI

128

12135-FRI
NOLTR 69-219

SIMULATION OF THE DYNAMICAL LOADING OF PMMA IN THE NOL REGULAR CARD GAP TEST

E. E. Fisher
R. G. Johnson
R. F. Paulson
Honeywell Inc., Systems and Research Division
Research Department, St. Paul, Minnesota

ABSTRACT: Results are presented of a computer simulation of the flow induced in a Plexiglass (PMMA) rod by a charge of tetryl. The charge and the rod are the standard donor and attenuator of the Naval Ordnance Laboratory Large Scale Gap Test (LSGT). The computations provide a better understanding of the flow and hence of phenomena which have been observed in PMMA rods during calibration studies of the LSGT. They also give data on the shape and duration of the pressure pulse (in the PMMA) which is transmitted into the acceptor explosive in the LSGT. Such data are needed in the study of shock sensitivity of explosives.

PUBLISHED 2 APRIL 1970

Approved by:

Carl Boyars, Chief
Advanced Chemistry Division
CHEMISTRY RESEARCH DEPARTMENT
U. S. NAVAL ORDNANCE LABORATORY
White Oak, Silver Spring, Maryland

12135-FRI
NOLTR 69-219

2 April 1970

SIMULATION OF THE DYNAMICAL LOADING OF PMMA
IN THE NOL REGULAR CARD GAP TEST

This work was performed by Honeywell, Inc., under contract N 60921-69-M-2003 for ORDTASK No. 331-0021/092-1/UF 19-332-302, Propellant and Ingredient Sensitivity. The computed results are useful in the calibration of gap tests such as the Naval Ordnance Laboratory Large Scale Gap Test, and in the interpretation of the results of such tests. Consequently, the hazards associated with both explosives and propellants used in military weaponry can be better assessed.

GEORGE G. BALL
Captain, USN
Commander

ALBERT LIGHTBODY
By direction

TABLE OF CONTENTS

ILLUSTRATIONS

SECTION 1
INTRODUCTION

The NOL gap tests have long been employed for characterizing "high" or detonating explosives. In such tests one usually observes the limiting gap for detonation in a receptor by the shock wave transmitted from a donor charge through a condensed inert medium. Due to the complex shock wave motion and the short duration of the gap test, a complete understanding of the test is difficult to obtain experimentally. For a more detailed understanding of the phenomena in this type of test a numerical simulation of the test should be of value. This report, prepared under Contract N60921-69-M-2003 for the Naval Ordnance Laboratory and partially funded under Honeywell corporate funds, summarizes the results of the numerically calculated flow in the simulation of the NOL regular card gap test.

The regular card gap test consists of a 2.0-inch-diameter cylinder of Plexiglas (PMMA) which is shocked by a charge of tetryl 2.0 inches in diameter and 2.0 inches long. It is described in References 1 and 2. In the course of calibrating the test, several interesting phenomena are observed. One of these is the "bump" in the plot of shock velocity, U_s, versus the distance from the interface. This phenomenon is observed between 20 and 40 mm from the interface between the explosive and the PMMA. Another interesting feature of the flow in the PMMA cylinder is a discontinuity in the curvature of the shock front which is observed at about 25 mm from the interface. Still another interesting feature of the flow is a sharp decrease in magnitude of the slope of the pressure at the shock front versus distance from the interface.

The purpose of the project reported here was to dynamically simulate the explosive loading of the PMMA and give, at least qualitative, theoretical understanding of the various phenomena observed experimentally. This report summarizes this simulation conducted with a Lagrangian strength of materials code called HEMP (Reference 3).

The results presented here do indicate a qualitative understanding of the phenomena and are thus encouraging considering the size of the effort involved. However, it is felt that they fall short in several respects. First, the study shows that if it is desired to obtain detailed quantitative information of effects such as abrupt changes in radius of curvature of the shock front, it will be necessary to zone the calculations much finer.

Secondly, if the simulation is to yield detailed aspects of inflections in flow quantity graphs and the like, more comprehensive equation-of-state data should be obtained. In this regard it is believed that more detailed information on failure must be obtained before that complicated phenomenon can be completely understood. In the last analysis, it must be said that there remains the possibility that a more time-consuming search of the voluminous data produced by this simulation could possibly yield new discoveries unnoticed by these authors.

SECTION 2
THE HEMP CODE

The HEMP code is a Lagrangian hydrodynamic-elasto-plastic code developed at the Lawrence Radiation Laboratory by Dr. Mark Wilkins and discussed in Reference 3. The basic equations of motion are presented in what follows:

Equations of motion are in x-y coordinates with cylindrical symmetry about the x axis. (It is desirable to have the problem formulated also in plane x-y coordinates; for this case the terms marked $|^*$ are set = 0.)

$$\frac{\partial \Sigma_{xx}}{\partial x} + \frac{\partial T_{xy}}{\partial y} + \frac{T_{xy}}{y}\Big|^* = \rho \ddot{x}, \quad \frac{\partial T_{xy}}{\partial x} + \frac{\partial \Sigma_{yy}}{\partial y} + \frac{\Sigma_{yy} - \Sigma_{\theta\theta}}{y}\Big|^* = \rho \ddot{y}, \tag{1}$$

$$\Sigma_{xx} = s_{xx} - (p+q), \quad \Sigma_{yy} = s_{yy} - (p+q), \quad \Sigma_{\theta\theta} = s_{\theta\theta} - (p+q). \tag{2}$$

Equations of continuity:

$$\frac{\dot{V}}{V} = \frac{\partial \dot{x}}{\partial x} + \frac{\partial \dot{y}}{\partial y} + \frac{\dot{y}}{y}\Big|^*. \tag{3}$$

Energy equation:

$$\dot{E} = -(p+q)\dot{V} + V(s_{xx}\dot{\varepsilon}_{xx} + s_{yy}\dot{\varepsilon}_{yy} + s_{\theta\theta}\dot{\varepsilon}_{\theta\theta} + T_{xy}\dot{\varepsilon}_{xy}) \tag{4}$$

Artificial viscosity (quadratic "q"):

$$q = C_0^2 \rho^0 (\dot{V}/V)^2 A/V \tag{5}$$

where C^0 = constant, A = zone area, and ρ^0 = reference density.

Equation of state:

$$\text{stress components} \quad \begin{cases} \dot{s}_{xx} = 2\mu(\dot{\epsilon}_{xx} - 1/3\ \dot{V}/V) + \delta_{xx}, \\ \dot{s}_{yy} = 2\mu(\dot{\epsilon}_{yy} - 1/3\ \dot{V}/V) + \delta_{yy}, \\ \dot{s}_{\theta\theta} = 2\mu(\dot{\epsilon}_{\theta\theta} - 1/3\ \dot{V}/V). \\ \dot{T}_{xy} = \mu(\dot{\epsilon}_{xy}) + \delta_{xy}, \end{cases} \tag{6}$$

where μ = shear modulus and δ = correction for rotation.

$$\text{velocity strains} \quad \begin{cases} \dot{\epsilon}_{xx} = \frac{\partial \dot{x}}{\partial x}, \quad \dot{\epsilon}_{\theta\theta} = \frac{\dot{v}}{y}\Big|^{*} \\ \dot{\epsilon}_{yy} = \frac{\partial \dot{y}}{\partial y}, \quad \dot{\epsilon}_{xy} = \frac{\partial \dot{y}}{\partial x} + \frac{\partial \dot{x}}{\partial y}. \end{cases} \tag{7}$$

Hydrostatic pressure:

$$p = a(\eta-1) + b(\eta-1)^2 + c(\eta-1)^3 + d\eta E, \tag{8}$$

$$\eta = 1/V = \rho/\rho^0.$$

Von Mises yield condition:

$$(s_1^2 + s_2^2 + s_3^2) - 2/3\ (Y^0)^2 \leq 0 \tag{9}$$

where Y^0 = material strength and (s_1, s_2, s_3) are the principal stress deviators.

Notation:

x, y	space coordinates	$\epsilon_{xx}, \epsilon_{yy}, \epsilon_{\theta\theta}, \epsilon_{xy}$	strains
$\dot{x}$	velocity in x direction	p	hydrostatic pressure
$\dot{y}$	velocity in y direction	V	relative volume
$\Sigma_{xx}, \Sigma_{yy}, \Sigma_{\theta\theta}$	total stresses	E	internal energy per original volume
T_{xy}	shear stress	ρ	density
$s_{xx}, s_{yy}, s_{\theta\theta}$	stress deviators		

The dot over a parameter signifies a time derivative along the particle path.

The finite difference equations solved in the HEMP code are based on the integral equations

$$\frac{\partial F}{\partial x} = \frac{\int_C F(\hat{n} \cdot \hat{t}) dS}{\lim_{A \to 0} A}$$

$$\frac{\partial F}{\partial y} = \frac{\int_C F(\hat{n} \cdot \hat{j})\, dS}{\lim_{A \to 0} A} \qquad (10)$$

where

C = boundary of area A

S = arc length

$\hat{n}$ = normal vector

$\hat{t}$ = tangent vector

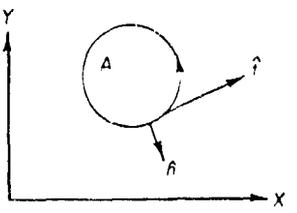

As such they yield more accurate expressions, especially in cases of high grid distortion.

SECTION 3
EQUATIONS OF STATE, ZONING AND INPUT DATA

CONSTITUTIVE RELATIONSHIP FOR PMMA

Hugoniot data listed in the contract and discussed in Reference 2 gives the shock velocity versus particle velocity as a piecewise linear function

$$U_s = S_o + S_1 U_p \tag{11}$$

with

$$\begin{pmatrix} S_o \\ S_1 \end{pmatrix} = \left\{ \begin{pmatrix} 0.257 \\ 1.61 \end{pmatrix} \text{ for } U_p \geq 0.05 \quad \begin{pmatrix} 0.295 \\ 0.85 \end{pmatrix} \text{ for } U_p < 0.05 \right\}$$

with velocity measured in centimeters per microsecond. This yields, via the Rankin-Hugoniot equations,

$$p_H(\rho) = \frac{\rho_o S_o^2 \left(\frac{m}{m+1}\right)}{\left(1 - S_1 \frac{m}{m+1}\right)^2} \tag{12}$$

$$\rho_o = 1.185 \text{ gm/cm}^3, \; m = \rho/\rho_o - 1 \tag{13}$$

$$\begin{pmatrix} S_o \\ S_1 \end{pmatrix} = \left\{ \begin{pmatrix} 0.257 \\ 1.61 \end{pmatrix} \text{ for } p \geq 0.02, \quad \begin{pmatrix} 0.295 \\ 0.85 \end{pmatrix} \text{ for } p < 0.02 \right\} \tag{14}$$

where $p_H(\rho)$ is the Hugoniot pressure and ρ_o is the initial density of PMMA. Pressure is measured in megabars.

The piecewise linearity of the shock velocity-particle velocity plot yields a discontinuity in the derivative of pressure with respect to density along the Hugoniot. This discontinuity shows up on isentropes as well, and thus affects the sound speed. Such discontinuities in sound speed cause separations in rarefaction wares. The pressure Hugoniot curve is shown in Figure 1.

It is well known that the isentropes for plastics diverge rapidly from the Hugoniot. Thus some energy dependence is required in the equation of state. For our simulations the general form of the Mie-Grüneisen equation.

$$p - p_H(\rho) = \frac{\gamma(\rho)}{\tau}\left[E - E_H(\rho)\right] \tag{15}$$

was chosen. Here $\gamma(\rho)$ is the Gruneisen ratio, E is the specific internal energy in megabars - cm^3/gm, τ is the specific volume, p is the pressure in megabars for states not necessarily on the Hugoniot, and $E_H(\rho)$ is the Hugoniot specific energy

$$E_H(\rho) = \frac{1}{2}\frac{p_H(\rho)}{\rho_o}\left(\frac{m}{1+m}\right) \tag{16}$$

From the viewpoint of material physics it is most appropriate to view Equation (15) as a first-order expansion of the pressure about the Hugoniot. Thus

$$\left(\frac{\partial p}{\partial E}\right)_\rho \Bigg|_{p = p_H(\rho)} = \frac{\gamma(\rho)}{\tau} \; . \tag{17}$$

With this interpretation, $\gamma(\rho)$ does not necessarily have the statistical mechanical identity of the analogous quantity in Grüneisen's original work on metals.

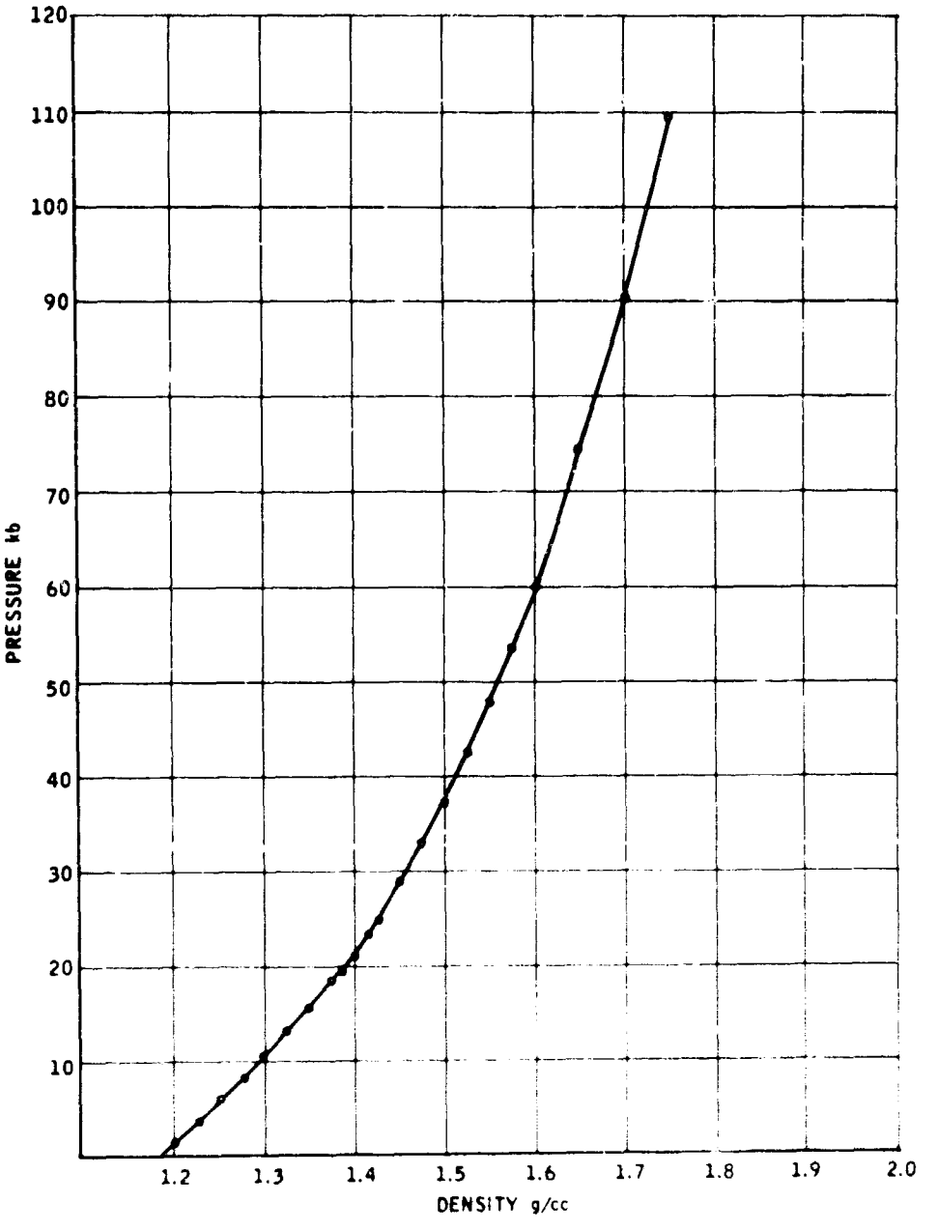

Figure 1. Pressure Hugoniot for PMMA

Since the appropriate value of γ for PMMA was not available from NOL sources, data for Lucite from Wilkins was used. This value is

$$\gamma = 0.6 \tag{18}$$

With these values inserted in Equation (15) the equation of state becomes

$$p = A(\rho) + B(\rho)\epsilon \,, \quad \epsilon = \rho_o E \tag{19}$$

with

$$B(\rho) = \frac{0.6\rho}{\rho_o} \tag{20}$$

$$A(\rho) = p_H(\rho) \left[1 - 1/2\,(0.6)\,(\rho/\rho_o - 1)\right] \tag{21}$$

The material's strength in tension, Y_o, was taken from the data of Keller and Trulio (Reference 5):

$$Y_o = 1 \text{ kb} \tag{22}$$

The material was allowed to flow plastically after yield. The shear modules of elasticity, μ, was taken from the Handbook of Physics and Chemistry,

$$\mu = 0.0143 \tag{23}$$

EQUATIONS OF STATE FOR TETRYL

A gamma-law equation of state was used for tetryl with the detonation velocity, D, and the initial density, ρ_o, given by

$$D = 0.72 \tag{24}$$

$$\rho_o = 1.51 \tag{25}$$

Since the gamma law is a three-parameter system, additional information is required. This was supplied as the initial chemical energy E_o of tetryl, given by the data of Donna Price (Reference 6) as

$$E_o = 0.0438 \tag{26}$$

The constant γ (the polytropic index) is then determined by the equation

$$\gamma^2 - 1 = \frac{0.5D^2}{E_o} \tag{27}$$

$$\gamma = 2.63017266 \tag{28}$$

Equation (27) is derived under the assumption that the detonation products expand from the Chapman-Jouguet state along an isentrope given by

$$p = \frac{p_{CJ}}{\rho_{CJ}^{\gamma}} \rho^{\gamma} . \tag{29}$$

While this system gives the correct detonation velocity, initial density, and energy release, it does not neccessarily yield the correct Chapman-Jouguet pressure and density. It is however self-consistent and satisfies the Rankin-Hugoniot equations and the Chapman-Jouguet hypothesis. The self-consistent values of the Chapman-Jouguet density ρ_{CJ}, and pressure p_{CJ} are then given by

$$\frac{\rho_{CJ}}{\rho_o} = \frac{\gamma+1}{\gamma}, \quad \rho_{CJ} = 2.0841068 \tag{30}$$

$$p_{CJ} = \frac{\rho_o D^2}{\gamma+1} = 0.2156327186 \tag{31}$$

Finally, the p, τ, E equation of state is given by

$$E = \frac{p\tau}{\gamma-1} \tag{32}$$

This equation does not result from the previous assumptions. It requires in addition the assumption that all isentropes from the detonation Hugoniot are polytropic with the same polytropic index γ (i.e., of the form of Equation (29) with the appropriate scale constant).

It is the opinion of these authors that better detonation data could be obtained if the measured value of the Chapman-Jouguet sound speed could be obtained. This together with the constants ρ_o and D would then determine the Chapman-Jouguet state. If, in addition, purely mechanical data on the expansion of the detonation products were available - for example data like that of Lee, et al. (Reference 7) - then the detonation and detonation products would be determined by purely mechanical means. At this time no such data exists.

Finally it should be stated that the detonation is simulated by an energy dump method (see Reference 3). This method gives the correct detonation speed but fails to give a detonation pressure as high as that given by Equation (31). This point will be discussed later in this report.

PROBLEM ZONING

The configuration simulated (as shown below) was a 4-inch-long, 2-inch-diameter cylinder of PMMA shocked by a 2-inch-long, 2-inch-diameter cylinder of tetryl which was initiated centrally at the end. The computation was carried out using 14 zones per inch (both radially and longitudinally). This resulted in 1,176 zones. The data storage and computer program together filled the core storage of the Control Data Corporation 3600 computer with 131,000 words of memory. This computation was carried out to a simulation time of 32.5 microseconds which corresponded to about 1.5 hours of computer time.

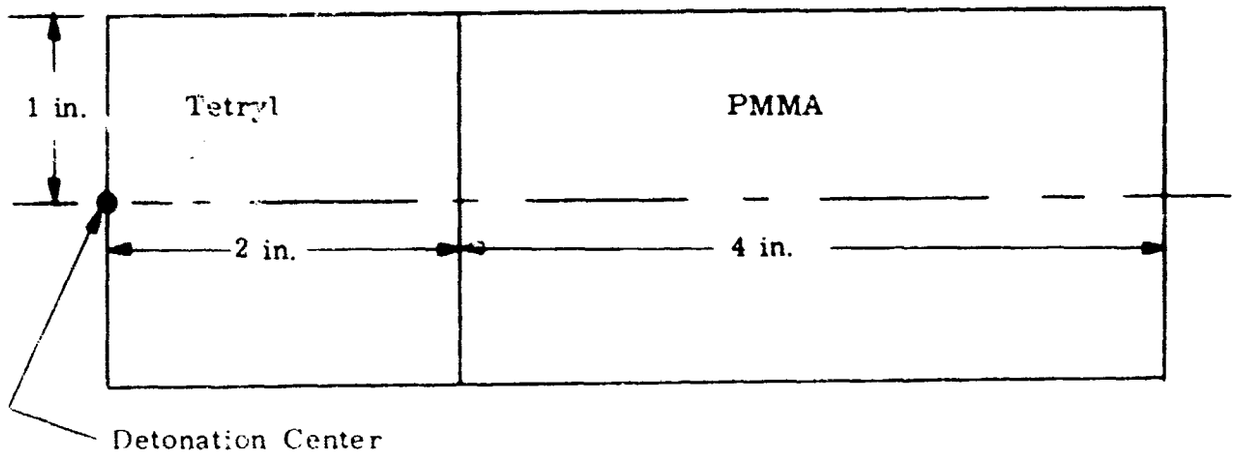

SECTION 4
COMPARISON OF SIMULATION WITH EXPERIMENTAL RESULTS

Comparison of the results presented here with the experimental results or results obtained elsewhere requires an explanation of how the graphs were obtained. For computational purposes, the zero of axial distance was taken to be the beginning of the tetryl. Thus, the interface between the tetryl and the Plexiglas was at 5.08 cm. Results, which are presented in such reports as NOLTR-65-43, place the zero of axial distance at the interface of tetryl and Plexiglas. Therefore, a distance of 5.08 cm had to be subtracted from axial distances presented here in order to compare them with axial distances presented in NOLTR-65-43. Also, zero time in reports such as NOLTR-65-43 is taken as the time when the shock enters the Plexiglas. For the results presented here zero time was taken as the time when the detonation was initiated in the tetryl. Determination of the time when the shock enters the Plexiglas in the numerical computation is resolved only to within the time step of the computation. From the numerical results, the shock entered the Plexiglas in the time interval of 7.0 μsec to 8.0 μsec. Rather arbitrarily, a zero time for the shock to enter the Plexiglas was taken as 7.25 μsec. This was done so the numerically obtained shock location versus time curve initially coincides with that given in NOLTR-65-43, Table A2. An explanation of how each graph was obtained follows.

SHOCK LOCATION VERSUS TIME

The numerical computation was carried out using the Q-method (Reference 3). For this graph (Figure 2), the shock location was defined as the position of maximum Q^* The zero of the numerical results has been adjusted so a comparison with results from NOLTR-65-43 can be made. The zero adjustment of the numerical results has been made by subtracting 5.08 cm from each axial distance and 7.25 μsec from each time.

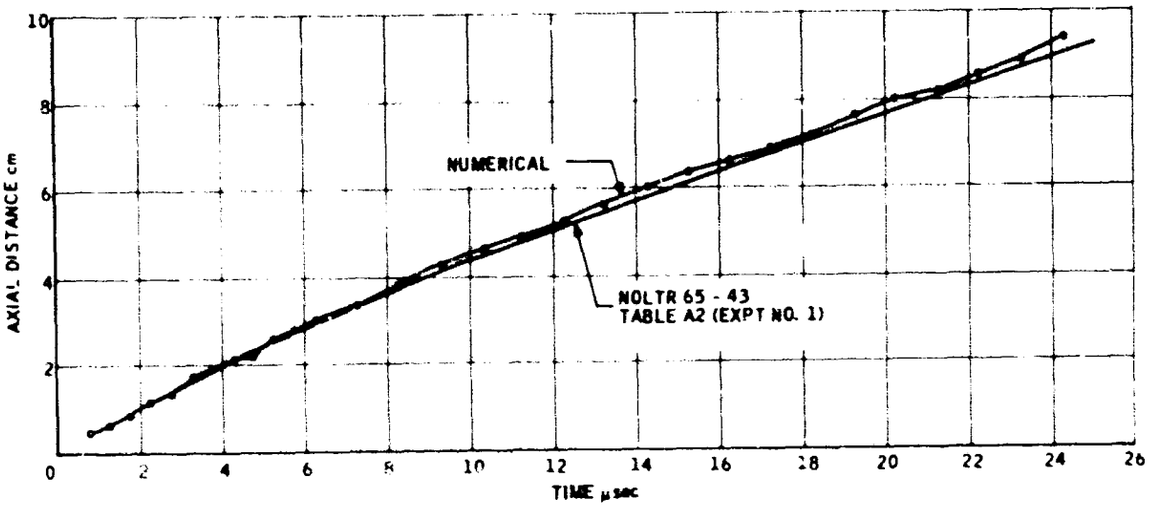

Figure 2. Shock Location versus Time

*This method, which seems to be part of the folklore of numerical hydrodynamics, gives very accurate results (dependent only on the problem zoning) when checked against one-dimensional problems with known analytical solutions.

PARTICLE VELOCITY AT SHOCK FRONT ON CYLINDER AXIS

In this graph (Figure 3), the shock front for the numerical results was defined to be at the point where the particle velocity is a maximum. This graph is then a plot of maximum particle velocity in the shock versus axial distance. The zero of axial distance has been adjusted by subtracting 5.08 cm from computational values in order to compare the results with those of NOLTR-65-43.

Since it is well known (see Reference 8) that all flow quantities overshoot their true values when the Q-method is used, these results should be somewhat high, which they are. A more accurate method of the determination of the particle velocity of the shock front would involve some averaging. Since such techniques are somewhat subjective this was not done. Such a technique is, however, recommended for final evaluation of this data.

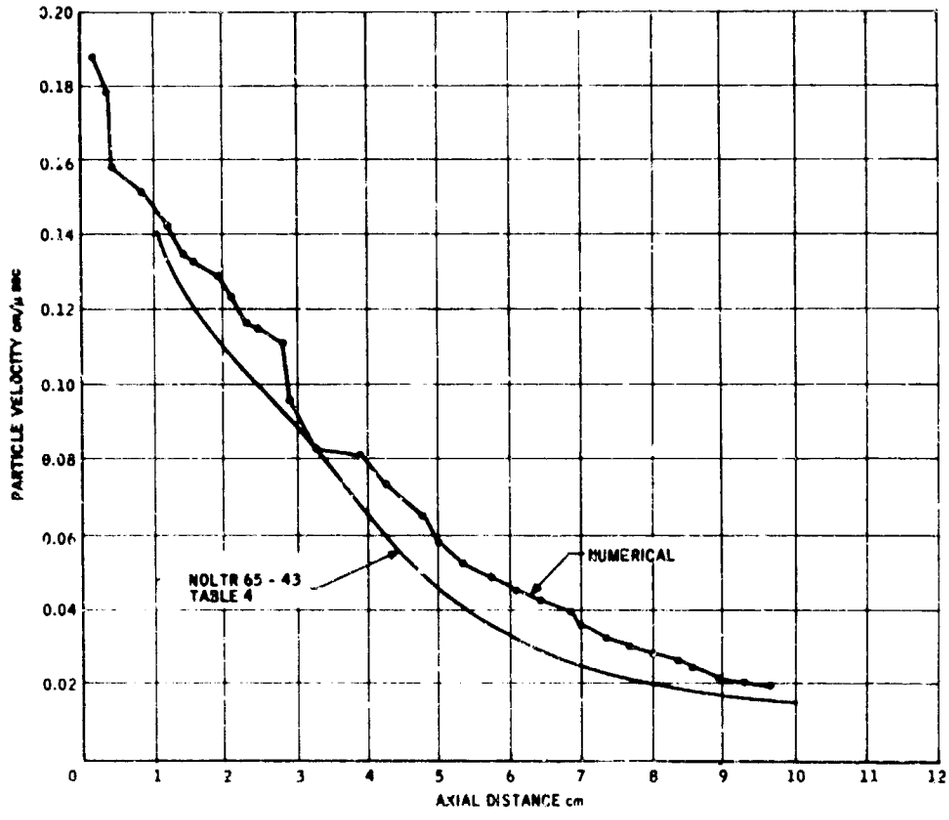

Figure 3. Particle Velocity at Shock Front on Cylinder Axis

SHOCK SHAPE

The shape of the shock was defined here by the position of maximum Q. These graphs (Figures 4, 5 and 6) are thus a plot of position of cells of maximum Q in the shock. No zero axial distance adjustment was made. Figure 32 in Reference 4 shows an apparent discontinuity in the radius of curvature of the shock wave between 20 and 40 mm in the Plexiglas. Examination of Figures 4, 5, and 6 does not conclusively demonstrate such behavior. It is the opinion of these authors that finer zoning could add much to the resolution of the problem, since the size of the phenomena in question is comparable with the current zone size. Again, some smoothing of the data would be helpful. This was not done because of the subjective nature of such analysis.

It should be mentioned that an abrupt decrease in the radius of curvature of the shock wave would be expected when the outside of PMMA material rarifies through 20 kb.. At this point the sound speed would decrease discontinuously, and sound signals would thus drive the shock wave with less strength. No attempt was made in our data analysis to correlate pressure levels with the observed discontinuity.

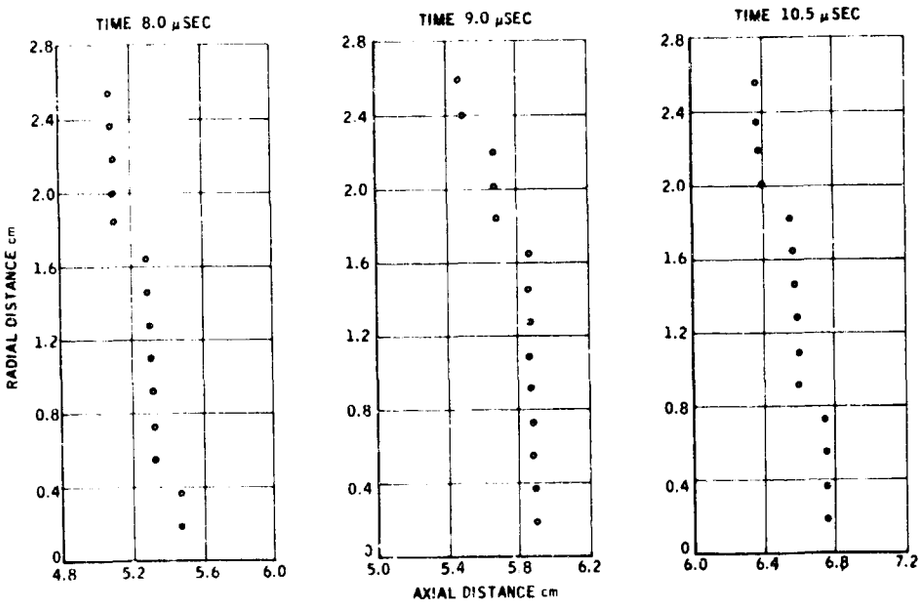

Figure 4. Shock Shape at 8, 9, 10.5 μsec

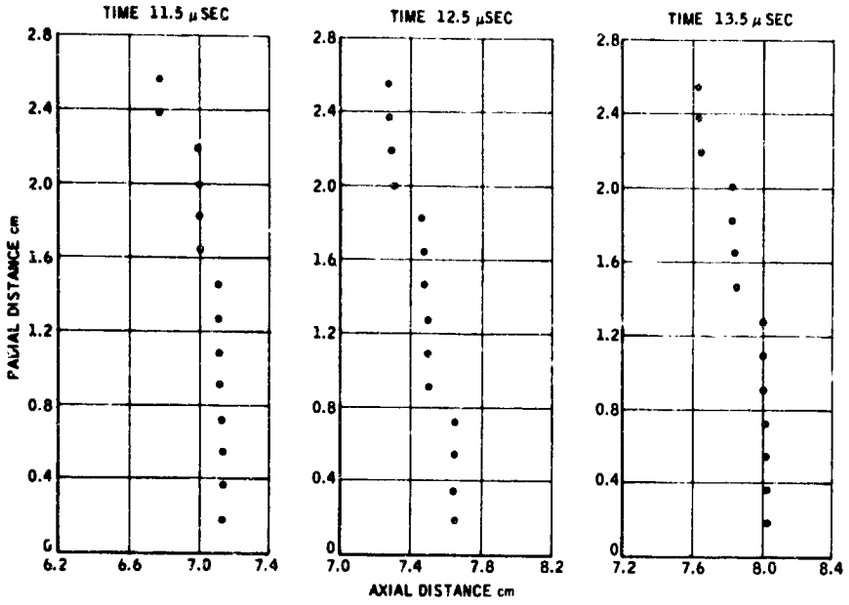

Figure 5. Shock Shape at 11. 5, 12. 5, 13. 5 μsec

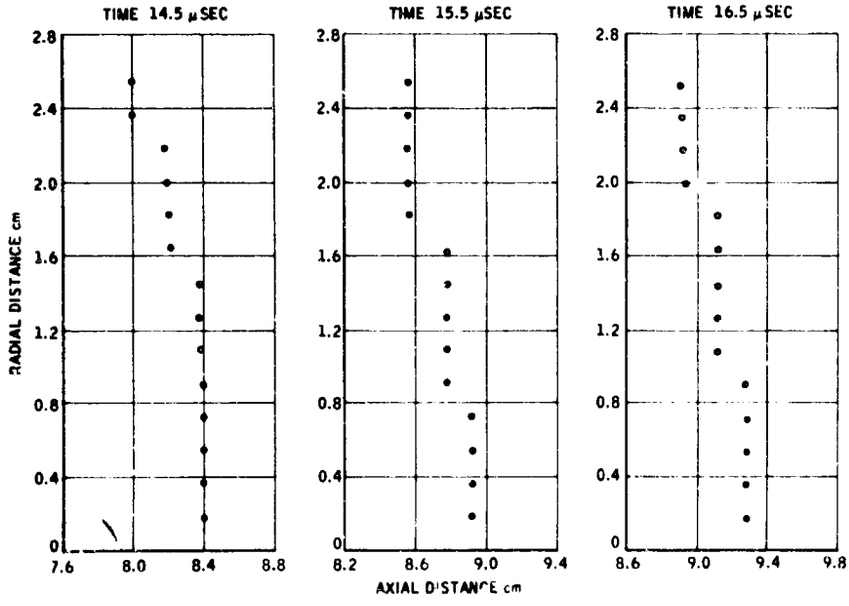

Figure 6. Shock Shape at 14. 5, 15. 5, 16. 5 μsec

PARTICLE VELOCITY

Due to the zoning of the problem, the location of particles of interest did not fall on zoned interfaces. Thus, particle velocities for particles between interfaces had to be determined by interpolation. In Figures 7 through 21, the particle velocities at the interface on either side of the location of interest are plotted. A linear interpolation is made between these points to determine the particle velocity at the location in question. No zero time adjustment was made. No attempt was made to correlate particle trajectories with elasto-plastic wave motion.

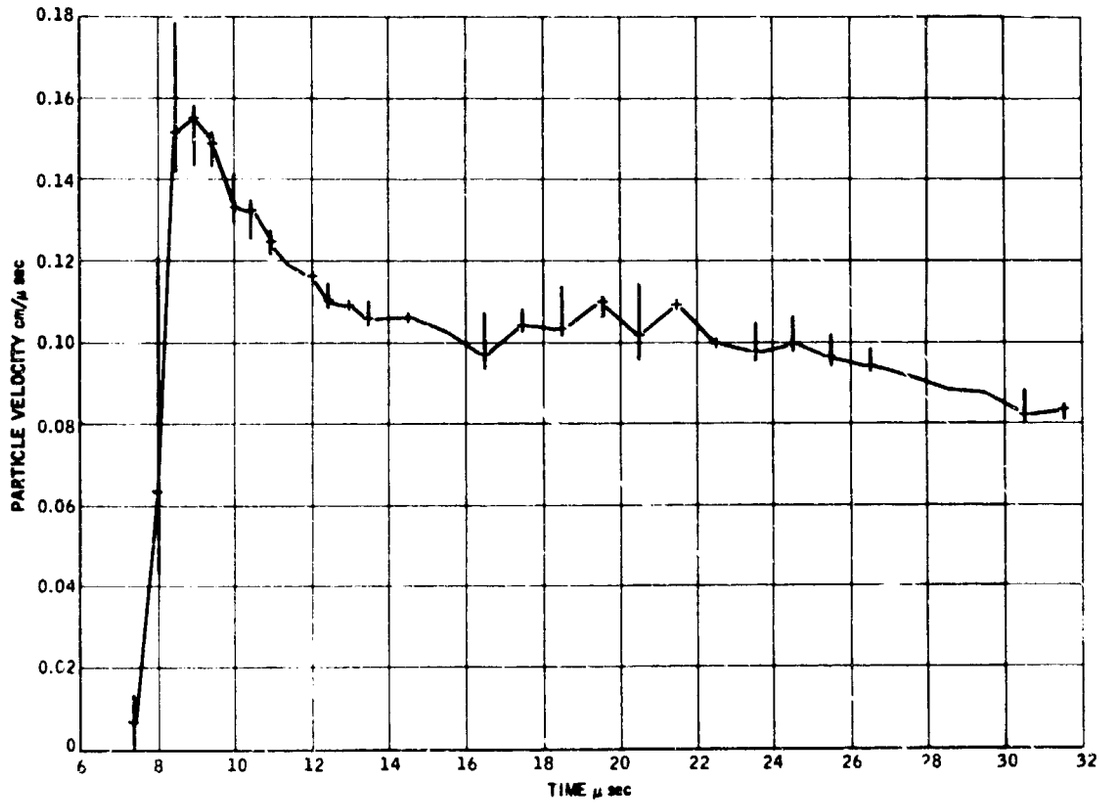

Figure 7. Particle Velocity versus Time (initial axial location - 0.5 cm)

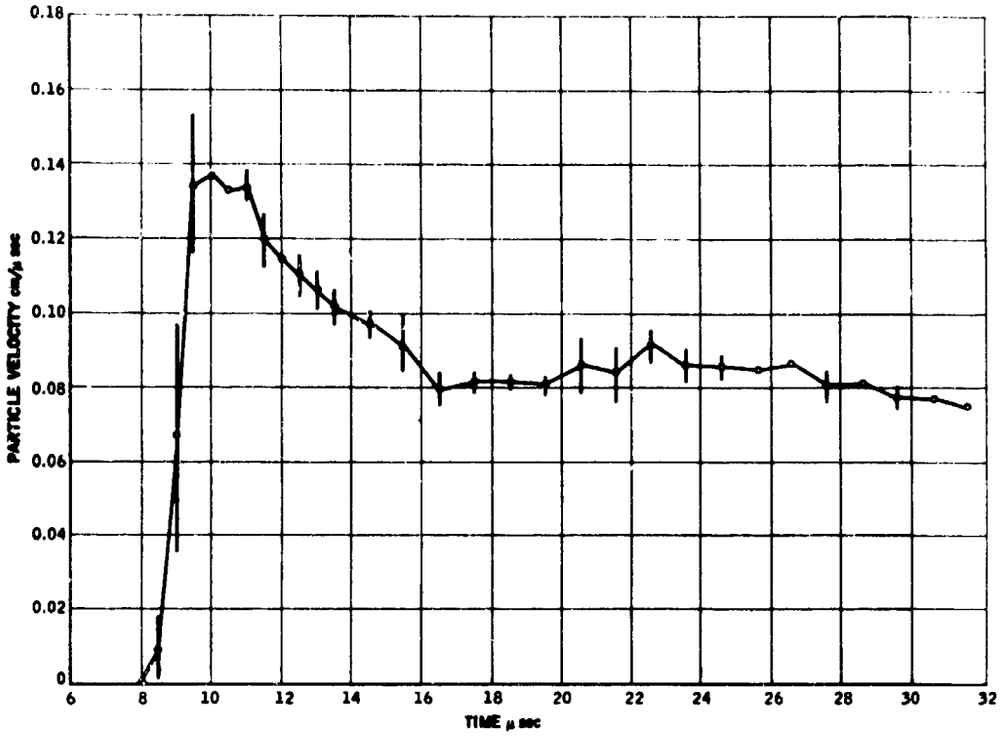

Figure 8. Particle Velocity versus Time (initial axial location - 1.0 cm)

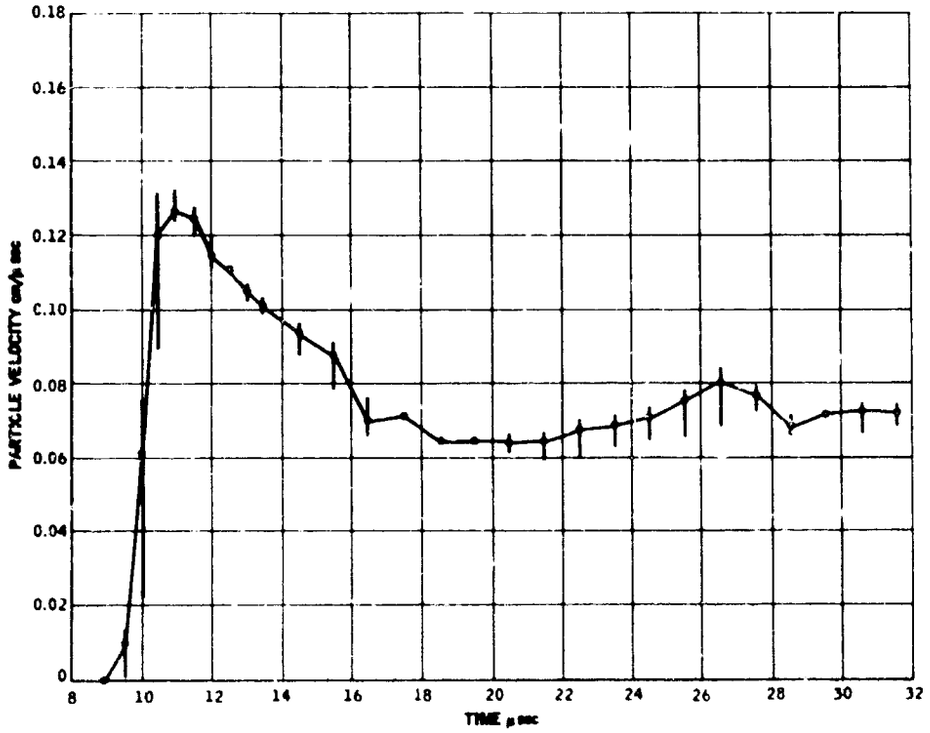

Figure 9. Particle Velocity versus Time (initial axial location - 1.5 cm)

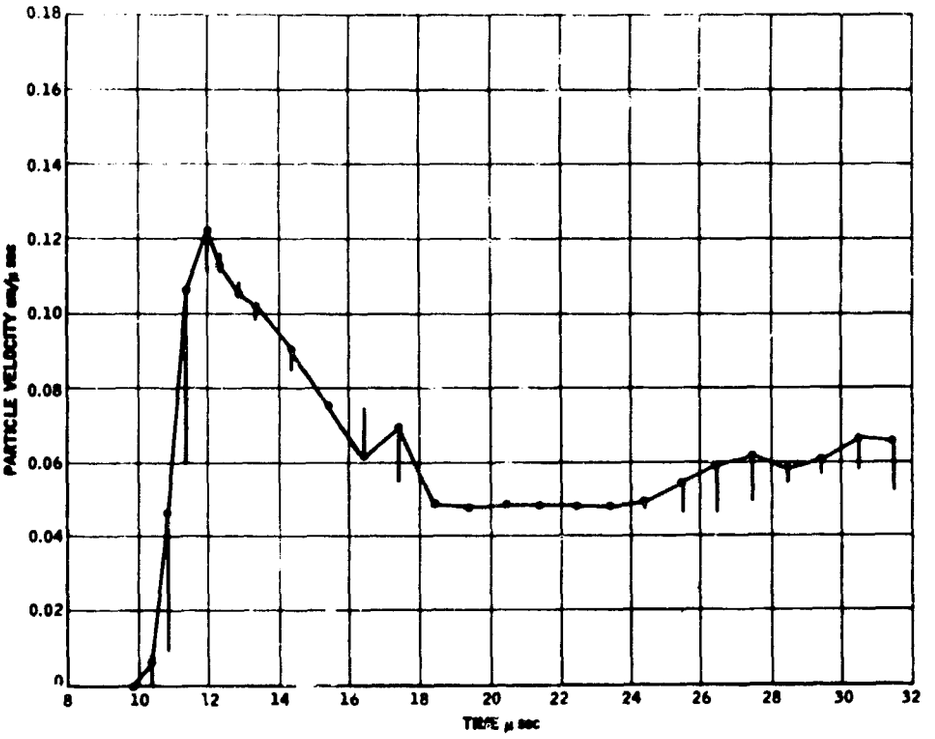

Figure 10. Particle Velocity versus Time (initial axial location -·2. 0 cm)

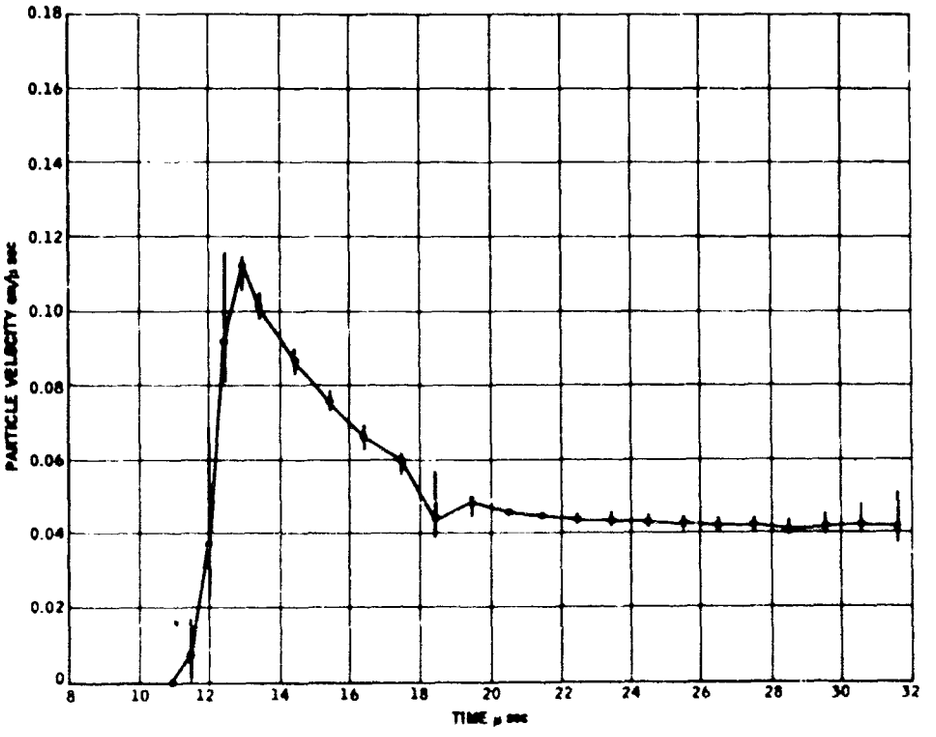

Figure 11. Particle Velocity versus Time (initial axial location - 2. 5 cm)

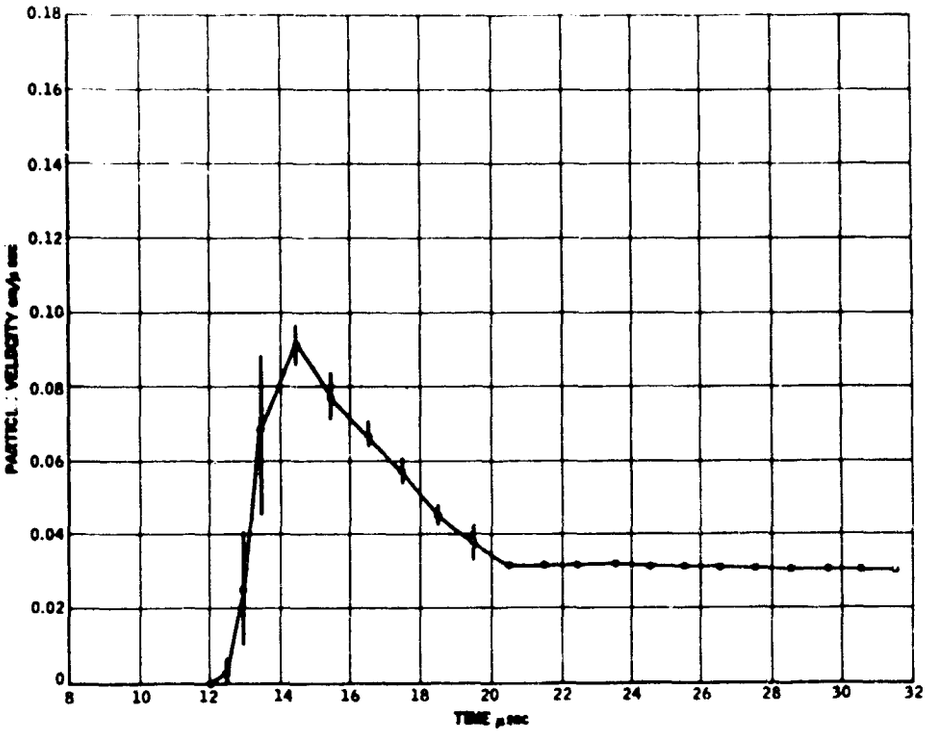

Figure 12. Particle Velocity versus Time (initial axial location - 3.0 cm)

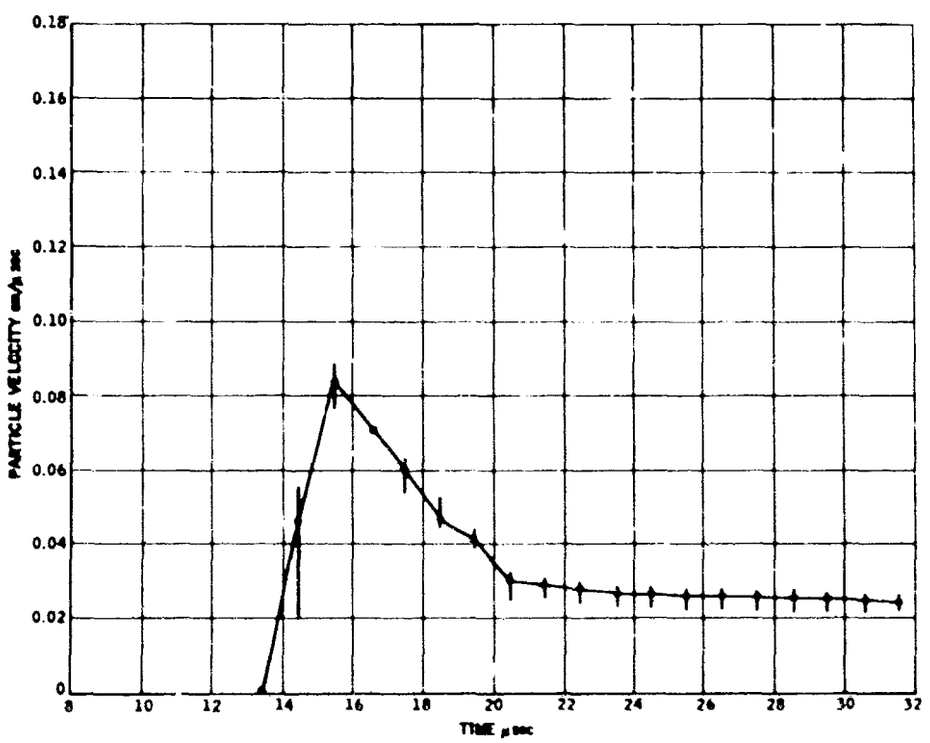

Figure 13. Particle Velocity versus Time (initial axial location - 3.5 cm)

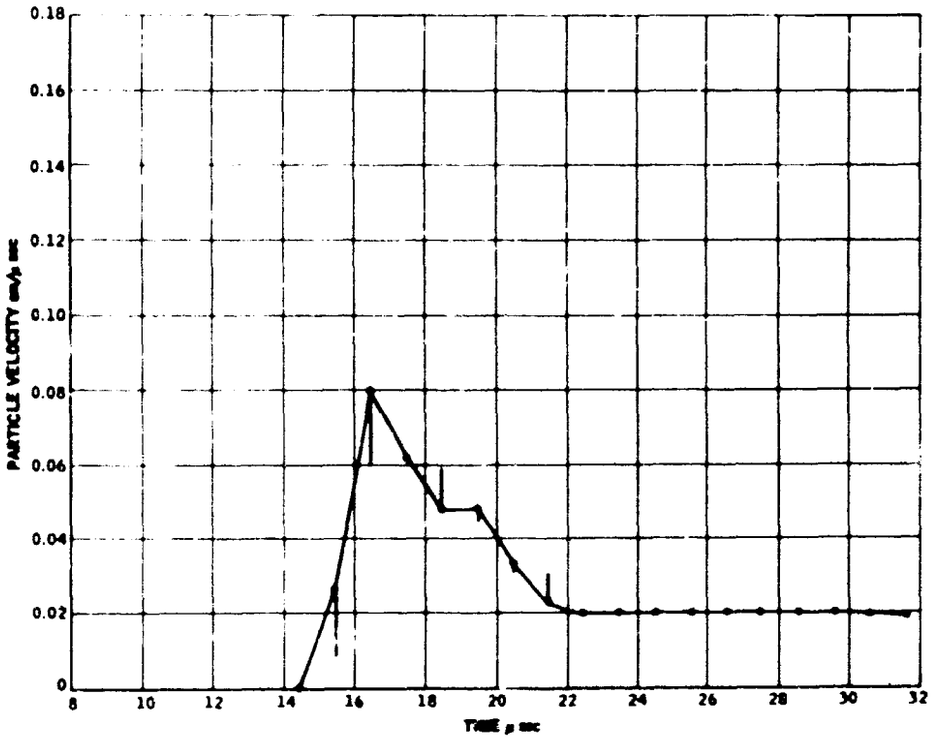

Figure 14. Particle Velocity versus Time (initial axial location - 4.0 cm)

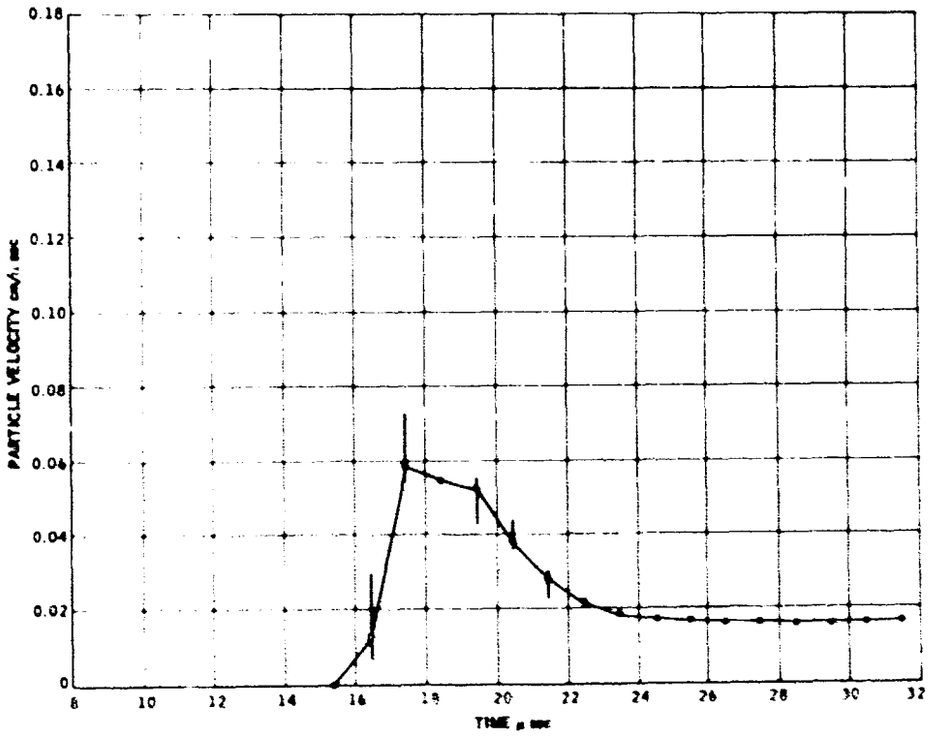

Figure 15. Particle Velocity versus Time (initial axial location - 4.5 cm)

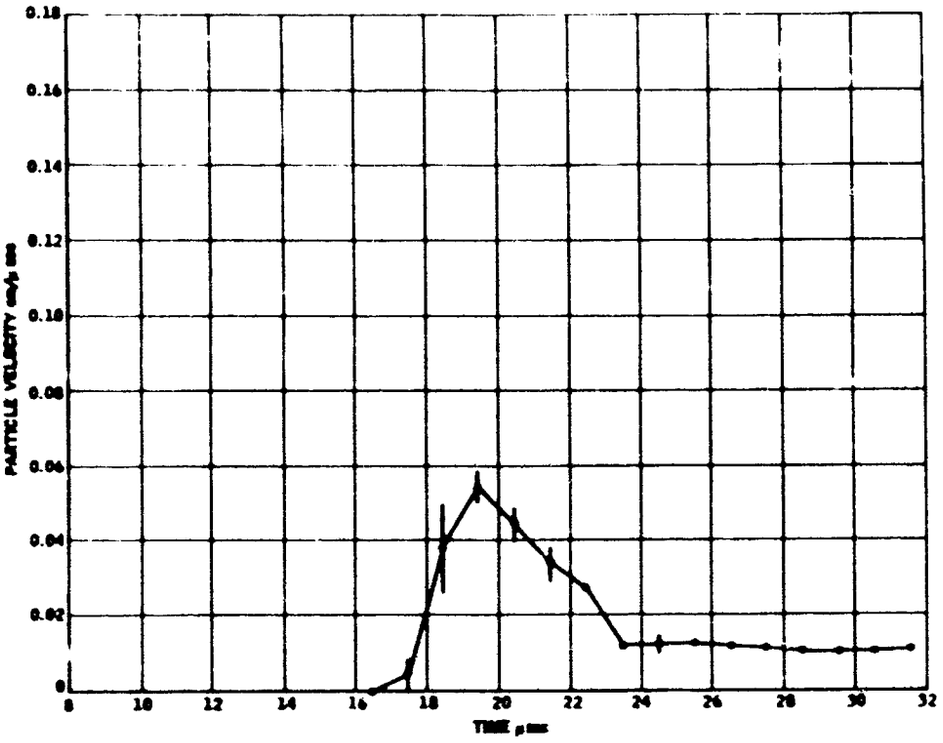

Figure 16. Particle Velocity versus Time (initial axial location - 5.0 cm)

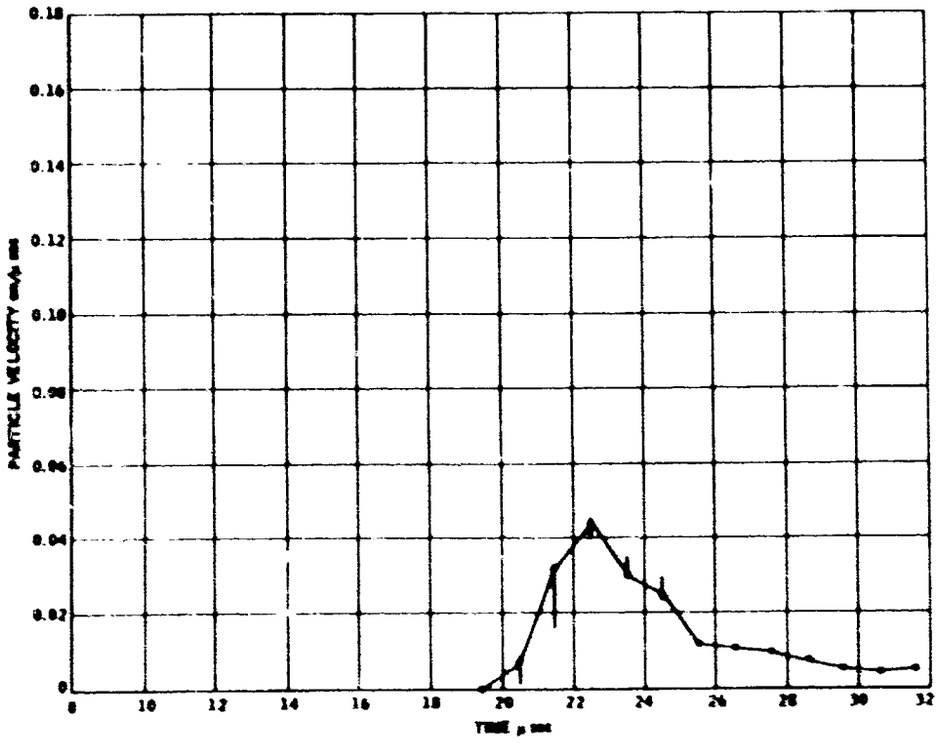

Figure 17. Particle Velocity versus Time (initial axial location - 6.0 cm)

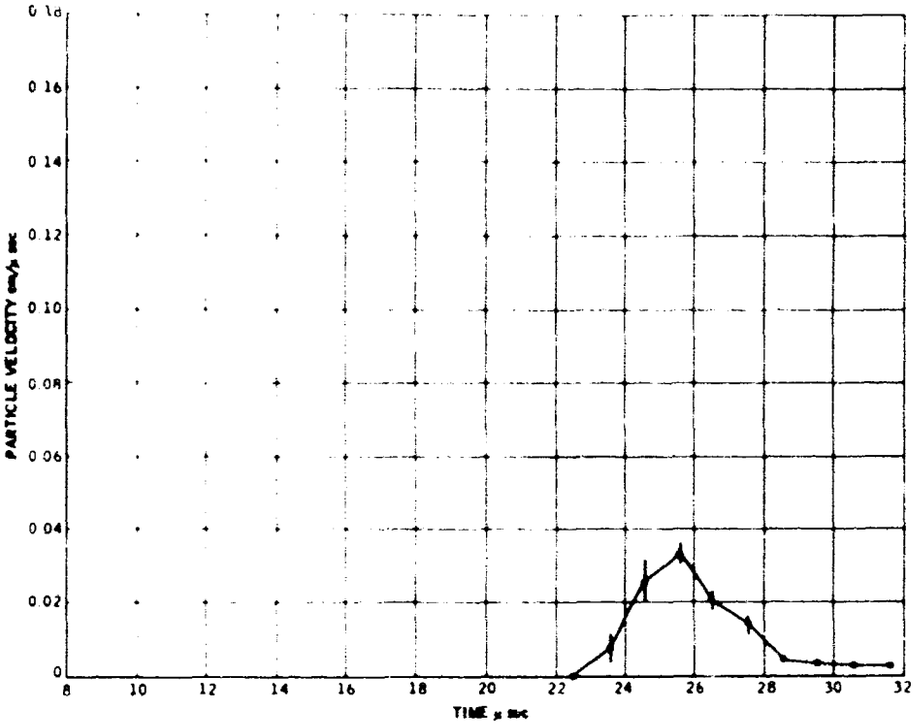

Figure 18. Particle Velocity versus Time (initial axial location - 7.0 cm)

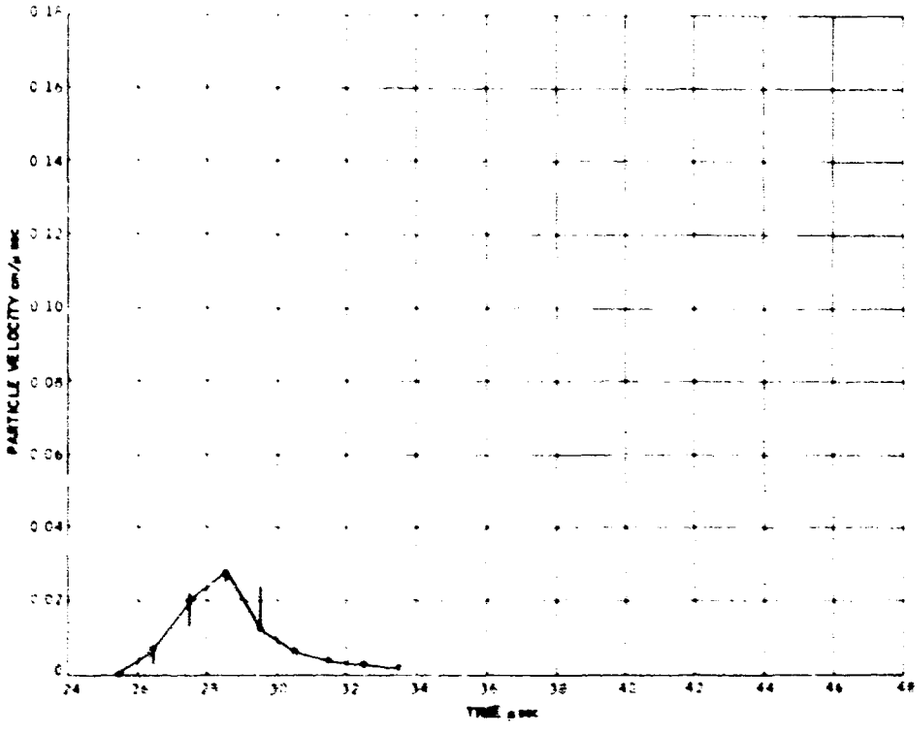

Figure 19. Particle Velocity versus Time (initial axial location - 8.0 cm)

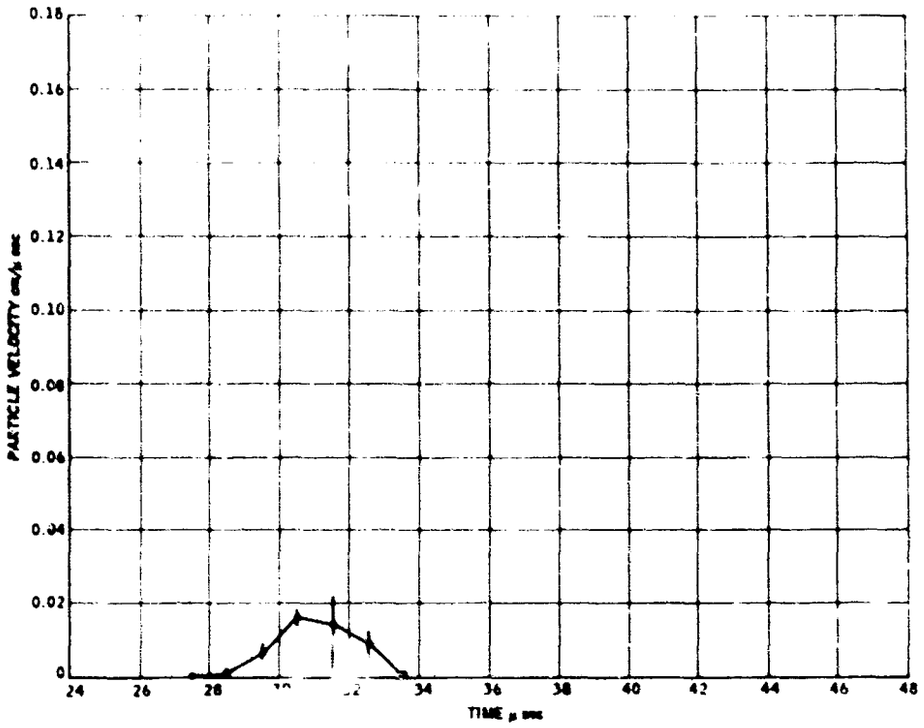

Figure 20. Particle Velocity versus Time (initial axial location - 9.0 cm)

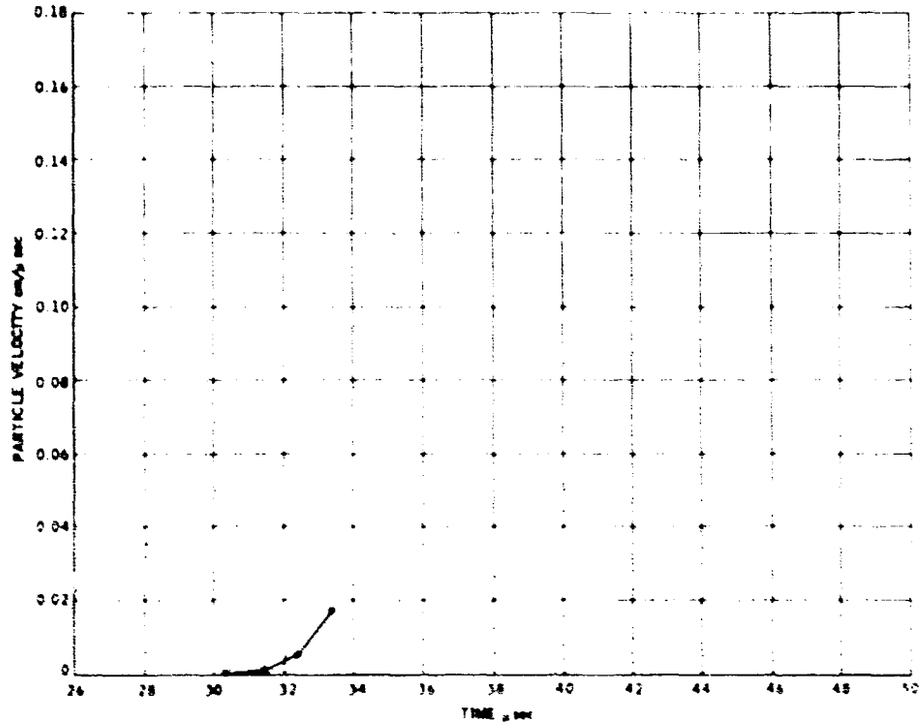

Figure 21. Particle Velocity versus Time (initial axial location - 10.0 cm)

AXIAL PRESSURE DISTRIBUTION

This graph (Figure 22) is typical of the axial pressure distribution across the shock front in the Plexiglas. It shows the shockwave and following rarefaction wave. Similar plots of the detonation wave in the tetryl indicated similar behavior. In that case, peak pressure values did not reach the Chapman-Jouquet value due to the extremely sharp (infinite derivative) decrease of the flow quantities from the Chapman-Jouquet values in the spherical Taylor wave, as discussed in Reference 9. Since peak shock values tend to smooth out in time, it is believed that the shock values in the Plexiglas may be quite accurate. Figure 23 tends to confirm this belief.

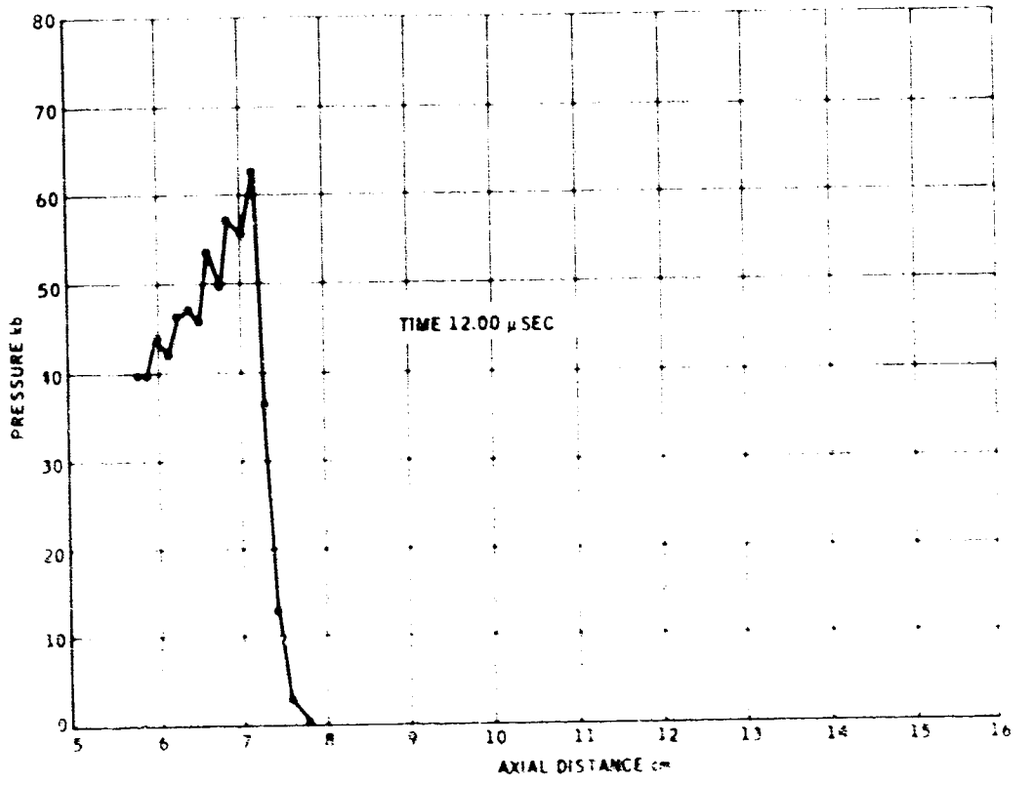

Figure 22. Axial Pressure Distribution at the Shock Front in the PMMA

AXIAL PRESSURE AT SHOCK FRONT

In this graph (Figure 23) the shock front was defined to be at the location where Q is a maximum. A zero axial distance adjustment was made by subtracting 5.08 cm from each of the numerical computed axial distance. Peak values of pressure which follow the shock front as defined above were plotted as the true pressure values at the shock front. It is the opinion of these authors that simulations with finer zoning would be required if a conclusive comparison of shock pressures were to be made. This is especially true in the region from 0 to 4 cm.

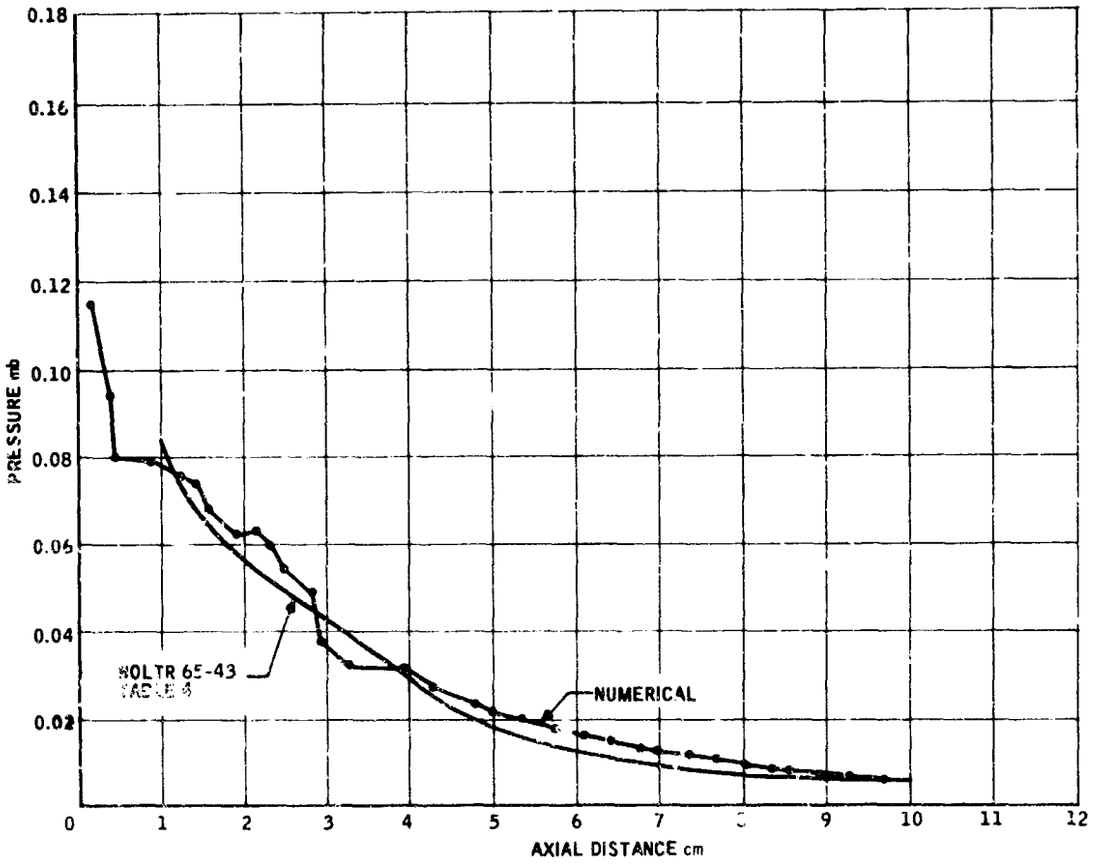

Figure 23. Axial Pressure at Shock Front

SECTION 5
DETAILED DISPLAY OF THE FLOW DYNAMICS

A detailed display of the flow dynamics was prepared in the form of Calcomp pen and ink plots of the flow field quantities. Because of their bulk, these are gathered in Appendix A as Figures A1 through A21 (representing the 21 simulation time intervals selected for plotting in the range from 0.01 μsec to 32.51 μsec.

Figures identified by the letter (a), e.g., Figure A1(a), are plots of the Lagrangian grid. The letter (b) following the figure number designates plots of particle velocity, and (c) indicates plots of the direction of maximum principal stress, with stress being measured positive in tension. These figures indicate regions of particular stress patterns, and should be compared qualitatively with the framing camera pictures of material failure in Reference 4. As discussed previously, the material was allowed to flow plastically at the yield strength after yield. For materials such as Plexiglas which fail due to brittle fracture it may have been more appropriate to set all the deviatoric stresses equal to zero for the remainder of the calculation, and set the pressure equal to zero until the material compresses again, if it does compress again. This would not substantially affect the particle velocity.

Figures with the letter (d) are isobar plots. Some indication of shock curvature can be obtained from these. Since rarefaction wave fronts are characteristic surfaces of the partial differential equations of motion, (i.e., they are surfaces along which the space and time derivatives of the flow field have discontinuities), isobar plots should have discontinuous slopes at a wave front. The computation performed did not have sufficient resolution to indicate such wave fronts. In examining the isobars of Reference 9 such wave fronts are visible. Those calculations were of course done with much more resolution. This again is another indication that finer zoned simulations would be desirable.

Finally, figures with a letter (e) indicate directions of maximum principal strain rate weighted with the magnitude of the local artificial viscosity. Such plots indicate positions of shock and detonation waves.

All graphs are labeled with the number of computer integration cycles (NCYCLE) and the simulation time (TIME) measured from the time the charge of tetryl was initiated.

It should be remarked at this point that all of the Calcomp plots give visual aid in understanding the flow, but do not replace the exact quantitative information available from the computer printouts. Indeed, the Calcomps should be used in conjunction with the printouts for future quantitative evaluation of the simulation.

SECTION 6
CONCLUDING REMARKS

Results of the simulation of the shock loading of PMMA have been presented. It is felt that more subjective analysis of the data, which would include such things as smoothing and interpolation, would be helpful. But, since these analyses are subjective, they were not done here. Beyond this it would be extremely helpful to simulate the configuration wit' finer zoning. For example, the shock loading at the PMMA interface could be simulated with very good accuracy by using the analytical Taylor wave for that portion of the "detonation head" which is bounded by the leading edge of the detonation, the lateral rarefactions, and the rarefactions from the rear. This part of the detonation wave would be put into the code as an initial condition. It would give very accurate information for that part of the flow which is determined by the appropriate domain of dependance.

A separate simulation of the total event, done with resolution at least double that used here would then determine events farther removed from the interface. This would probably determine these events as accurately as much higher resolution simulations, due to the lack of memory of hydrodynamic events. Finally it is recommended that a serious study be conducted on the fracture of PMMA. Such a study would involve the simulation of several constitutive models for PMMA.

ACKNOWLEDGEMENT

The authors of this report express their appreciation to M. L. Wilkins of the University of California, Lawrence Radiation Laboratory, Livermore, California for his cooperation in the use of the HEMP code. The code was used in this work to simulate the dynamical loading of PMMA in the NOL regular card gap test.

REFERENCES

1. T. P. Liddiard, Jr. and Donna Price, "Recalibration of The Standard Card-Gap Test," NOLTR 65-43, October 1965.

2. Donna Price and T. P. Liddiard, Jr. "The Small Gap Test: Calibration and Comparison with the Large Gap Test," NOLTR 66-87, 7 July 1966.

3. Mark L. Wilkins, "Calculation of Elastic-Plastic Flow," Methods in Computational Physics, Vol. 3, Fundamental Methods in Hydrodynamics, Academic Press, 1964.

4. I. Jaffe, J. Toscano, and D. Price, "Behavior of Plexiglas Under Shock Loading by a Tetryl Donor," NOL 64-66, 2 July 1964.

5. D. V. Keller, and John G. Trulio, "Mechanism of Spall in Lucite," J. Appl. Physics, 34, 172 (1963).

6. Donna Price, "Dependance of Damage Effects Upon Detonation Parameters of Organic High Explosives," Chem. Rev. 59, p. 801 (1959).

7. J. W. Kury, H. C. Hornig, E. L. Lee, J. L. McDonnel, D. L. Ornellas, M. Finger, F. M. Strange, M. L. Wilkins, "Metal Acceleration By Chemical High Explosives," Proceedings of the Fourth Detonation Symposium, October 12-15, 1965.

8. R. D. Richtmyer, "Difference Methods For Initial-Value Problems," Interscience Publishers, New York, 1964 Ch X.

9. D. Piacesi, Jr. "Numerical Hydrodynamic Calculations of the Flow of the Detonation Products From a Point-Initiated Explosive Cylinder," NOL 66-150, 13 January 1967.

APPENDIX A
CALCOMP PLOTS OF THE FLOW FIELD QUANTITIES AT VARIOUS TIMES

The Calcomp plots shown in Figures A1 through A21 are identified in the following manner:

Shown on the face of each plot are the number of computer integration cycles (NCYCLE) and the simulation time (TIME) measured from initiation of detonation in the tetryl.

Parenthetical letters following the figure number, e.g., Figure A1(a), indicate plots of:

(a) Lagrangian grid

(b) Particle velocity

(c) Direction of maximum principal stress

(d) Isobars

(e) Direction of maximum principal strain rate weighted with the magnitude of the local artificial viscosity

All figures do not necessarily include the full range of plots, (a) through (e).

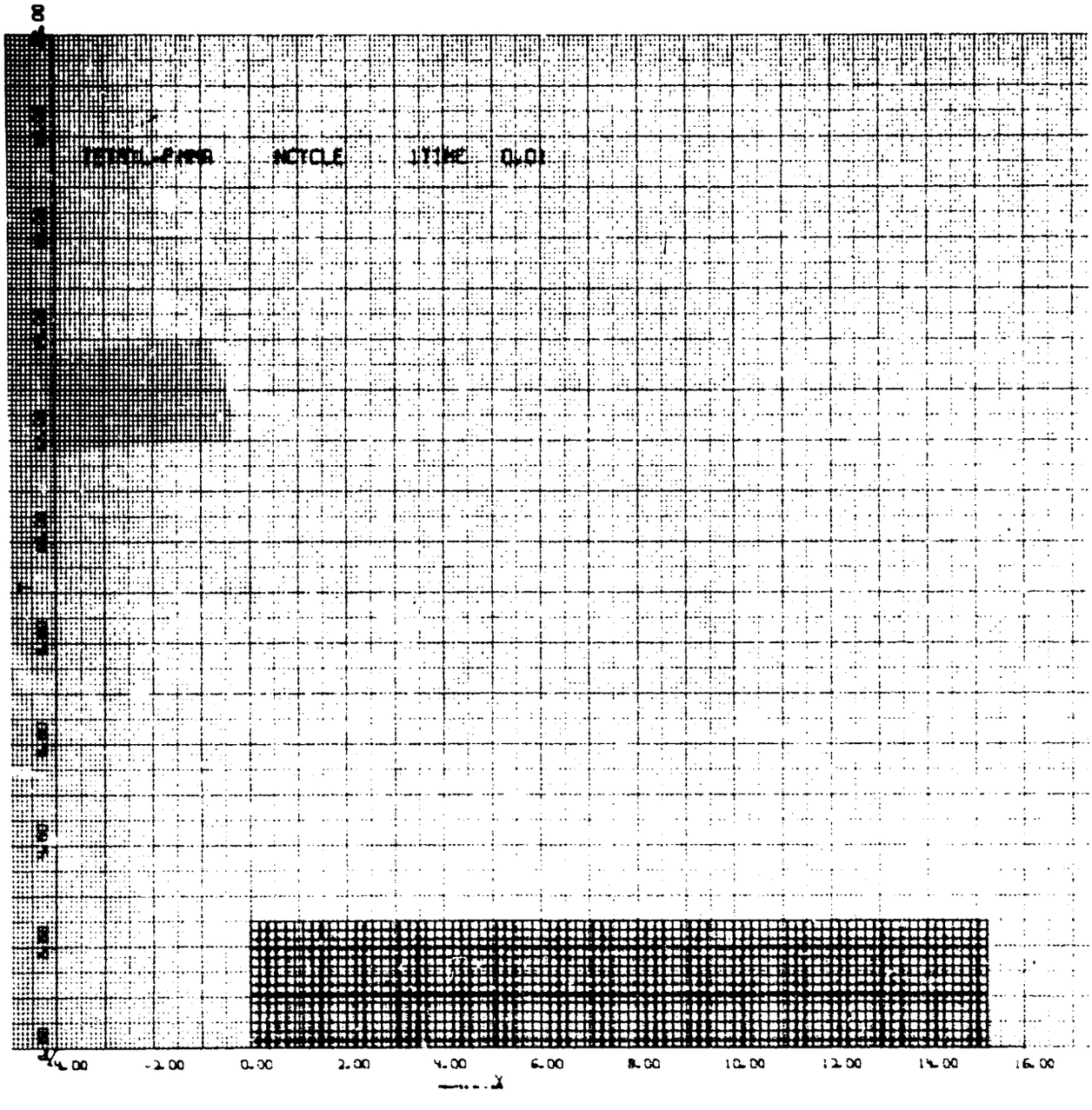

Figure A1(a)

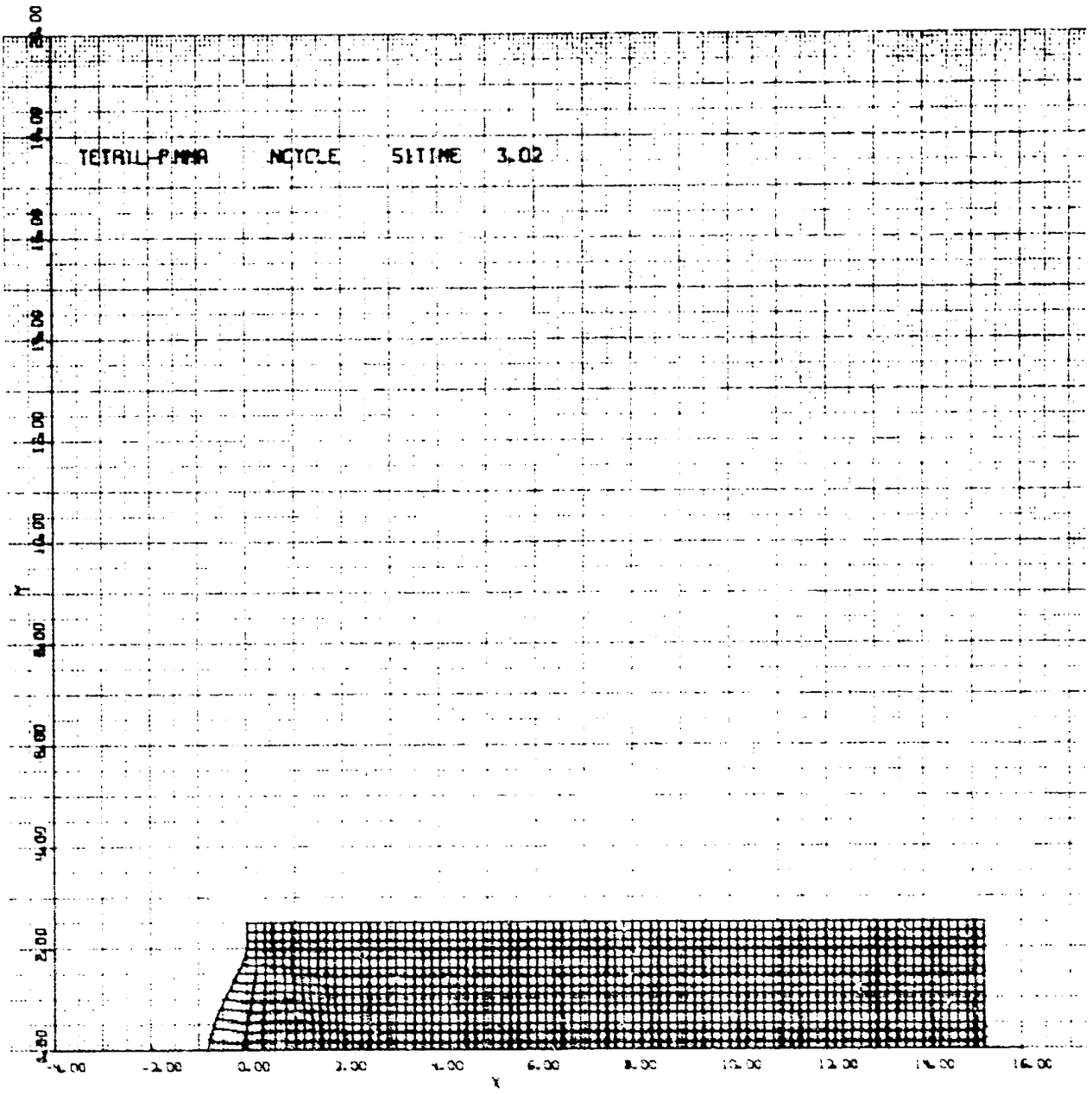
TETRYL-PMMA
NCYCLE
SITIME 3.02
Y
-4.00
-2.00
0.00
2.00
4.00
6.00
8.00
10.00
12.00
14.00
16.00

Figure A2(a)

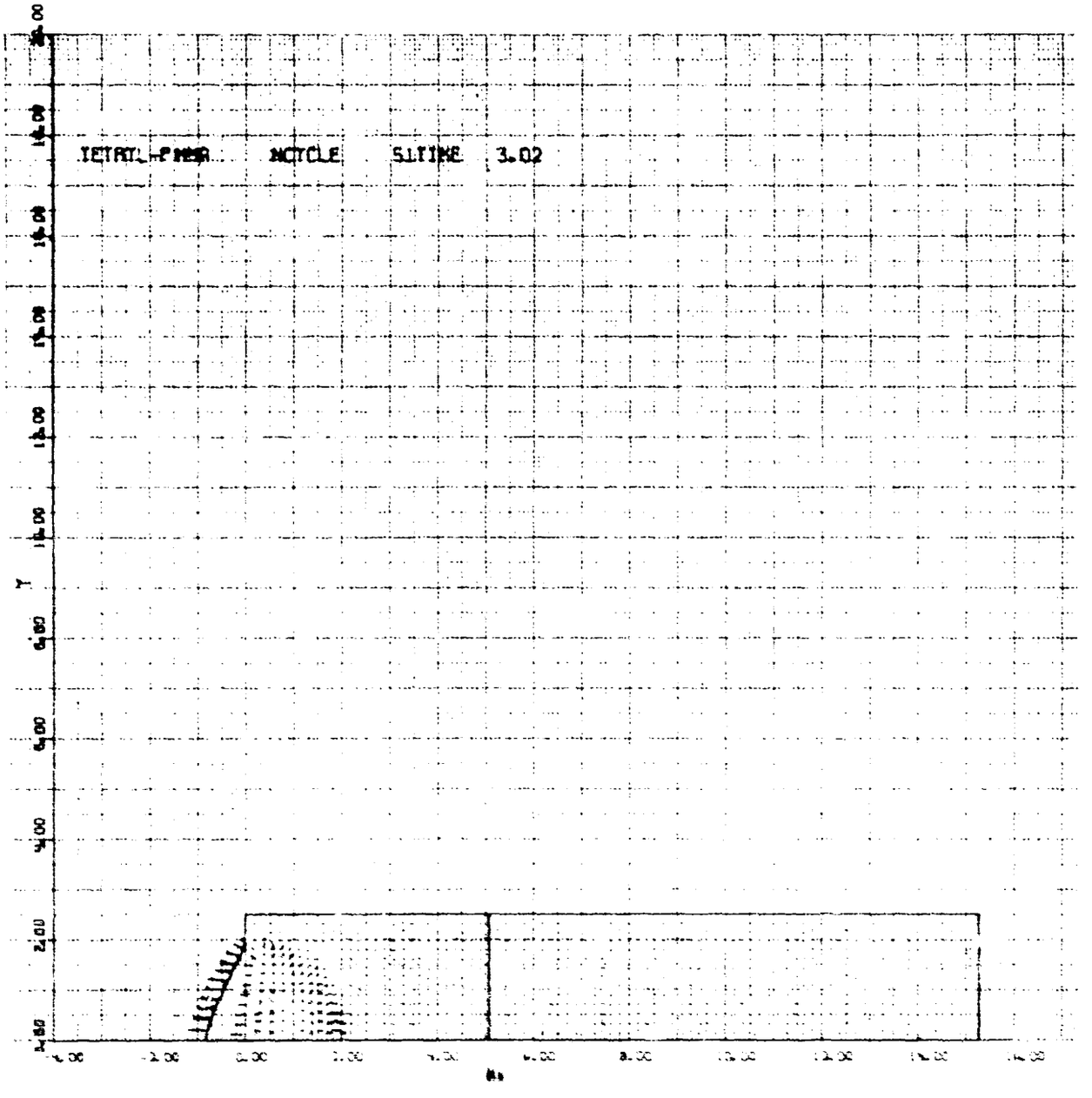

Figure A2(b)

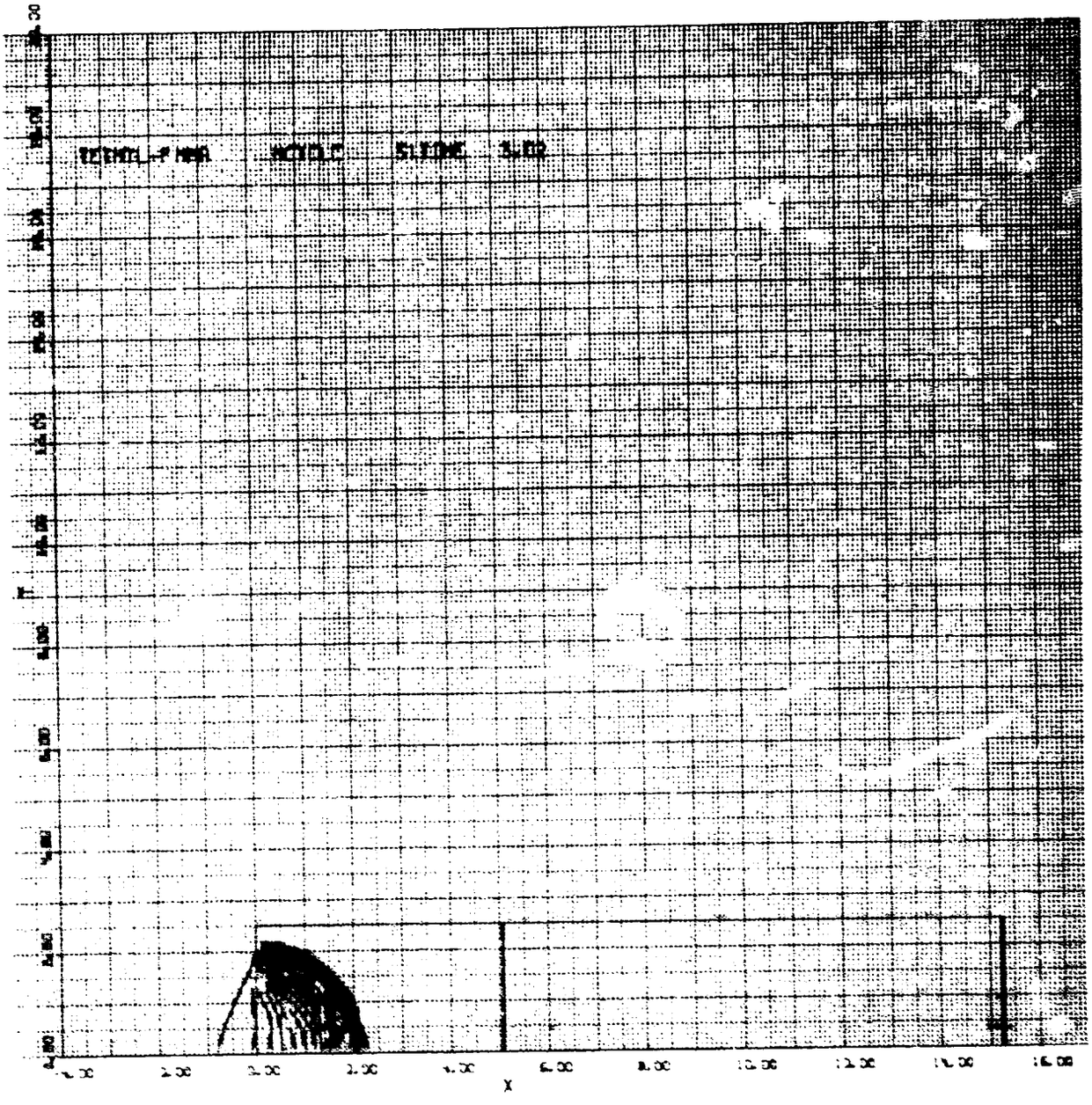

Figure A2(d

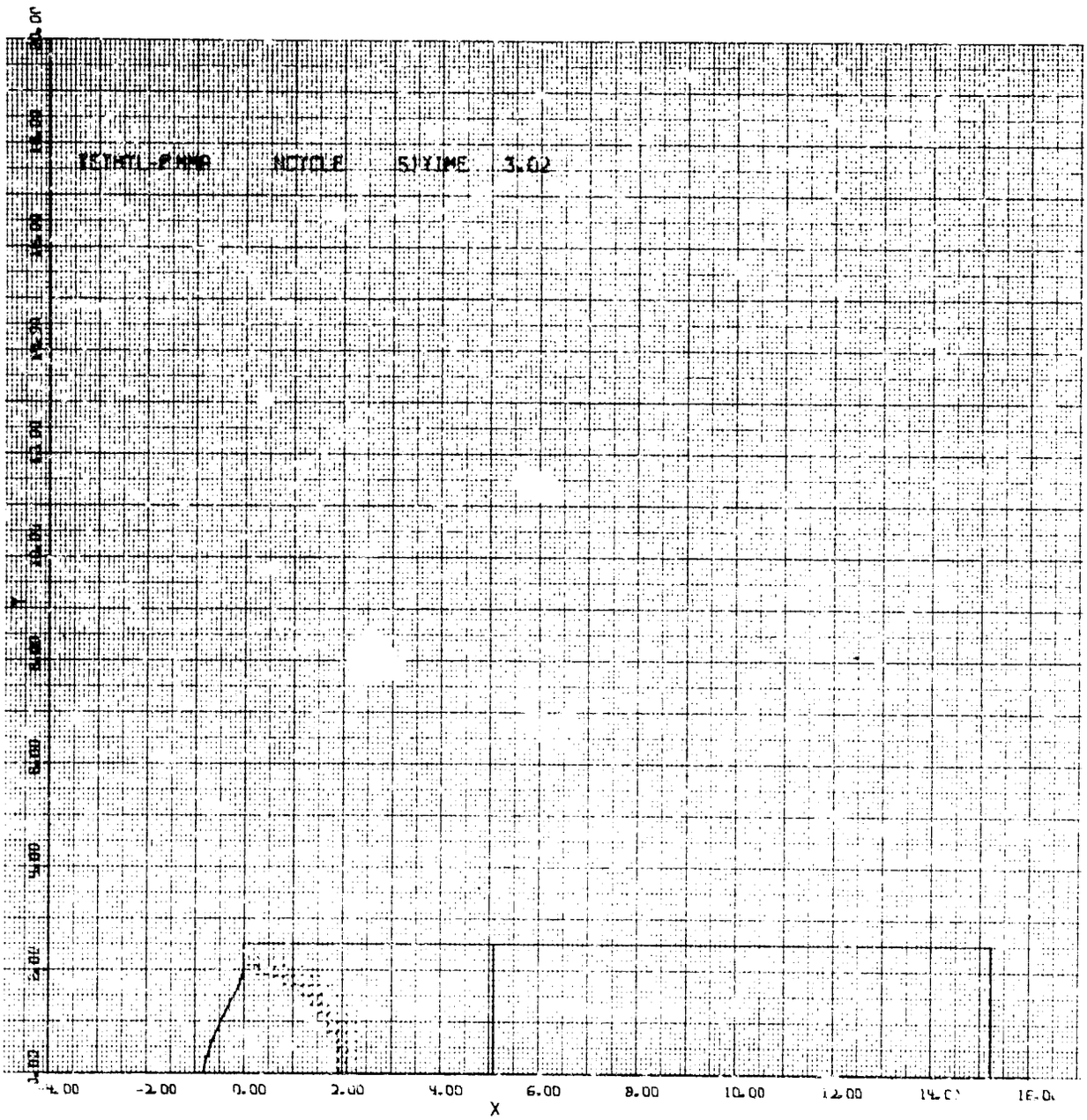

Figure A1(e)

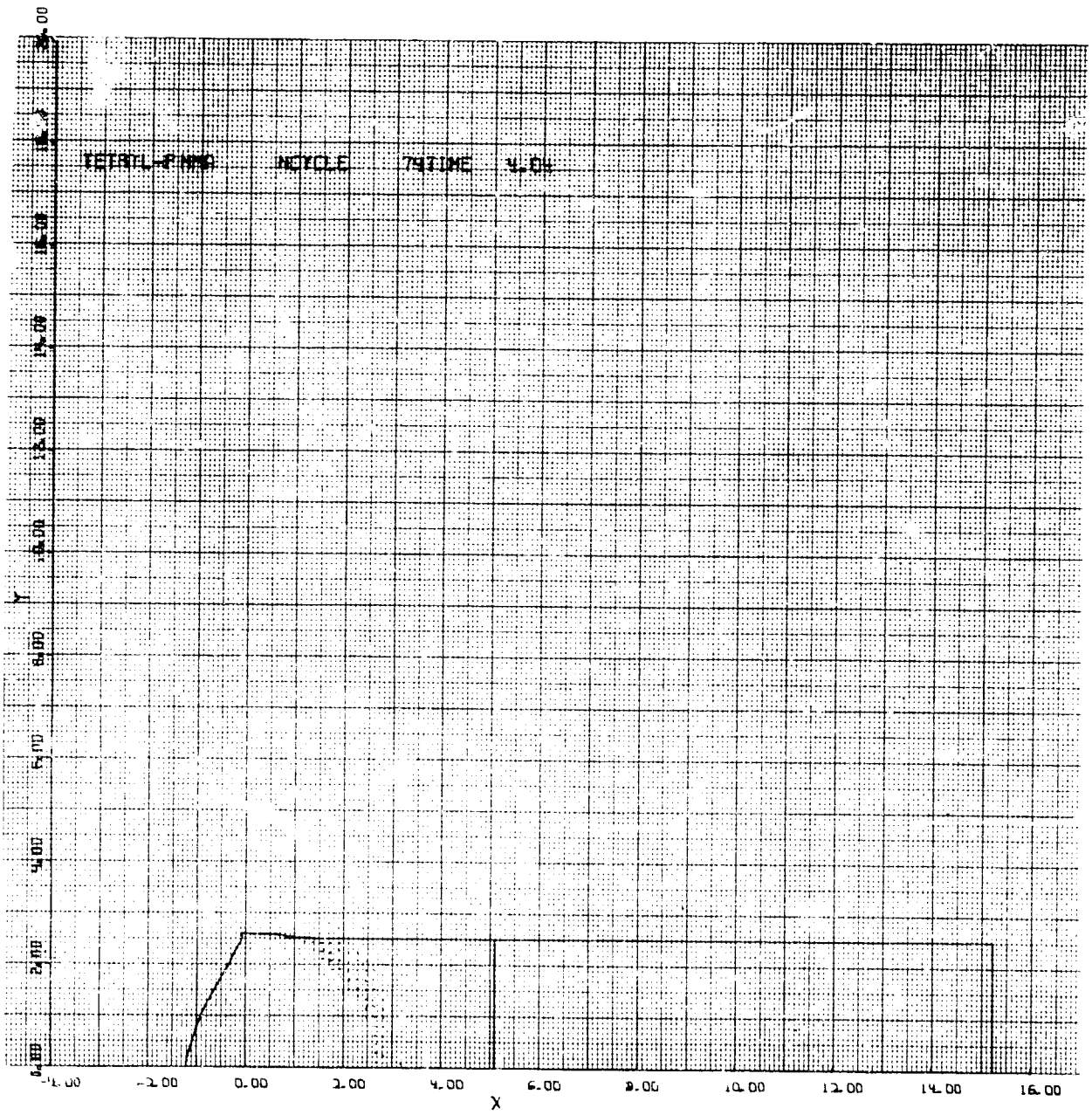
TETRYL-PMMA NOYCLE 791IME 4.04
Y
X
-2.00
0.00
2.00
4.00
6.00
8.00
10.00
12.00
14.00
16.00

Figure A3(e)

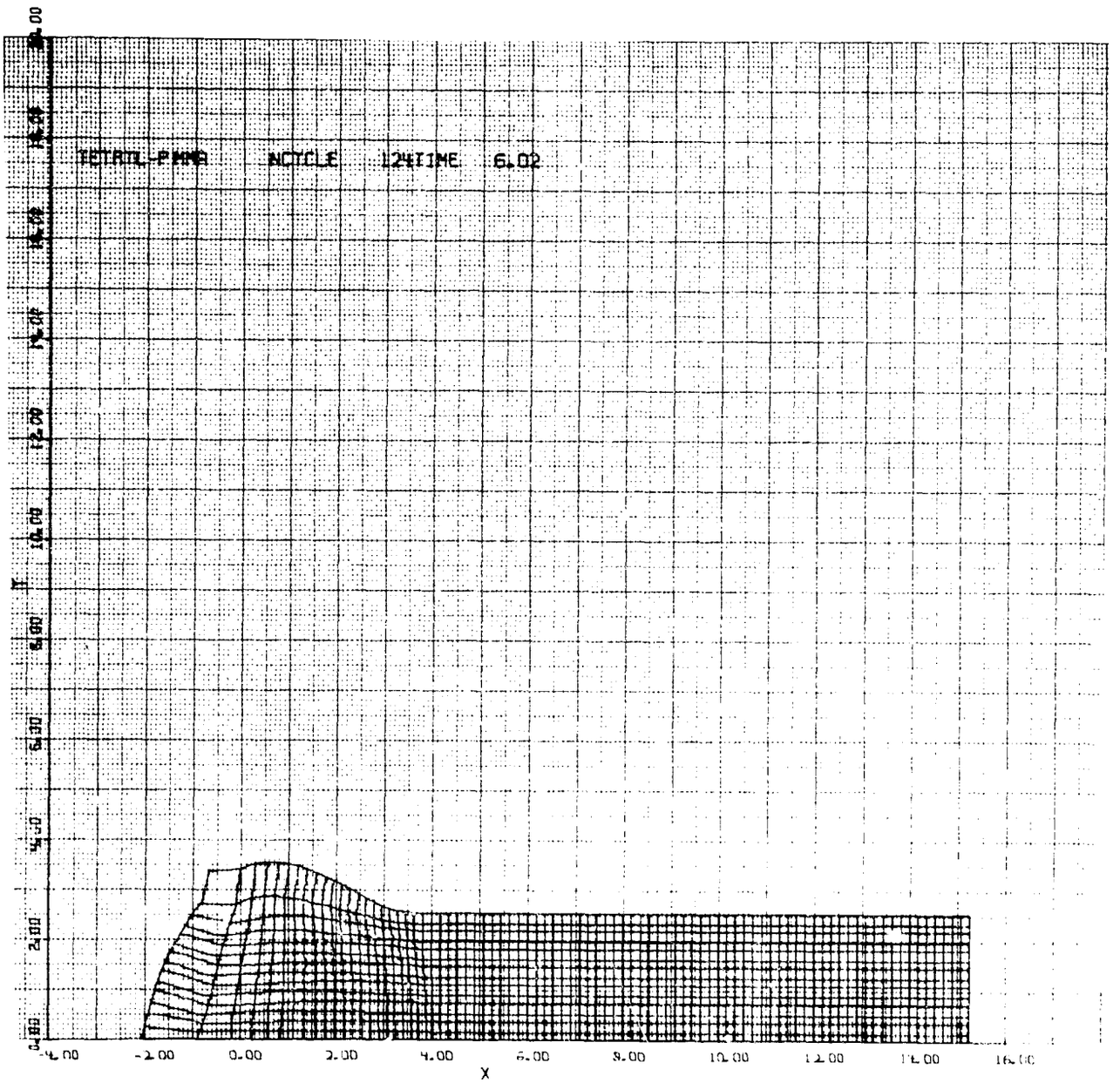
TETRAL-PMMA NOTCLE 124TIME 6.02
Y
X
-4.00
-2.00
0.00
2.00
4.00
6.00
8.00
10.00
12.00
14.00
16.00

Figure A4(a)

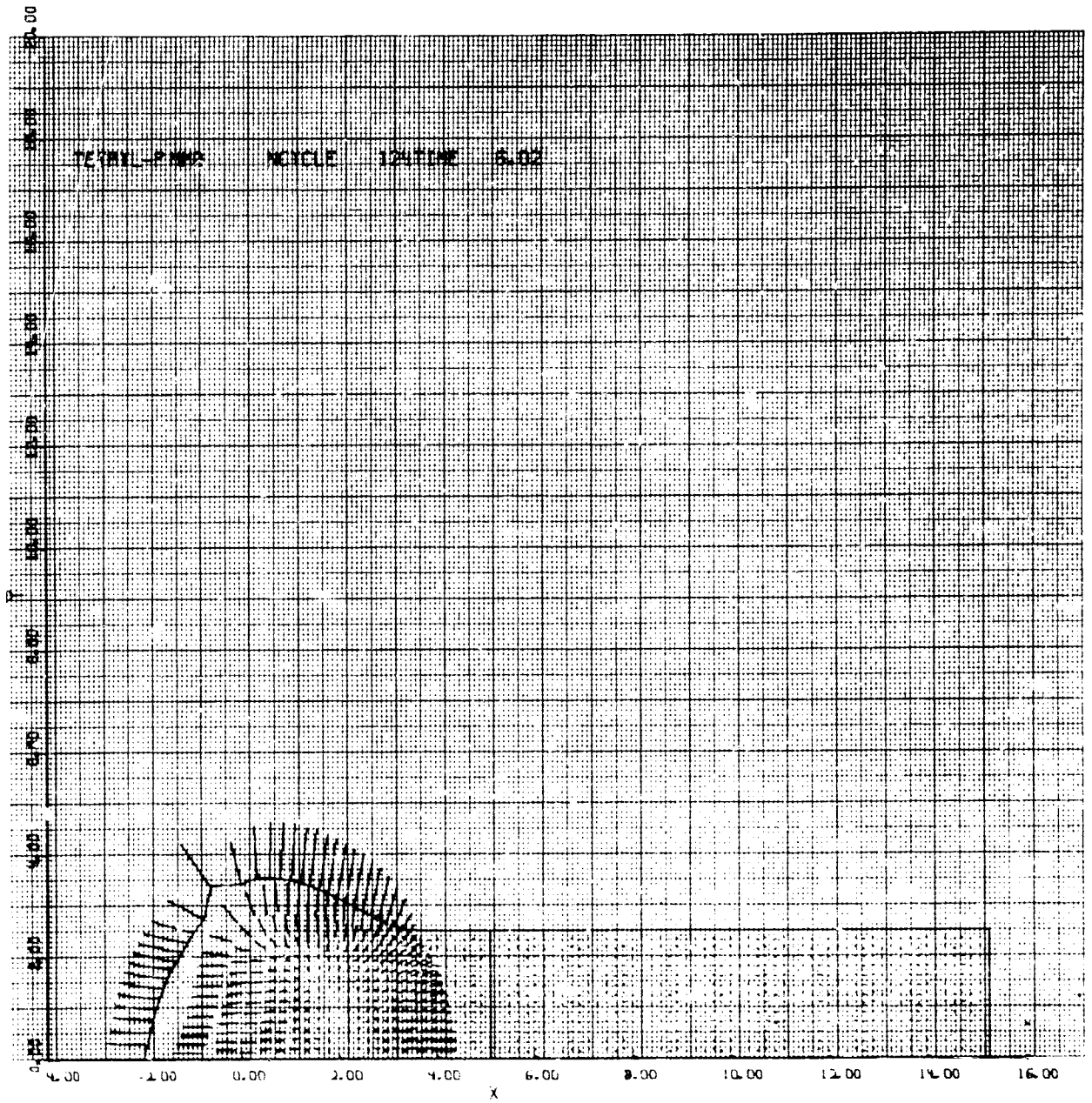
CYCLE 124 TIME 6.02
-4.00
-2.00
0.00
2.00
4.00
6.00
8.00
10.00
12.00
14.00
16.00
X

Figure A4(b)

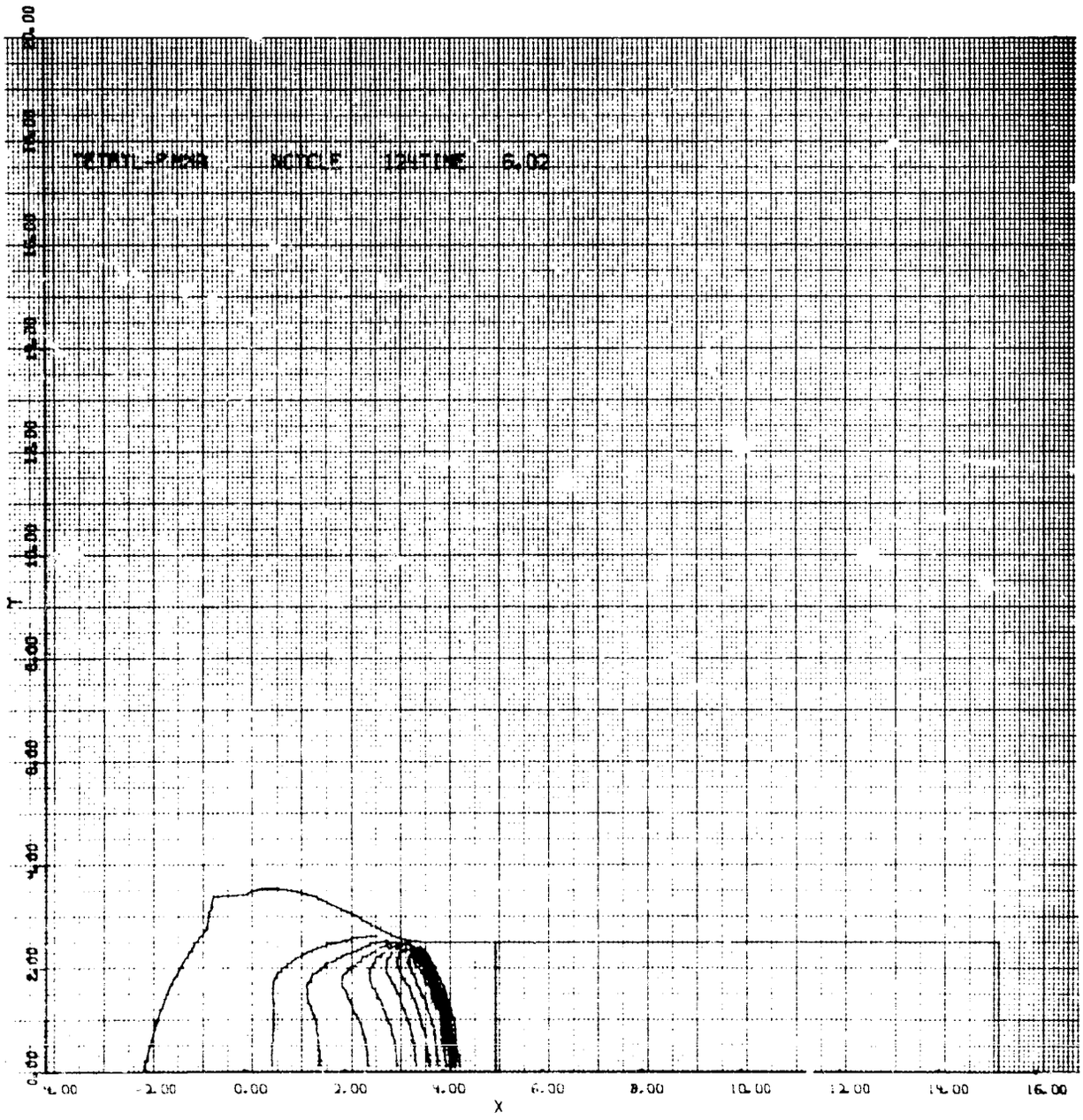
TOTAL-PMAS NCTCLF 12*TIME 6.02
Y
X
-4.00
-2.00
0.00
2.00
4.00
6.00
8.00
10.00
12.00
14.00
16.00
0.00
2.00
4.00
6.00
8.00
10.00
12.00
14.00
16.00
18.00
20.00

Figure A4(d)

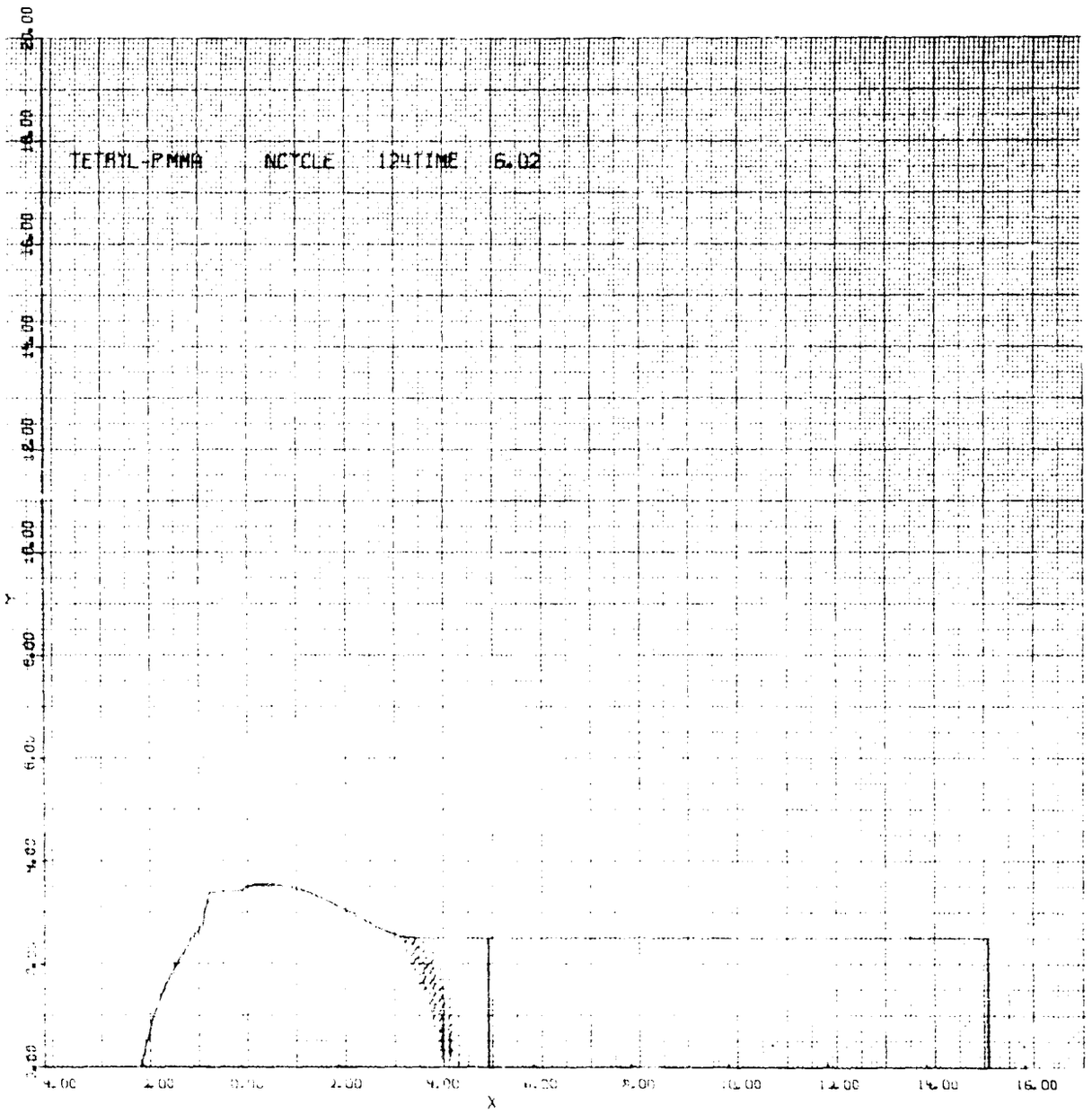
TETRYL-PMMA NCTCLE 124TIME 6.02
Y
X
20.00
16.00
12.00
8.00
4.00
16.00

Figure A4(e)

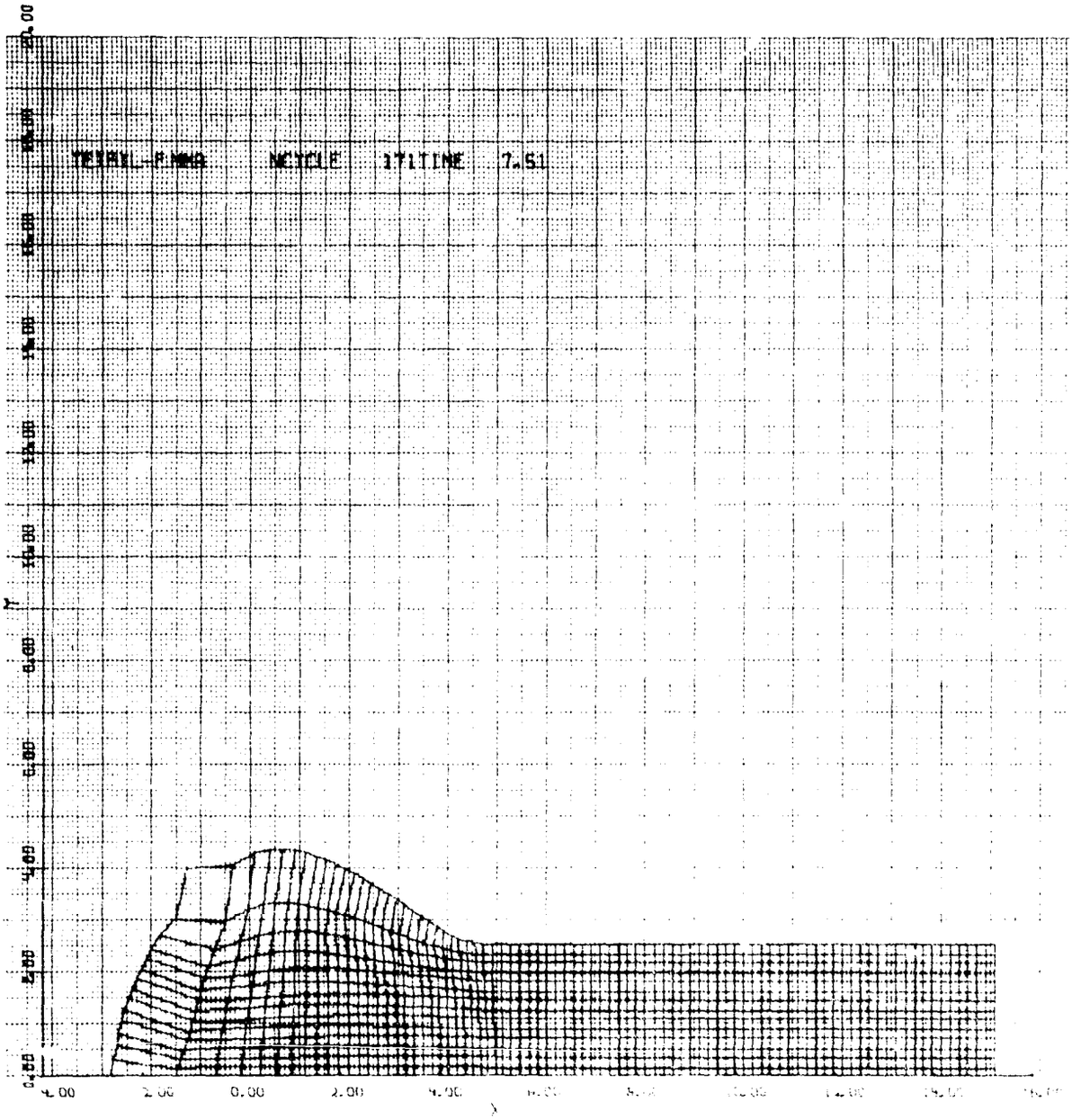

Figure A-6(c)

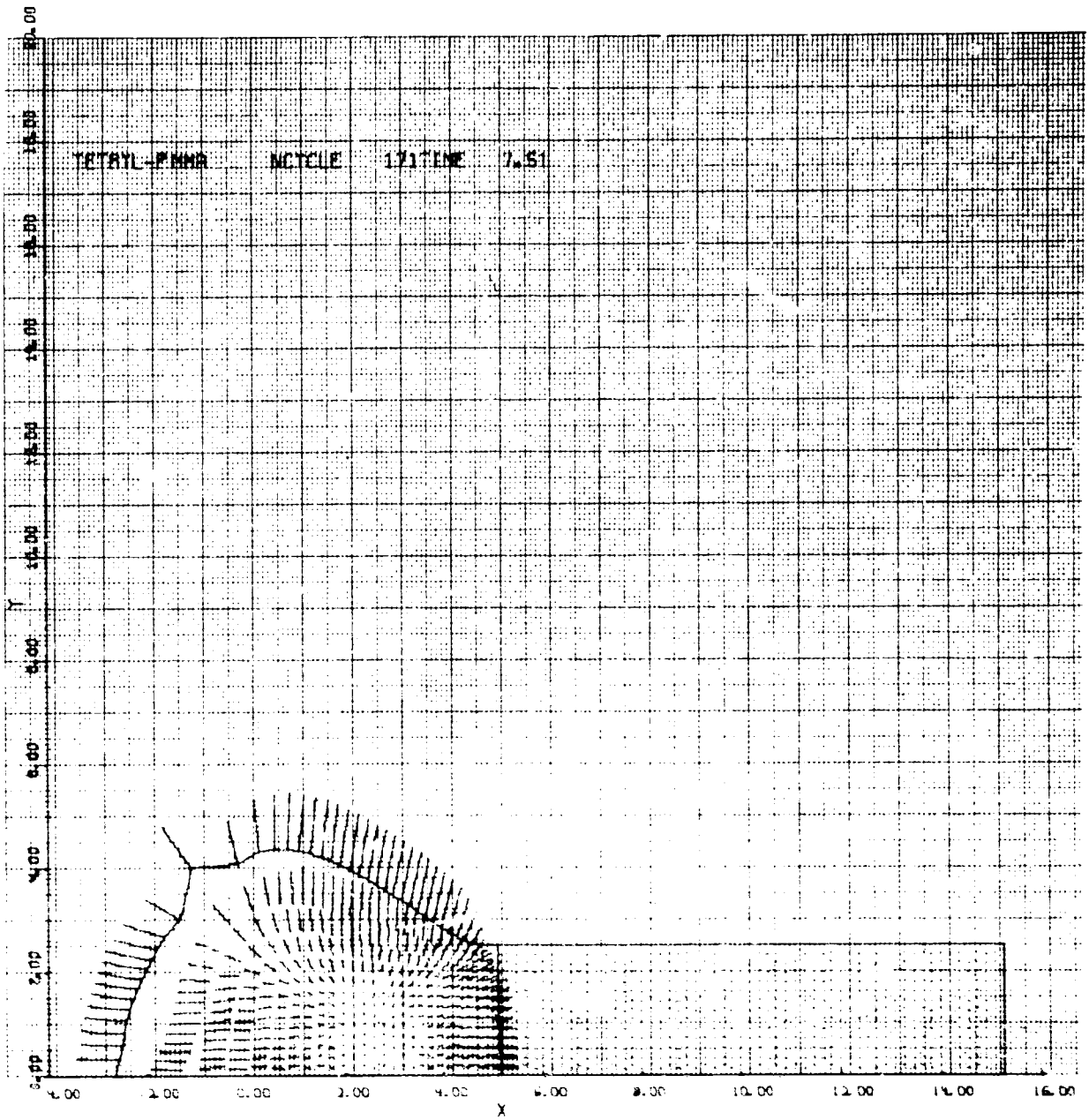

Figure A5(b)

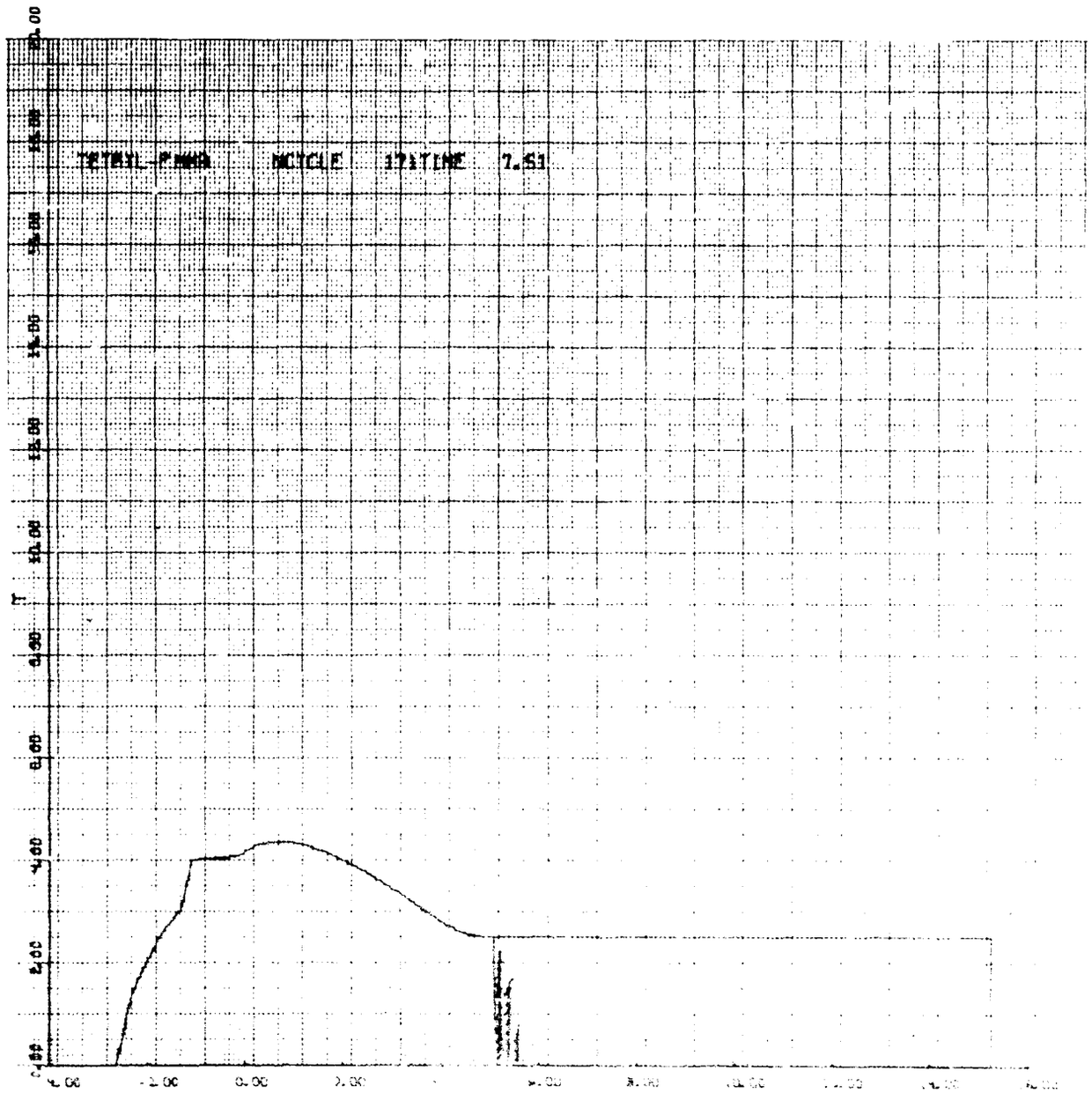

Figure A5(c)

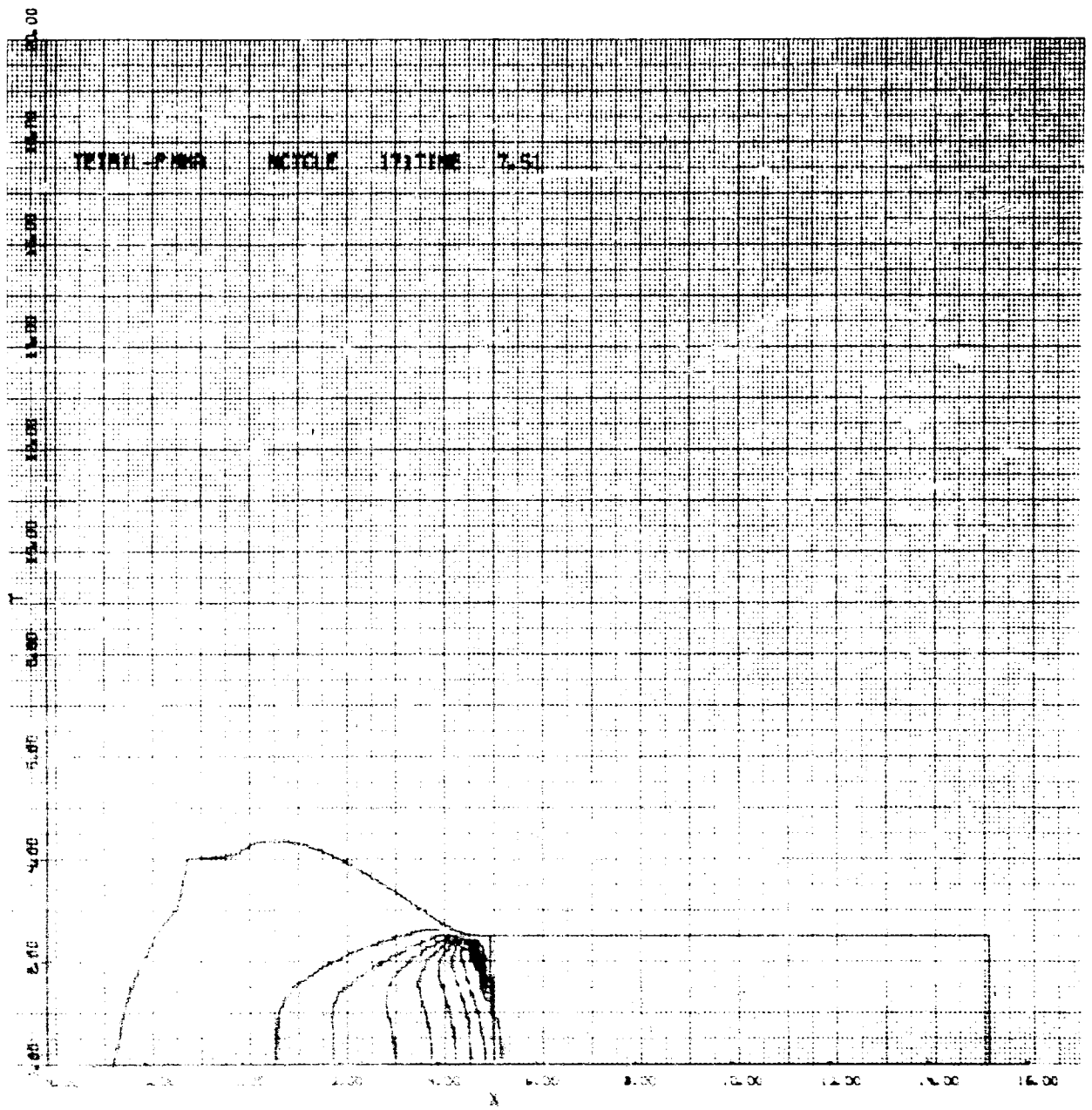

Figure A5(c)

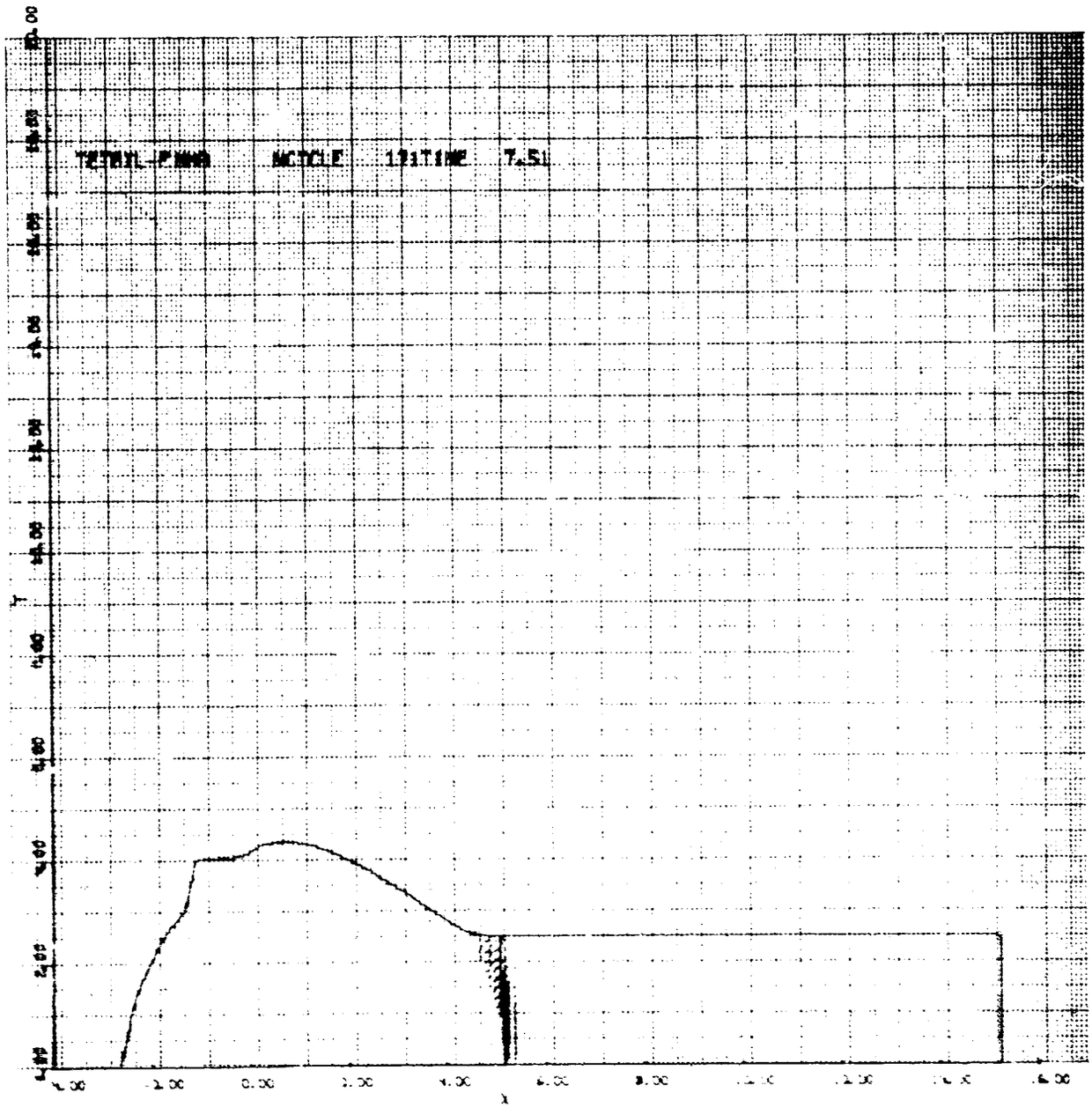

Figure A5(c)

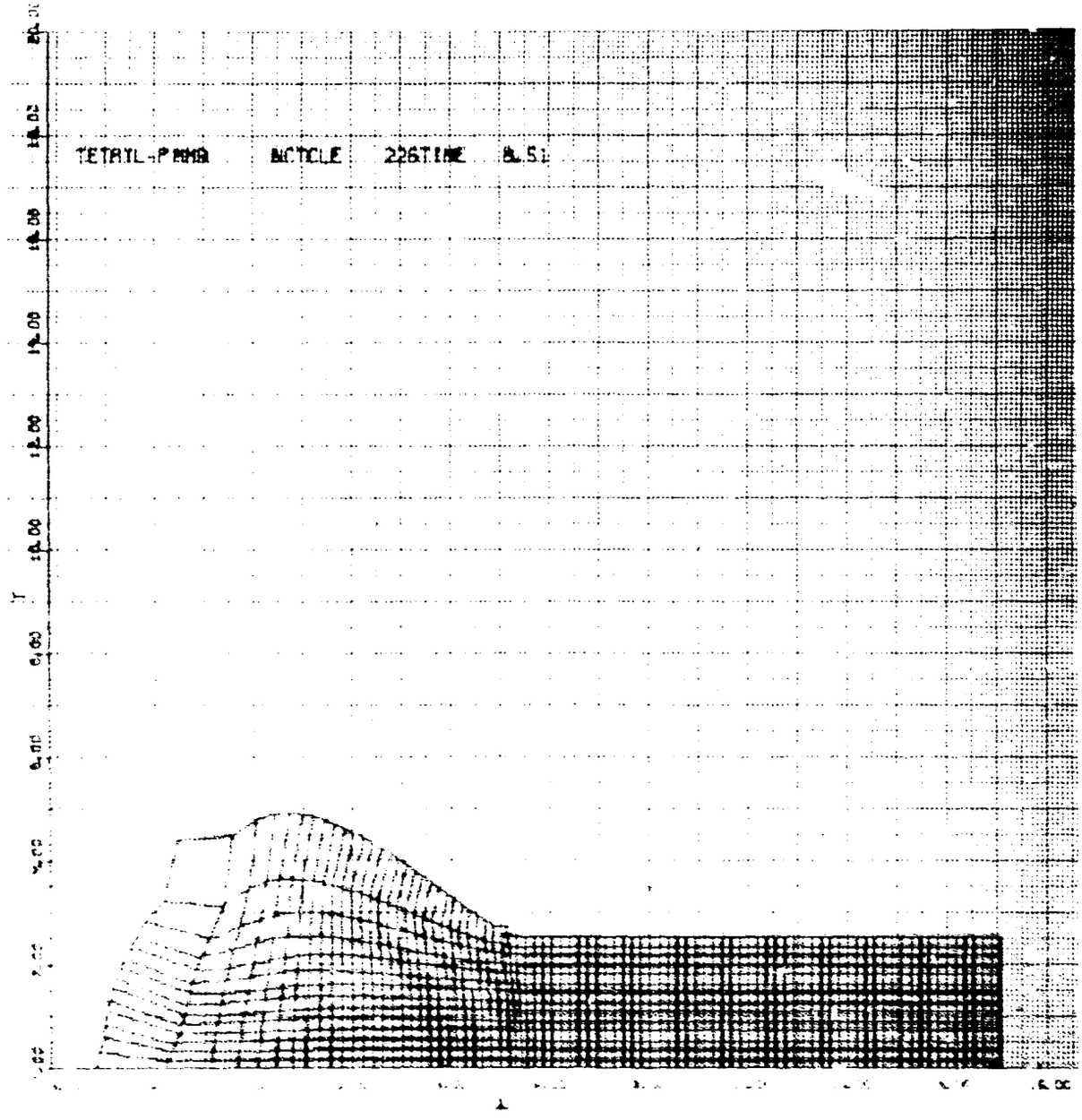
TETRYL-PMMA
ANGLE
226TIME
8.51

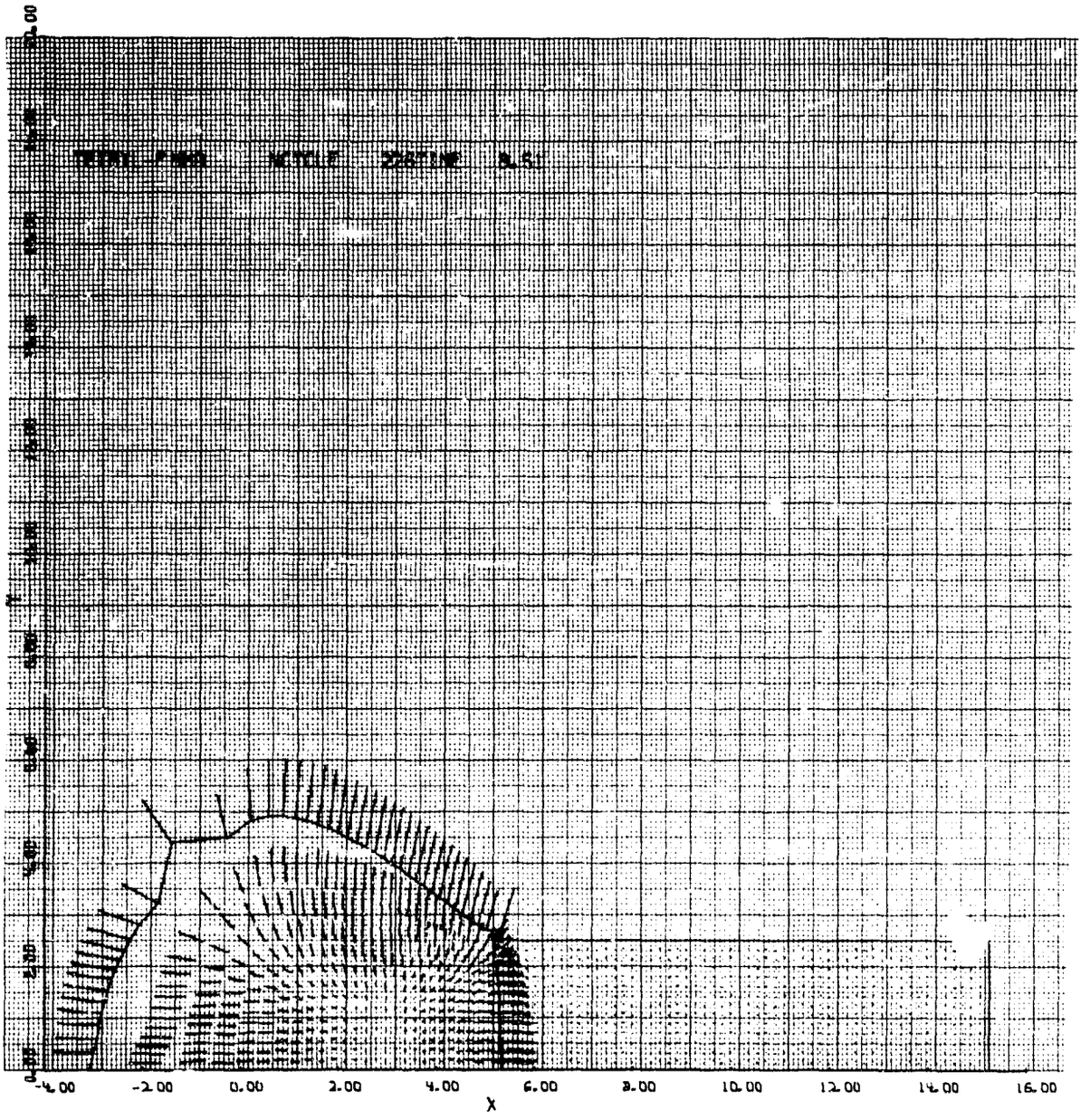

Figure A6(b)

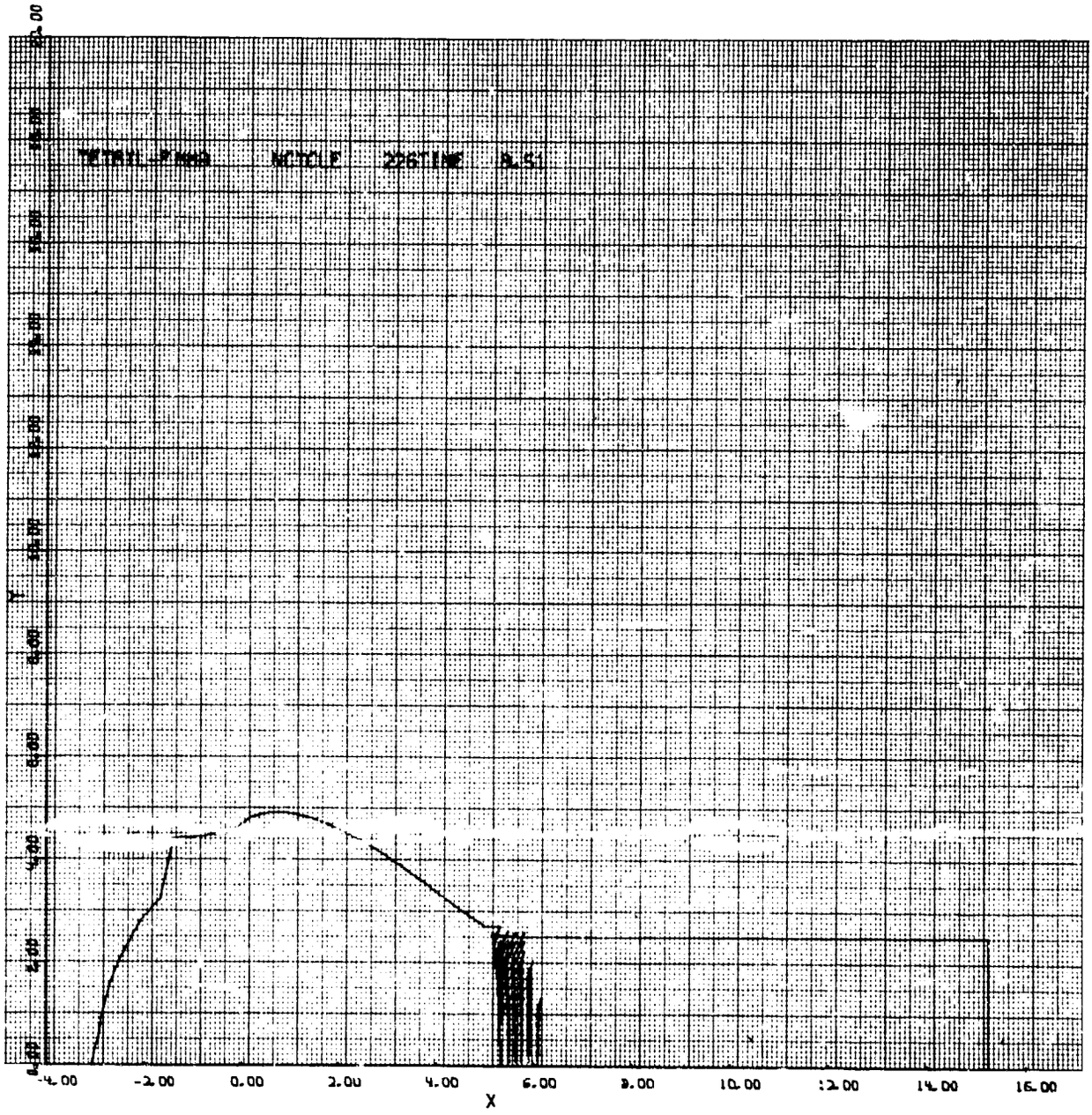

Figure A6(c)

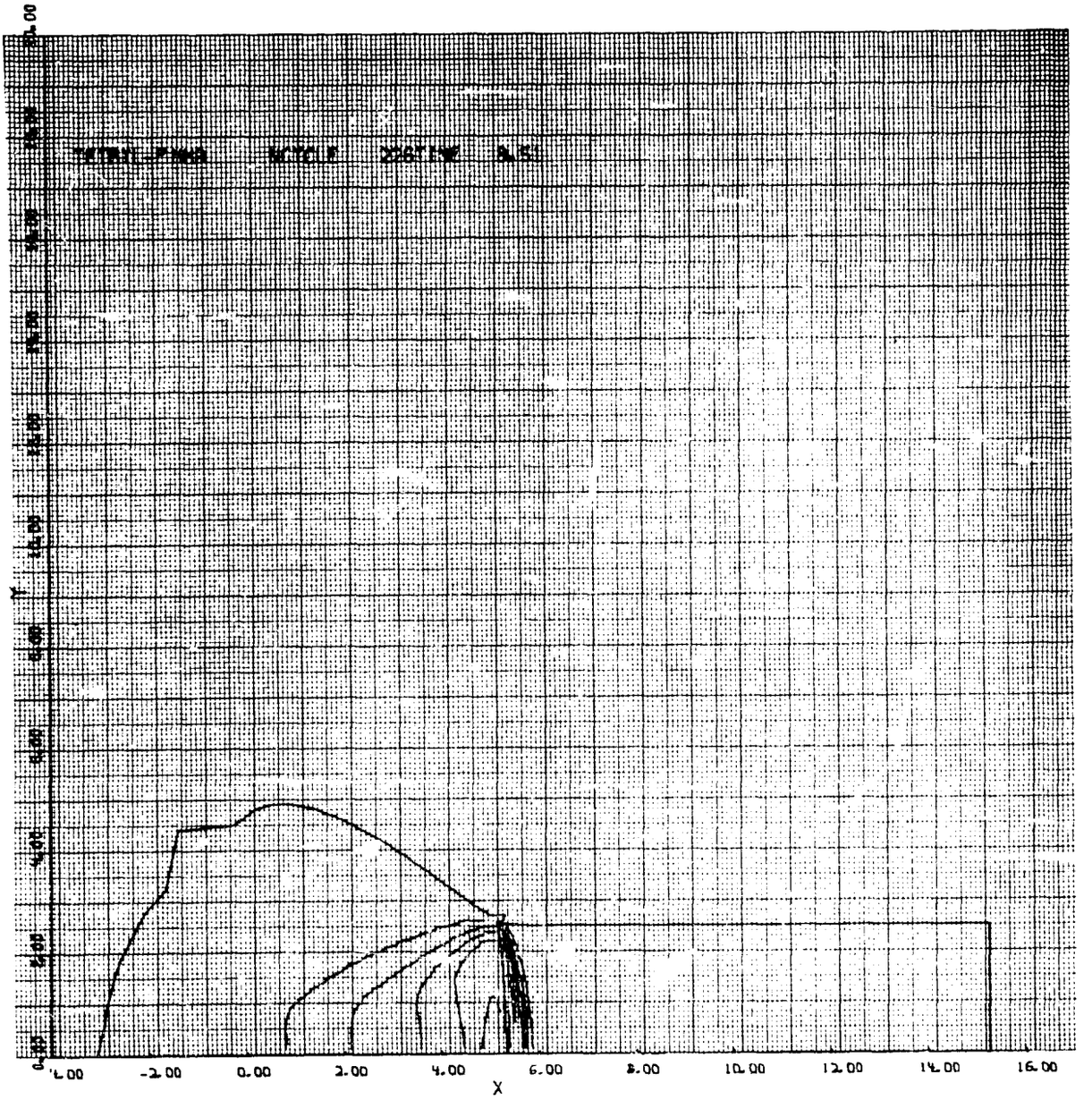

Figure A6(d)

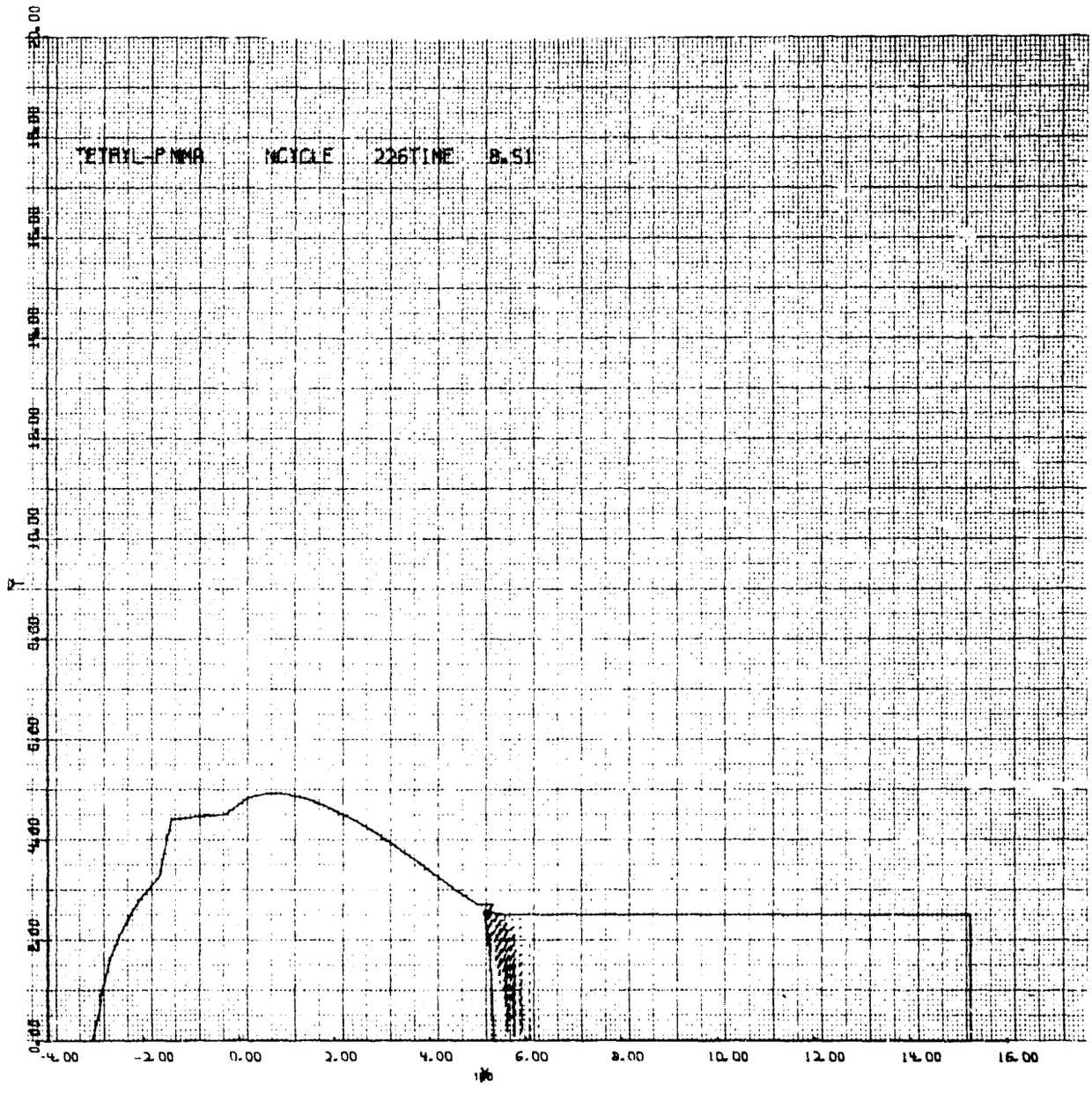
TETRYL-PMMA NCYCLE 226TIME 8.51
-4.00
-2.00
0.00
2.00
4.00
6.00
8.00
10.00
12.00
14.00
16.00

Figure A6(e)

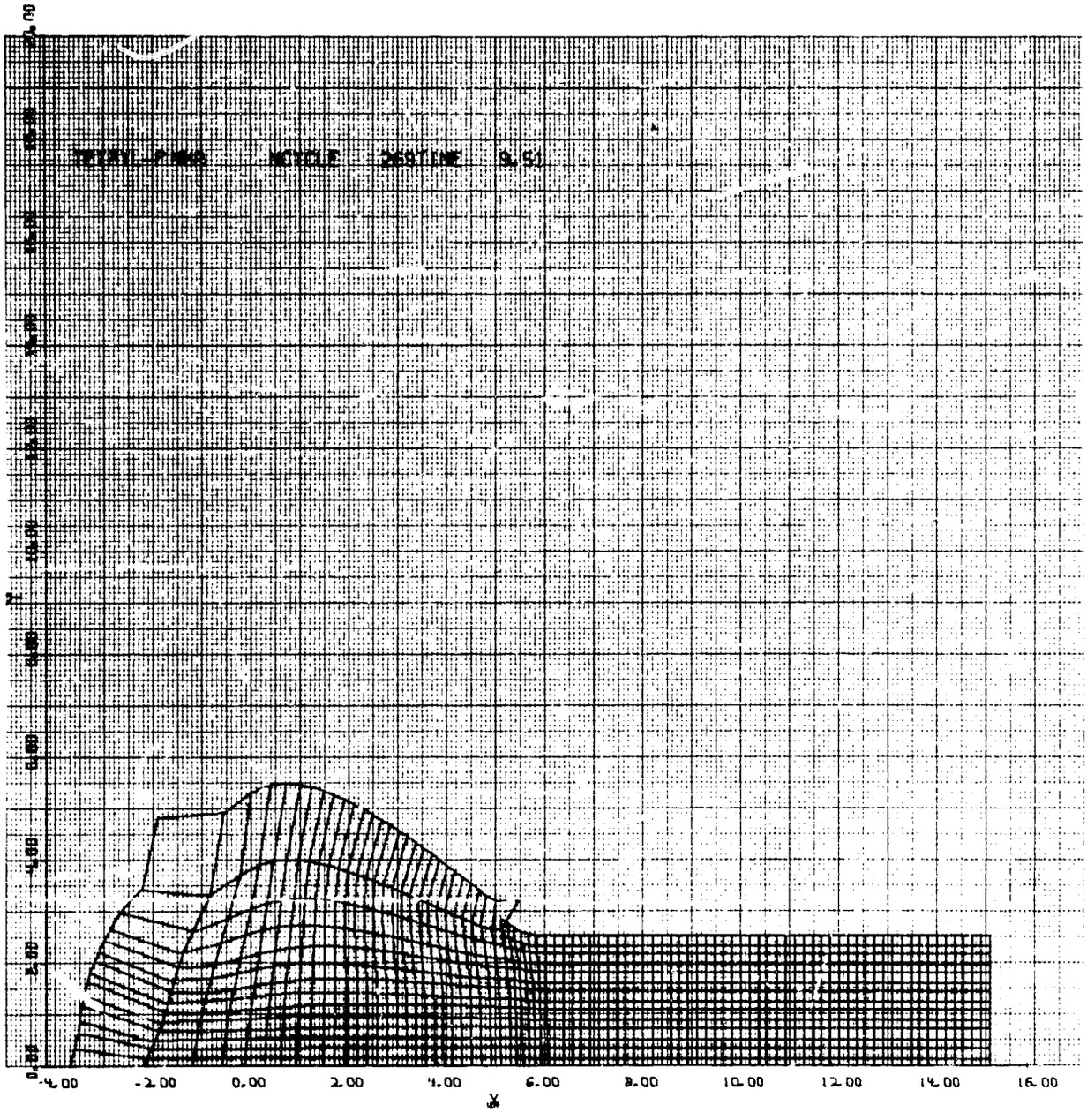
TOTAL POWER
CYCLE 269 TIME 9.51
-4.00
-2.00
0.00
2.00
4.00
6.00
8.00
10.00
12.00
14.00
16.00
X

Figure A7(a)

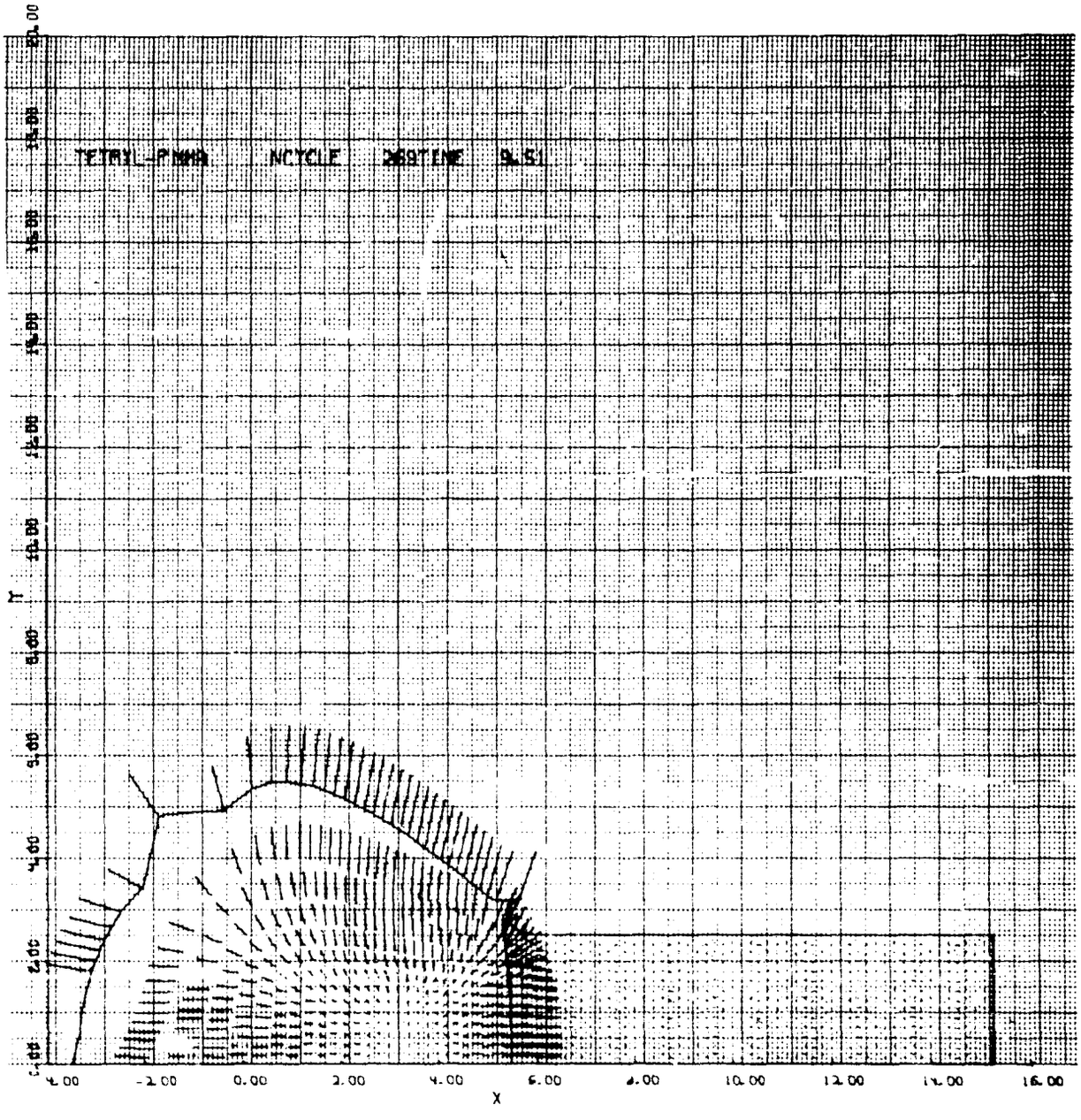
TETRYL-PMMA NCYCLE 268TIME 9.51
Y
X
-4.00
-2.00
0.00
2.00
4.00
6.00
8.00
10.00
12.00
14.00
16.00

Figure A7(b)

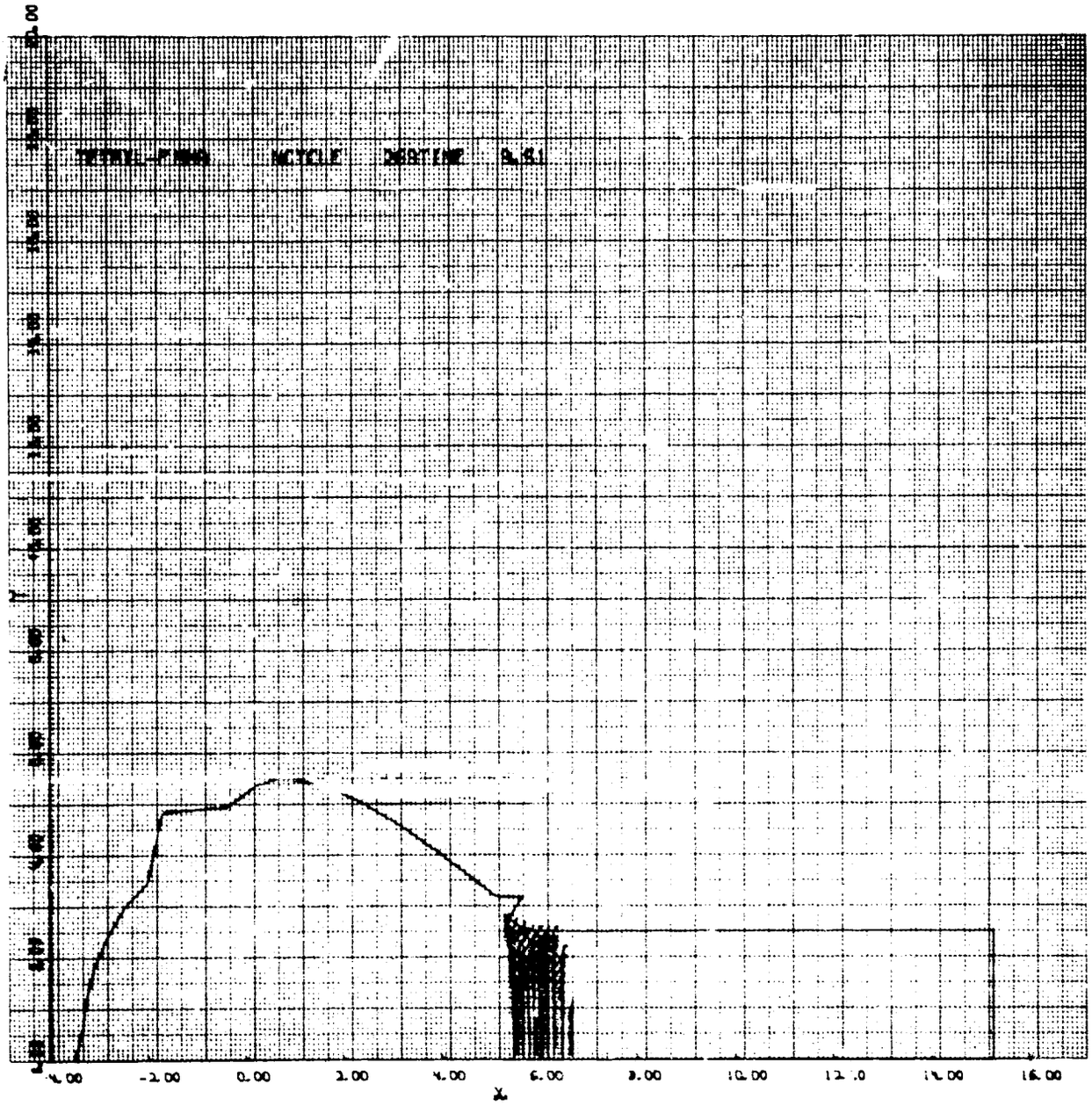

Figure A7(c)

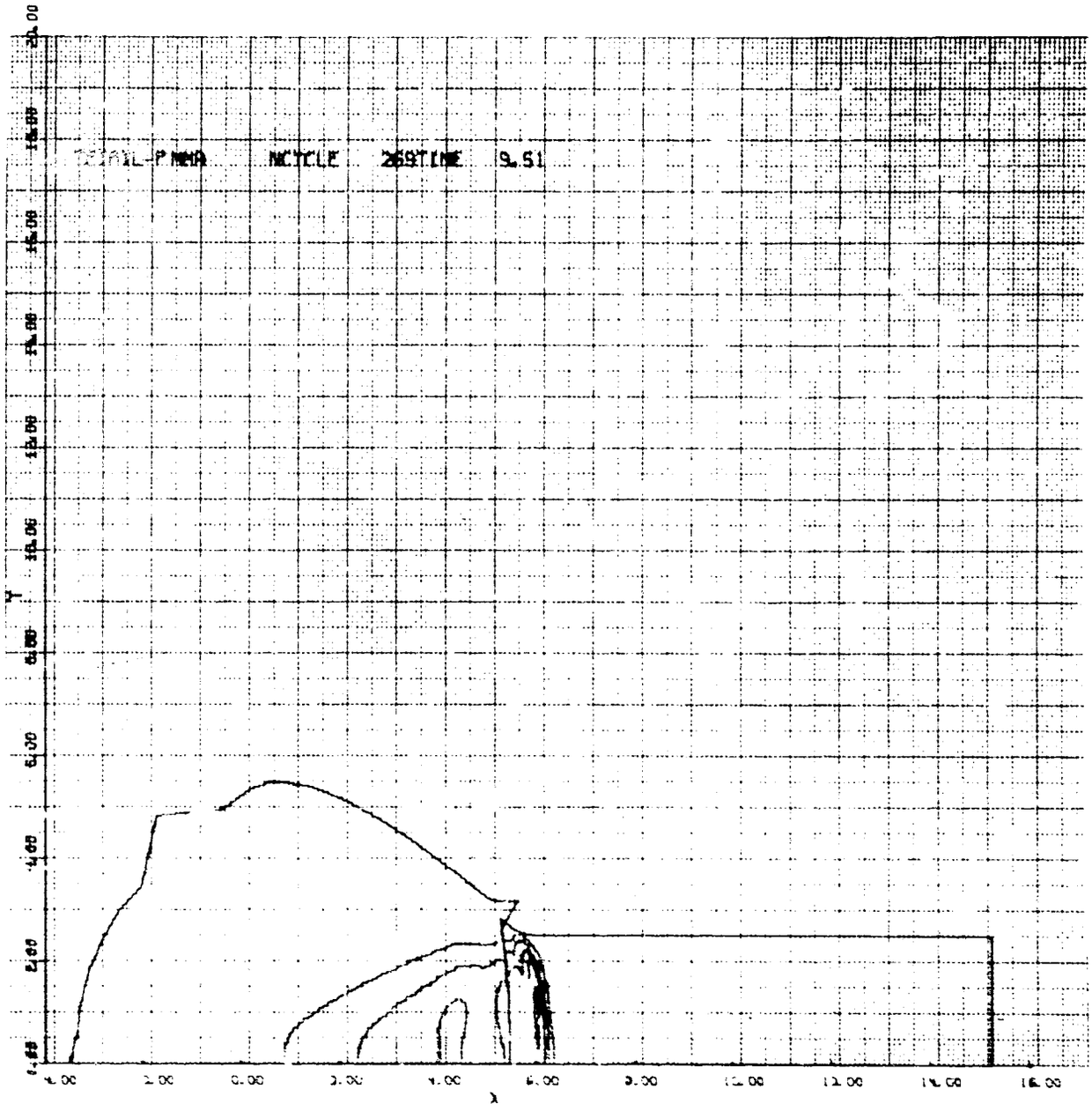

Figure A7(d)

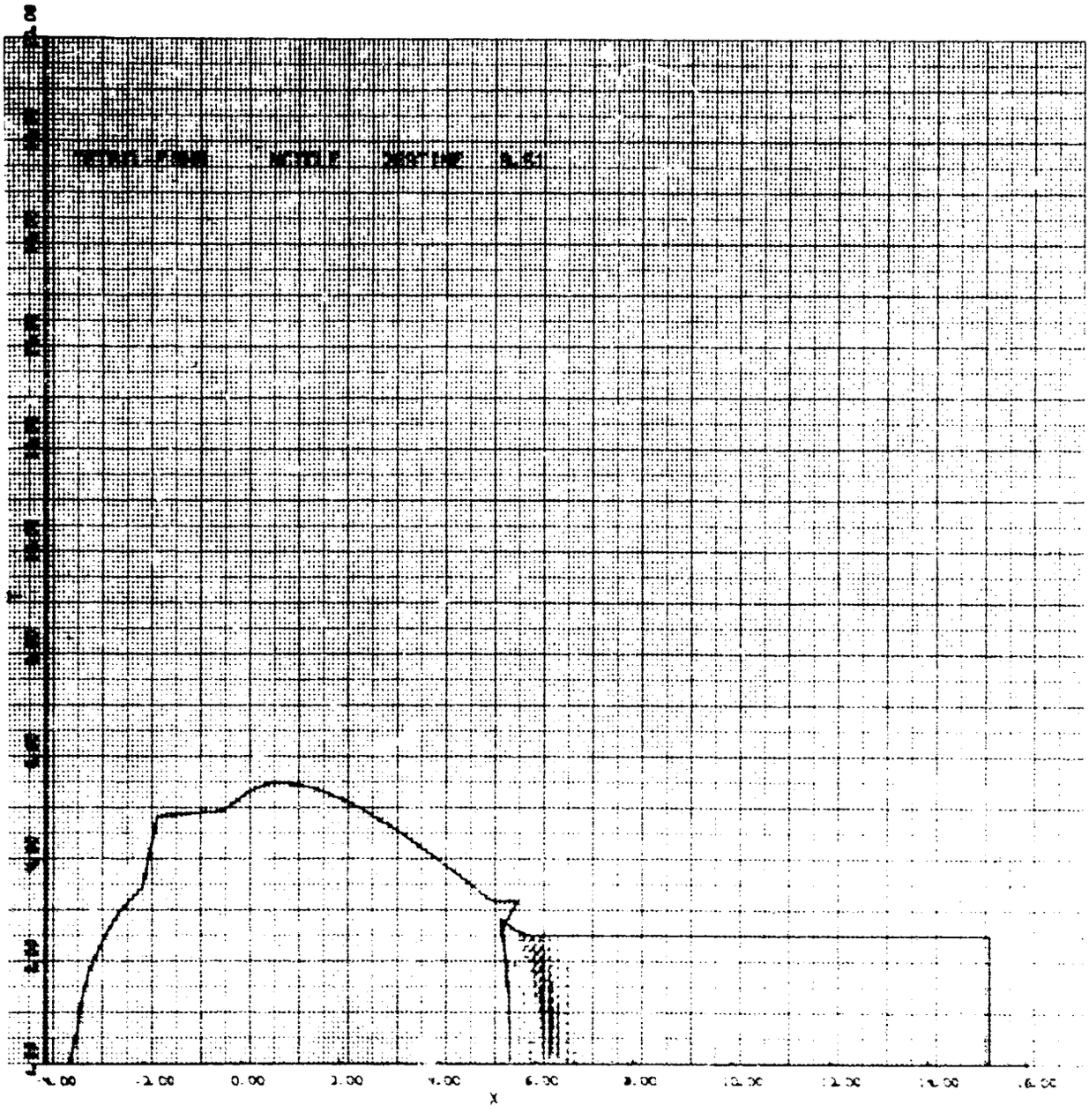

Figure A7(c)

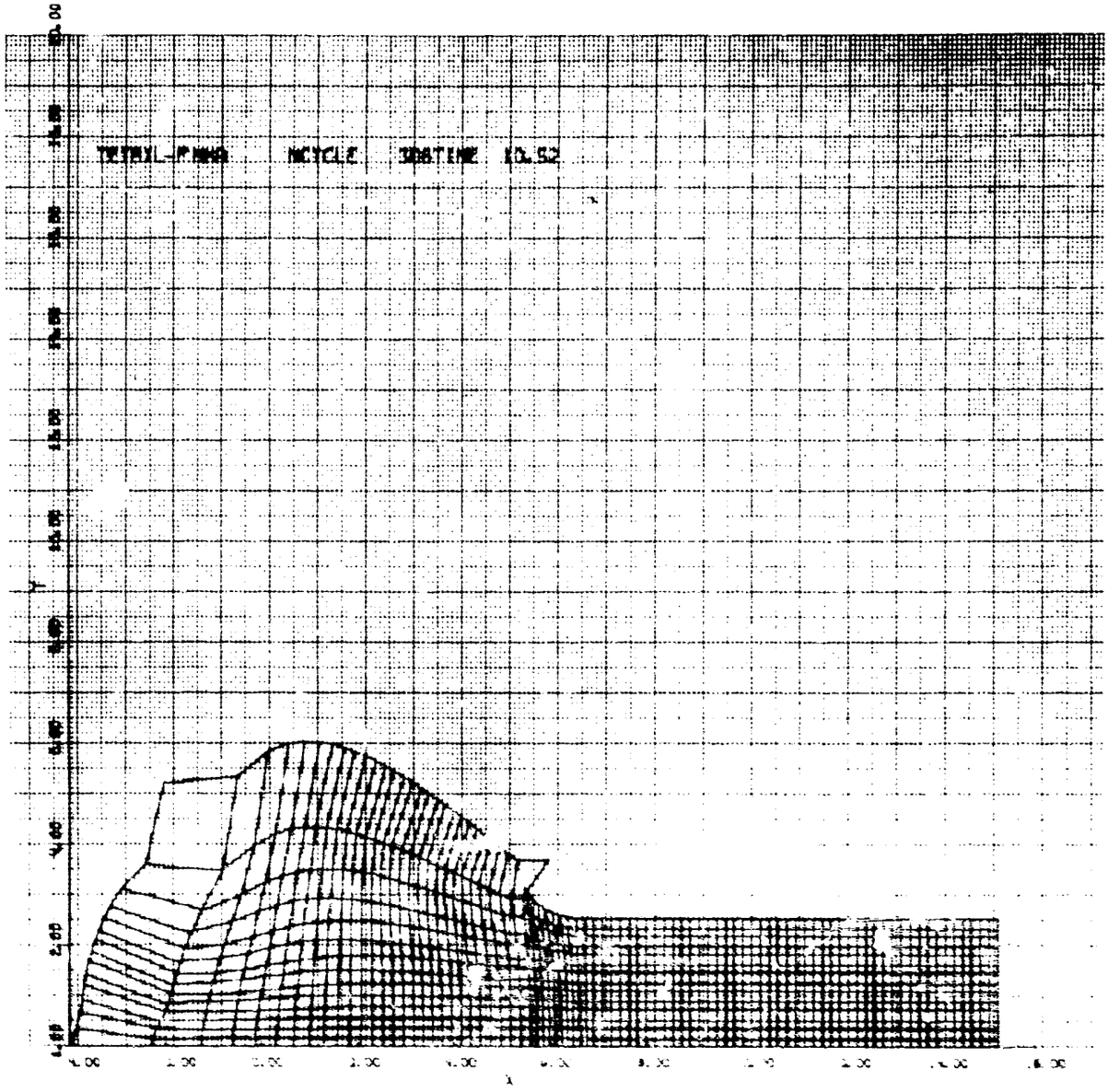

Figure A3(a)

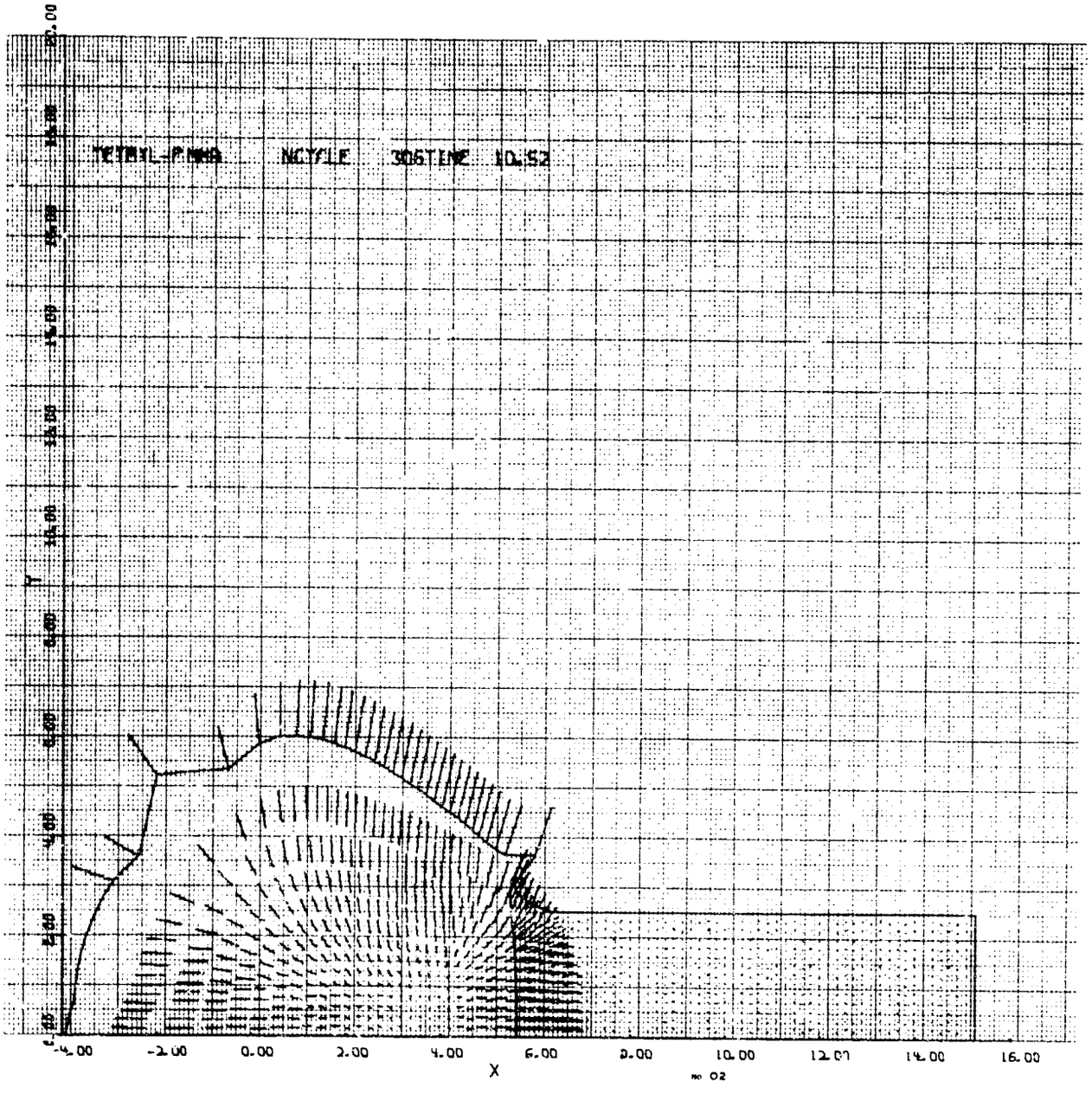

Figure A8(b)

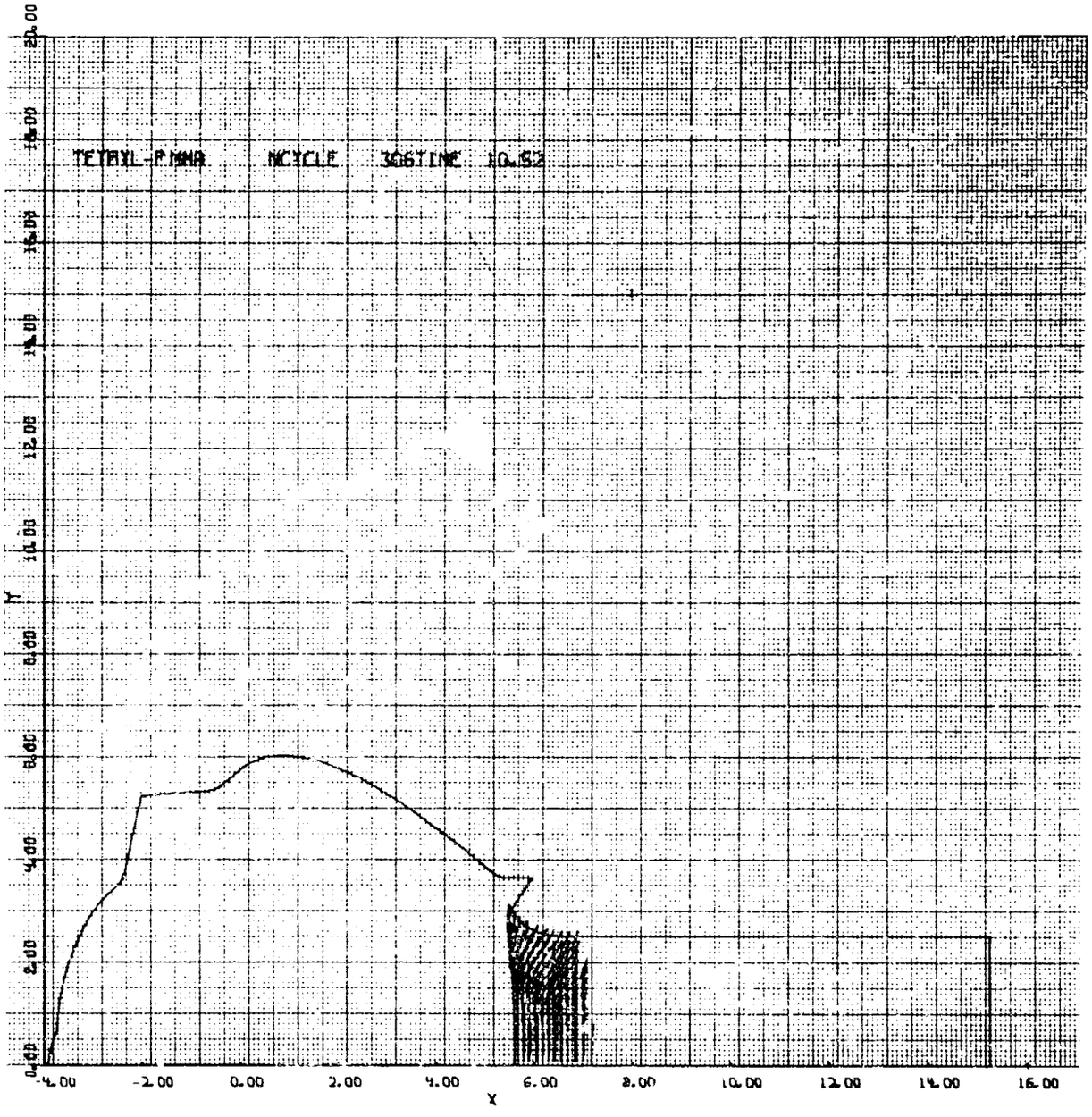

Figure A 8(c)

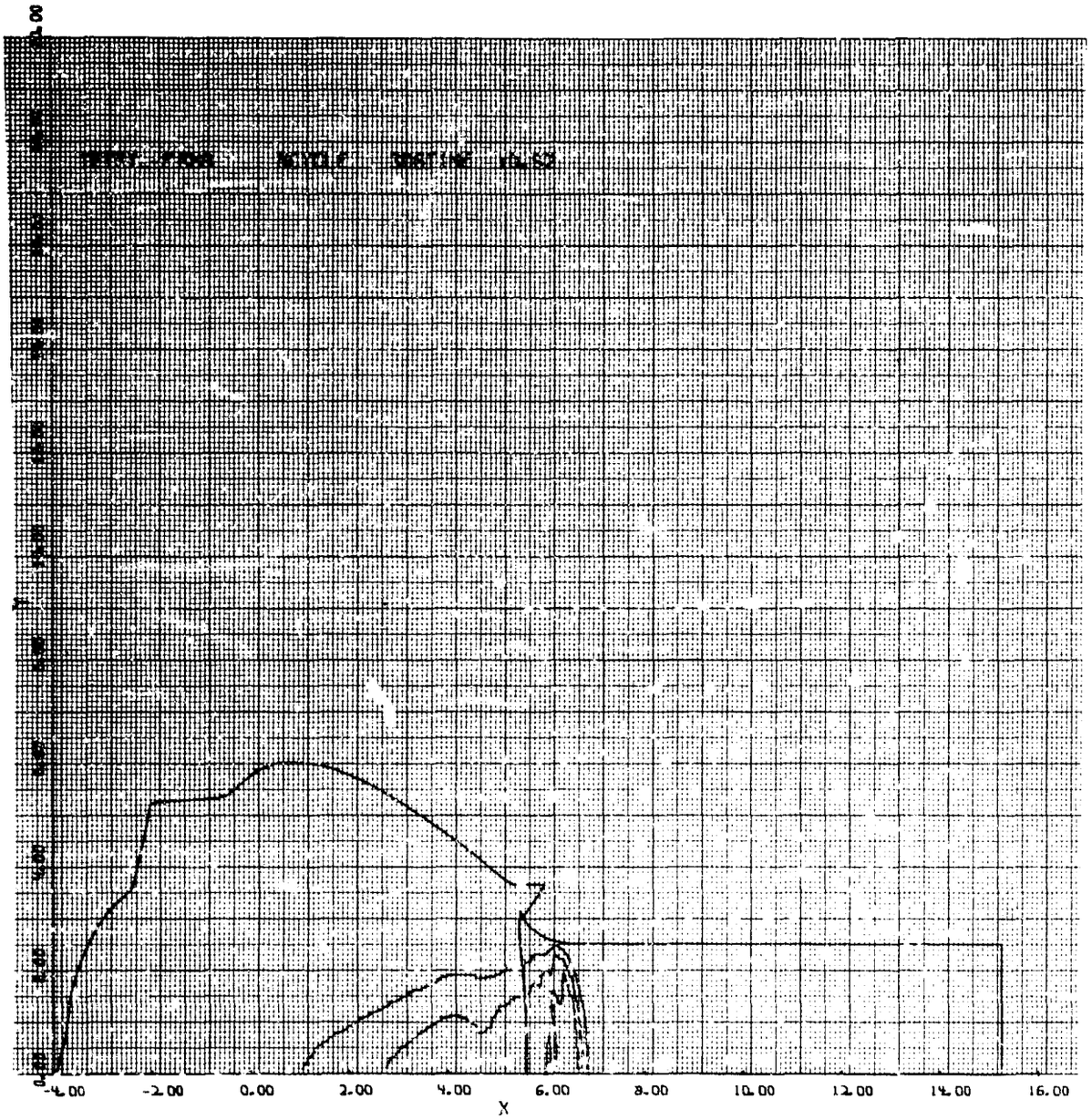

Figure A8(d)

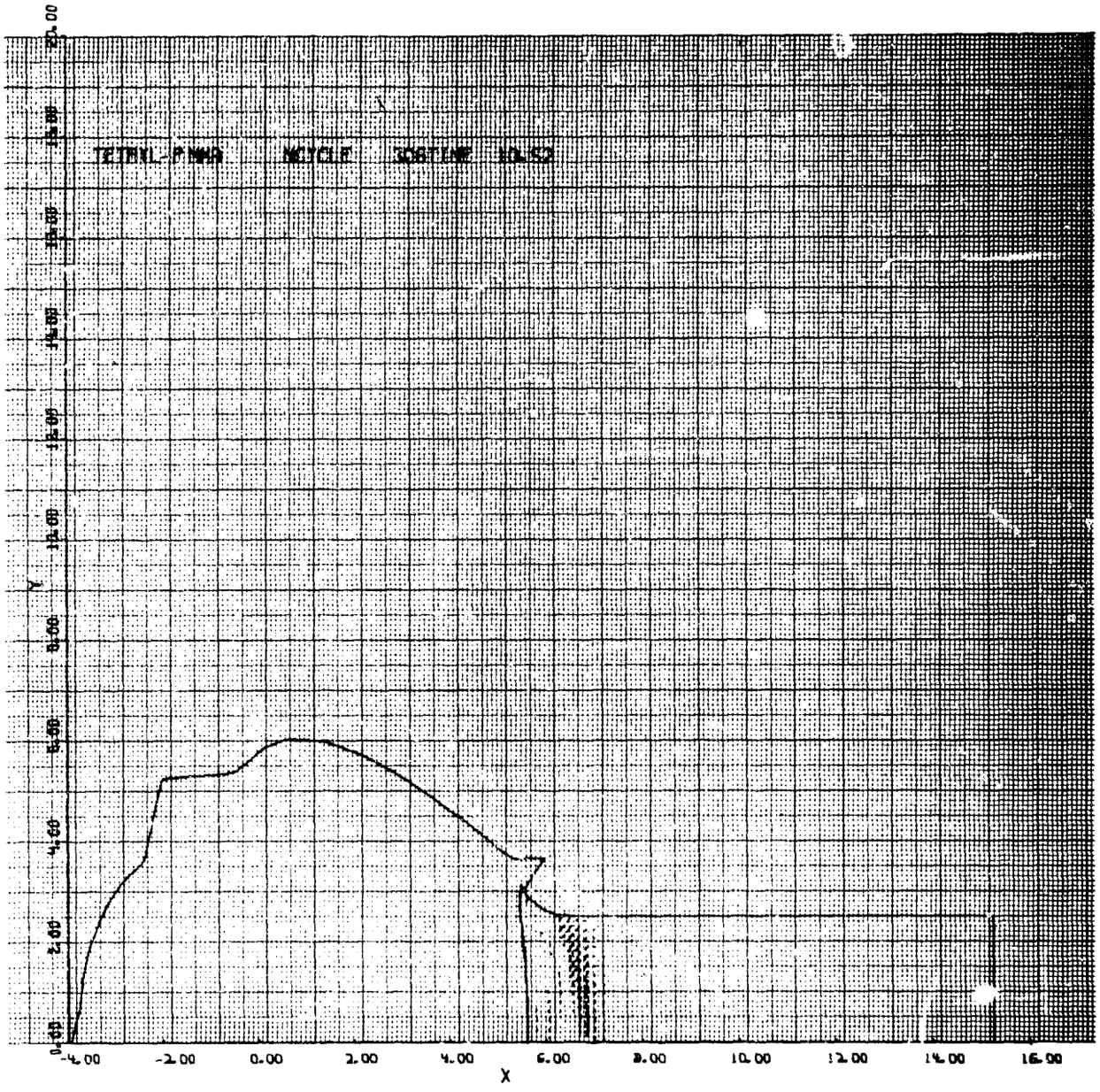
TETRYL-PMMA
METCLF
Y
X
-4.00
-2.00
0.00
2.00
4.00
6.00
8.00
10.00
12.00
14.00
16.00

Figure A8(e)

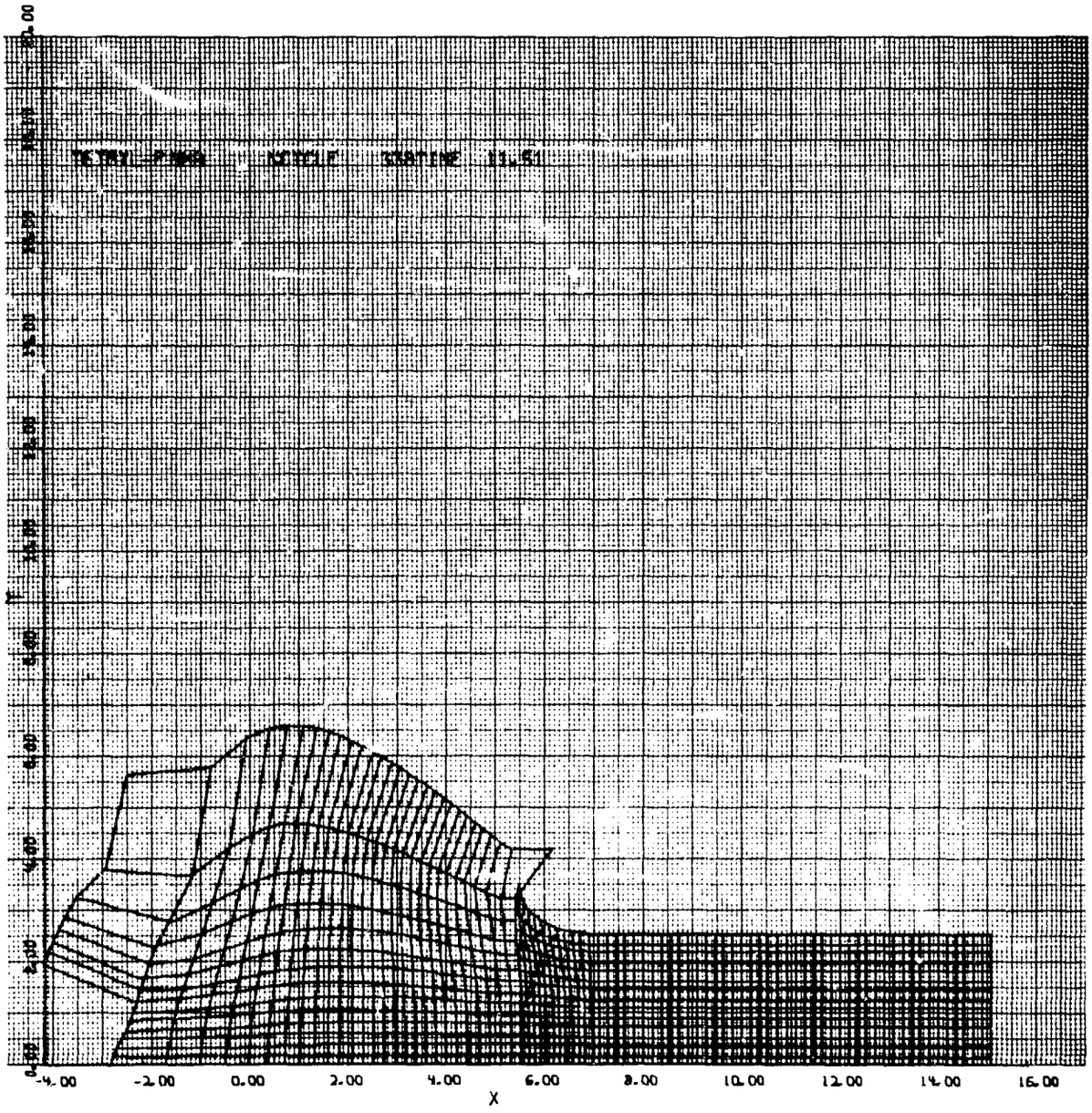

Figure A9(a)

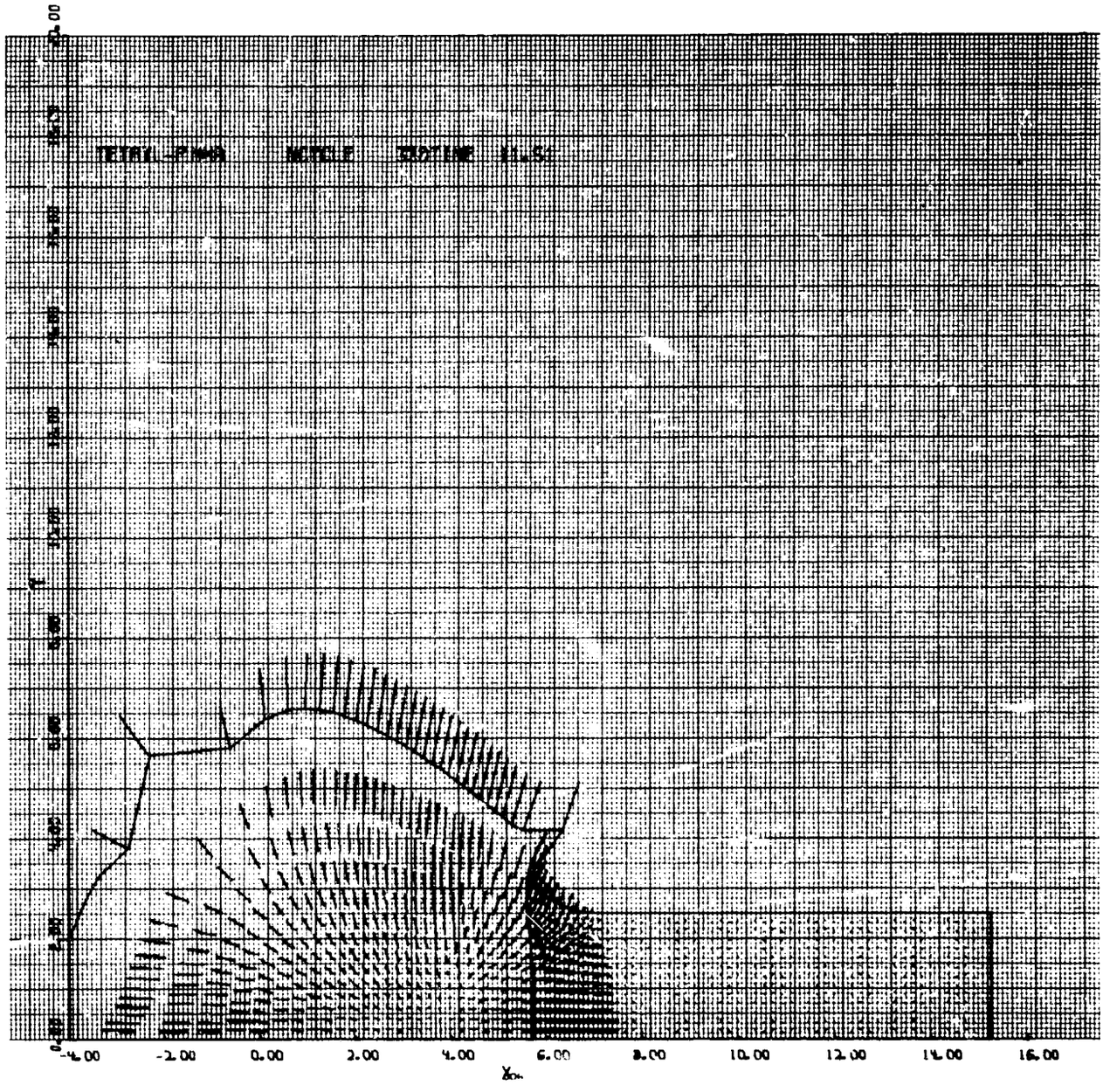

Figure A9(b)

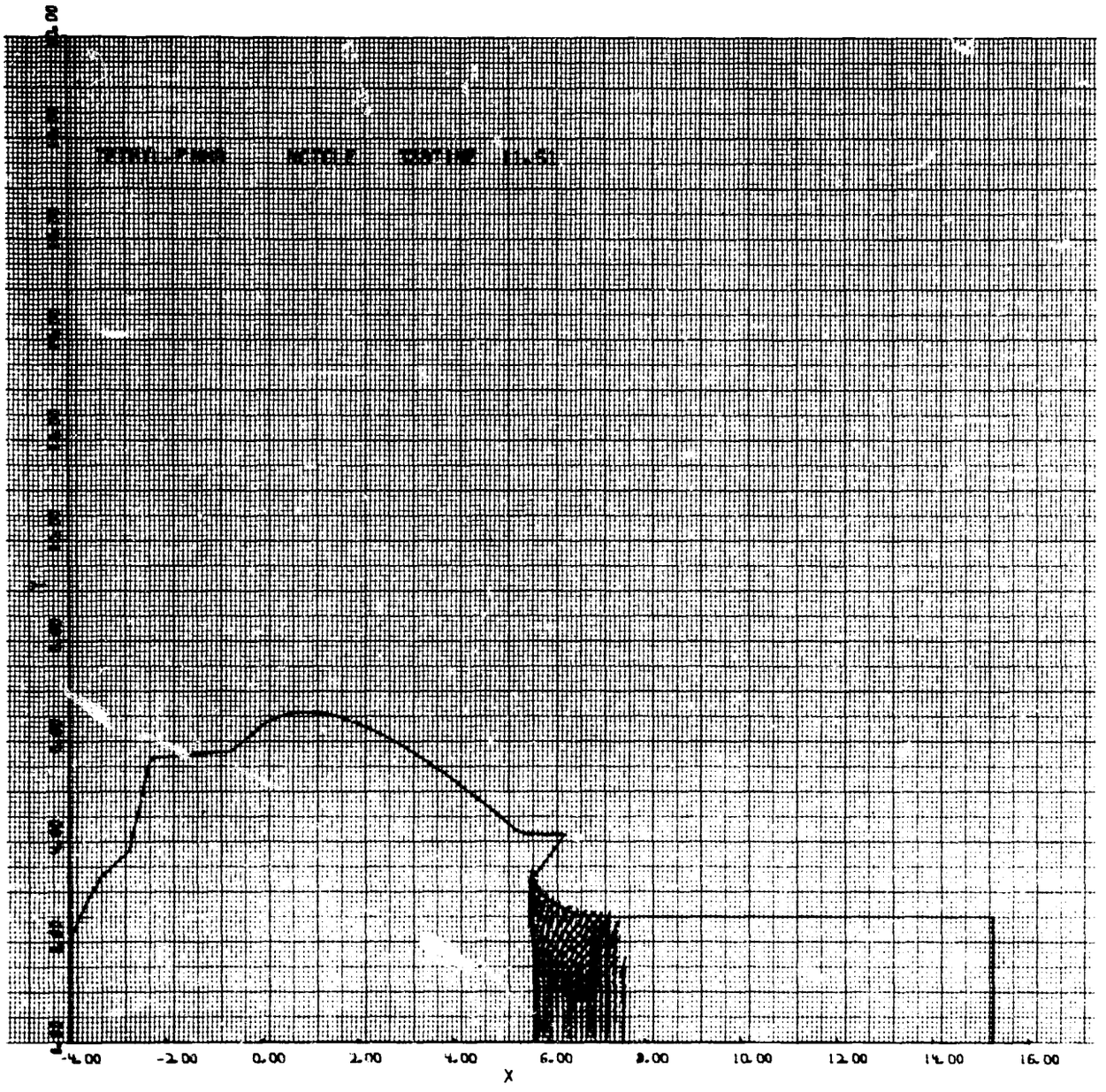

Figure A9(c)

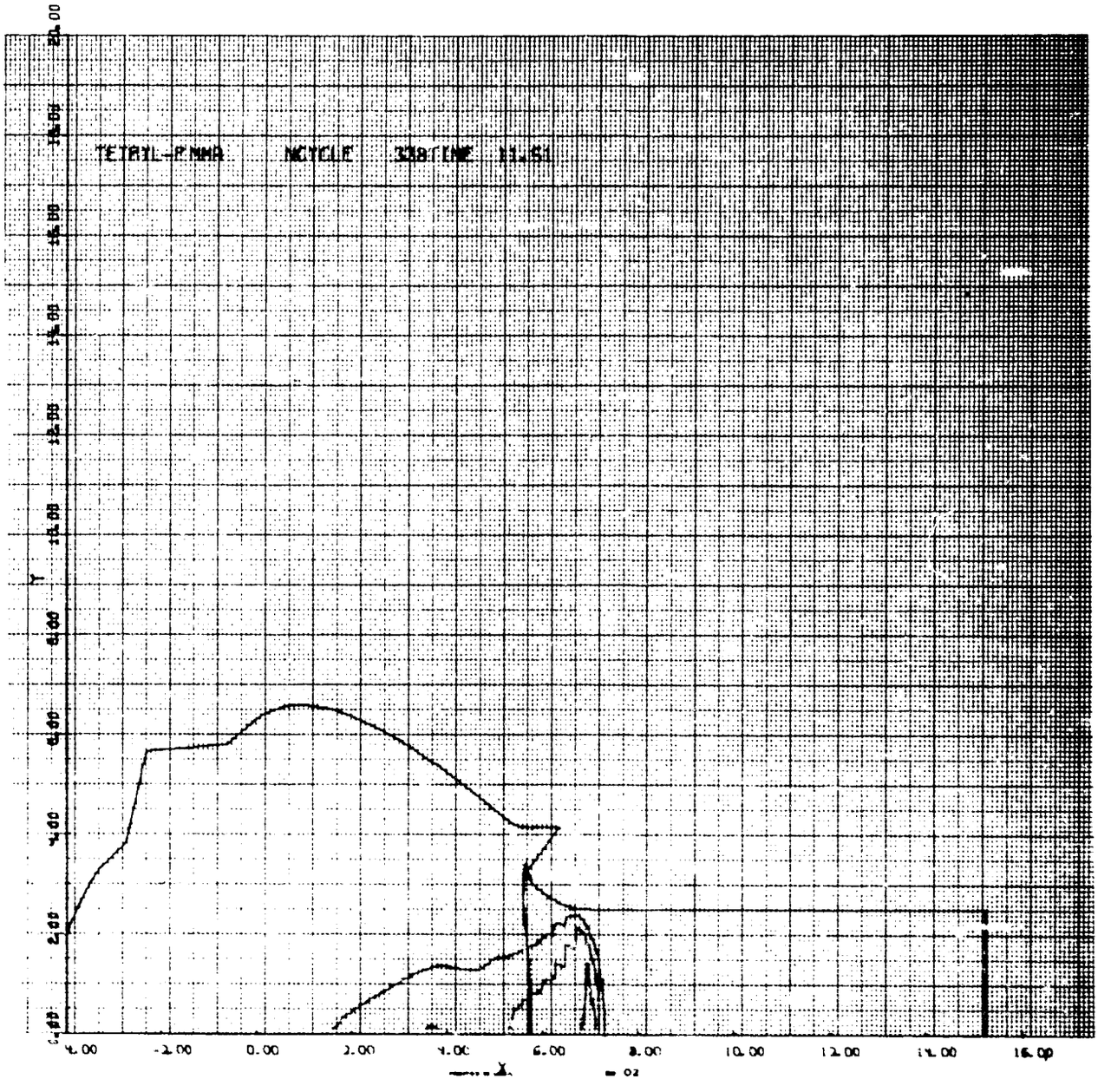

Figure A9(d)

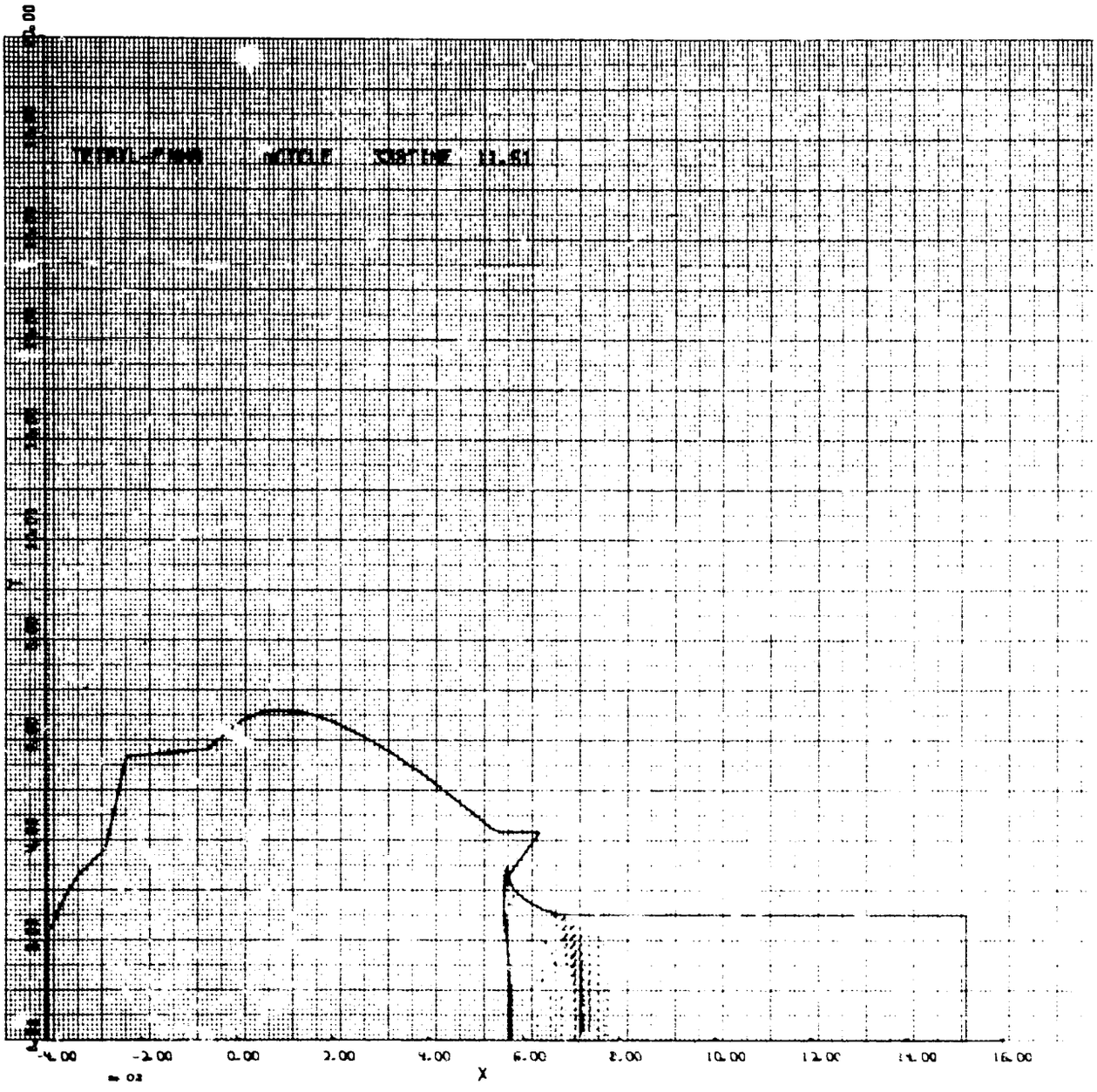

Figure A9(e)

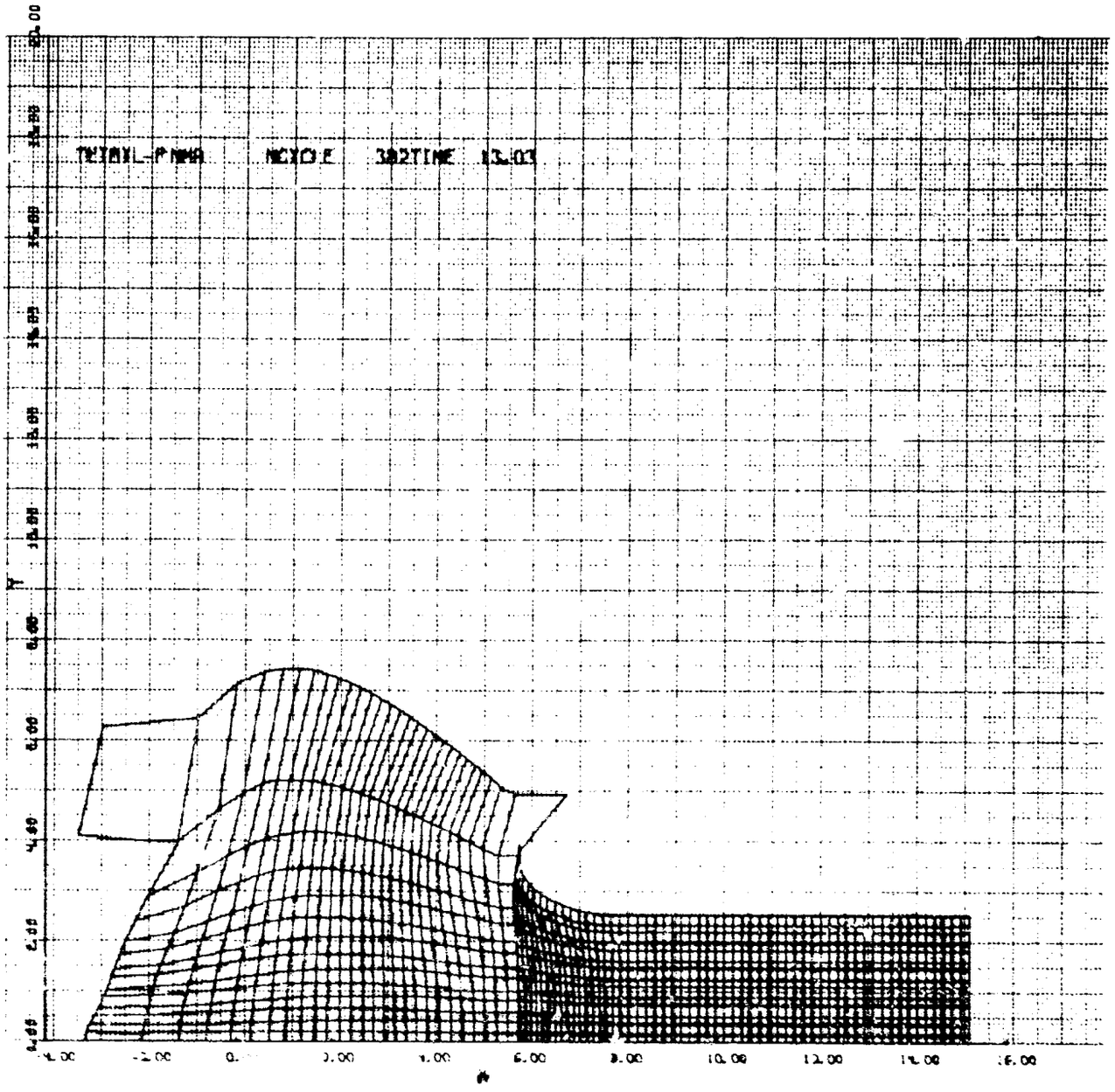

Figure A10(a)

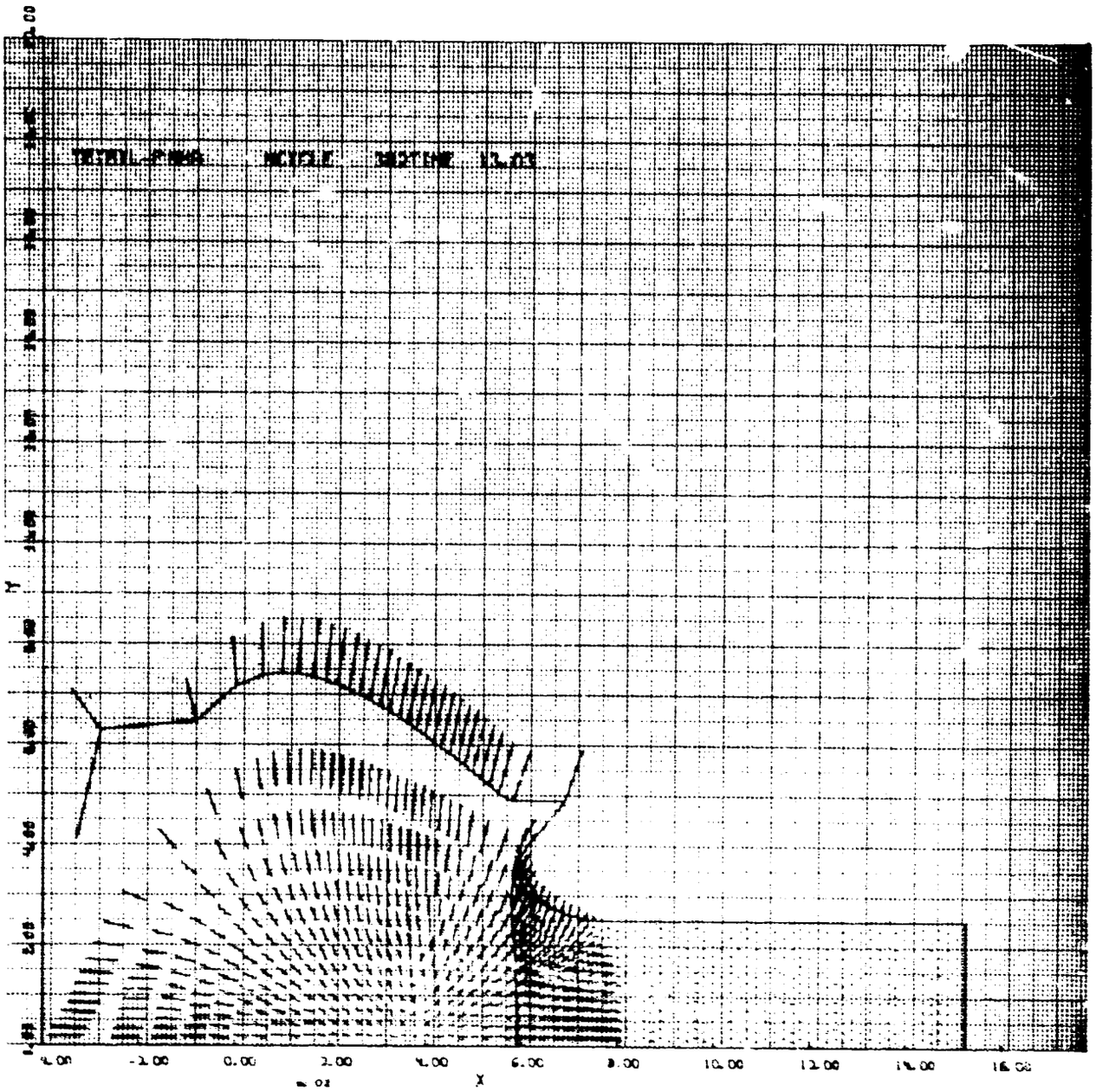

Figure A10(b)

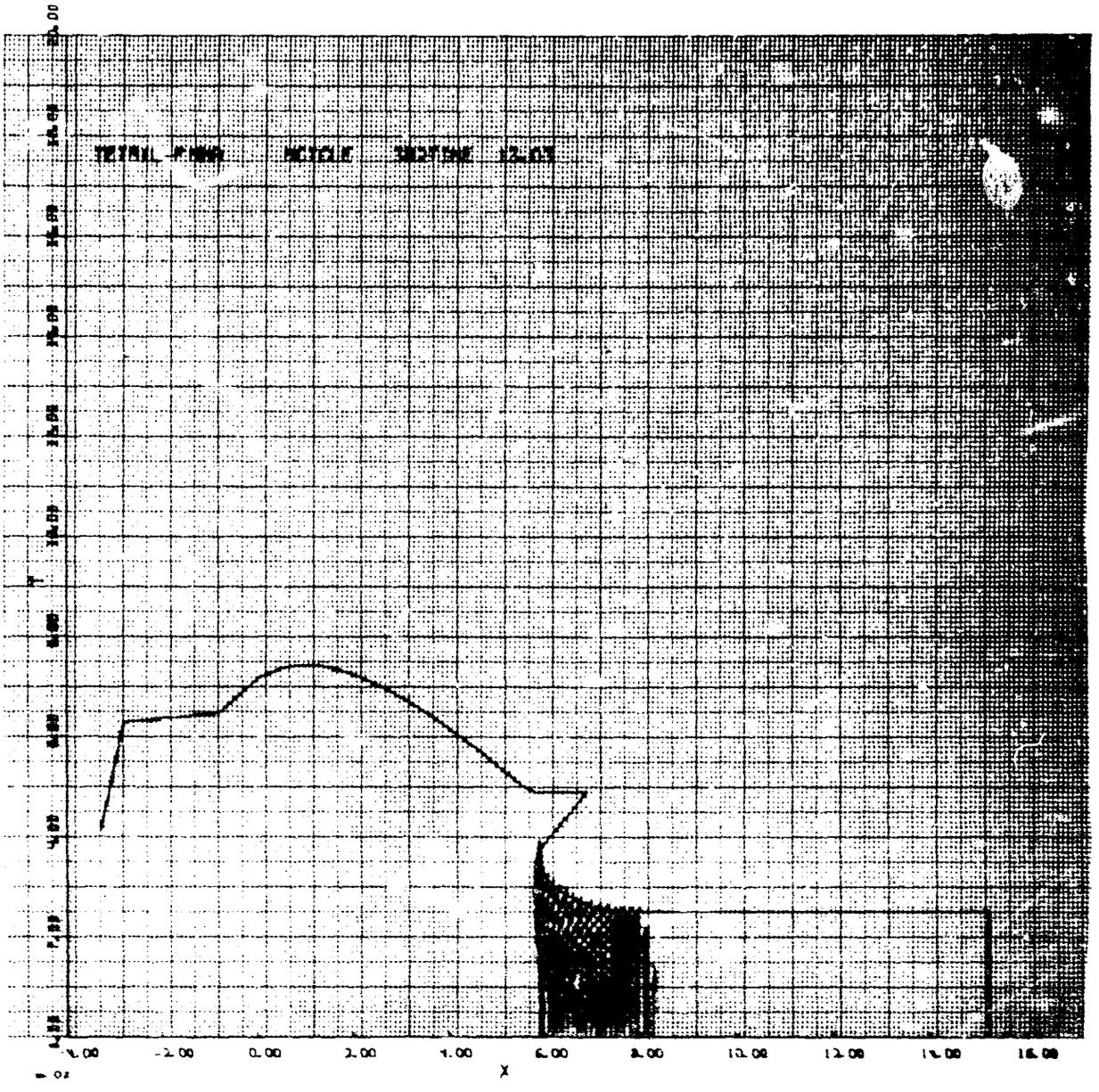

Figure A10(c)

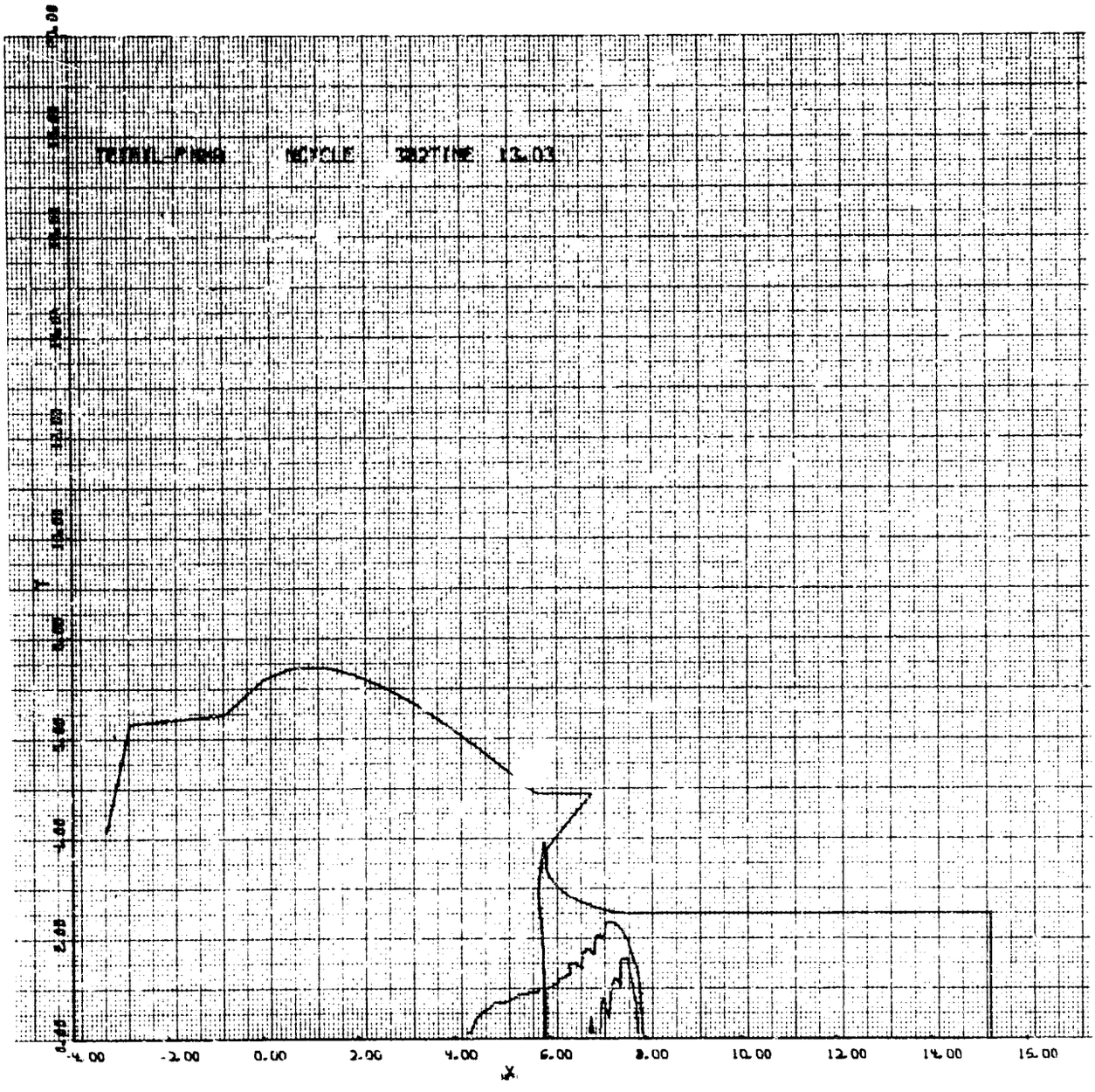

Figure A10(d)

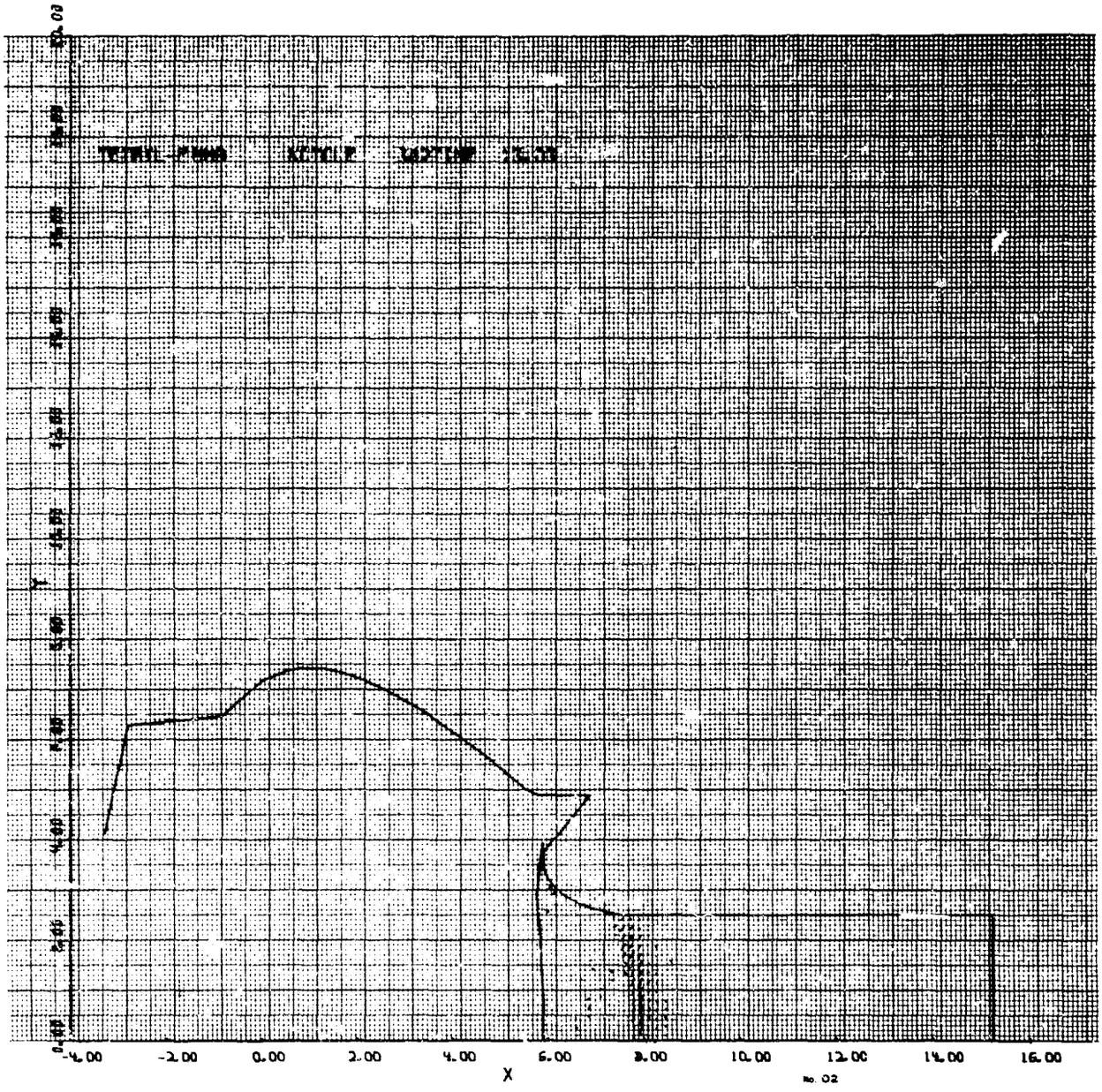

Figure A10(e)

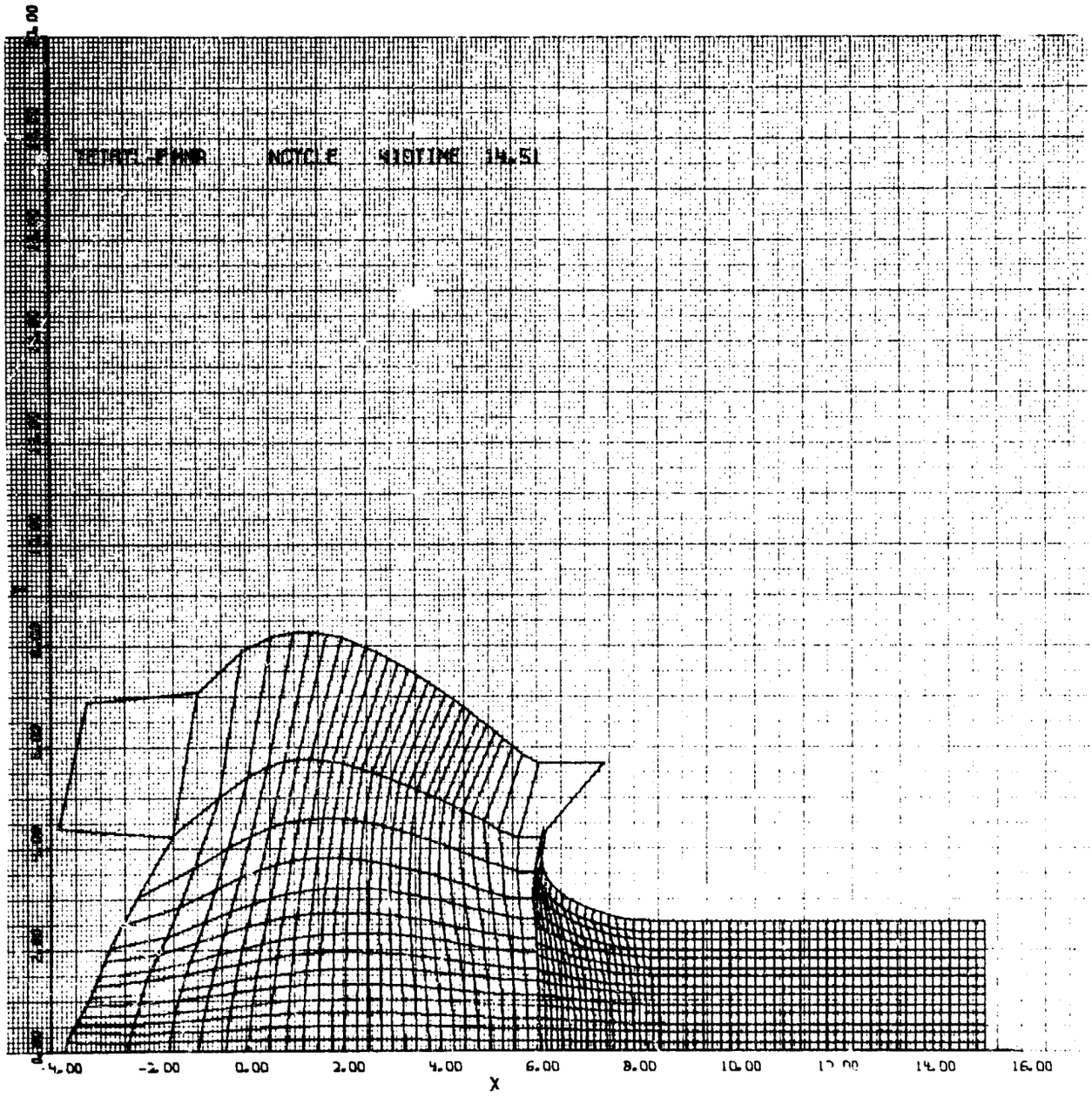

Figure A11(a)

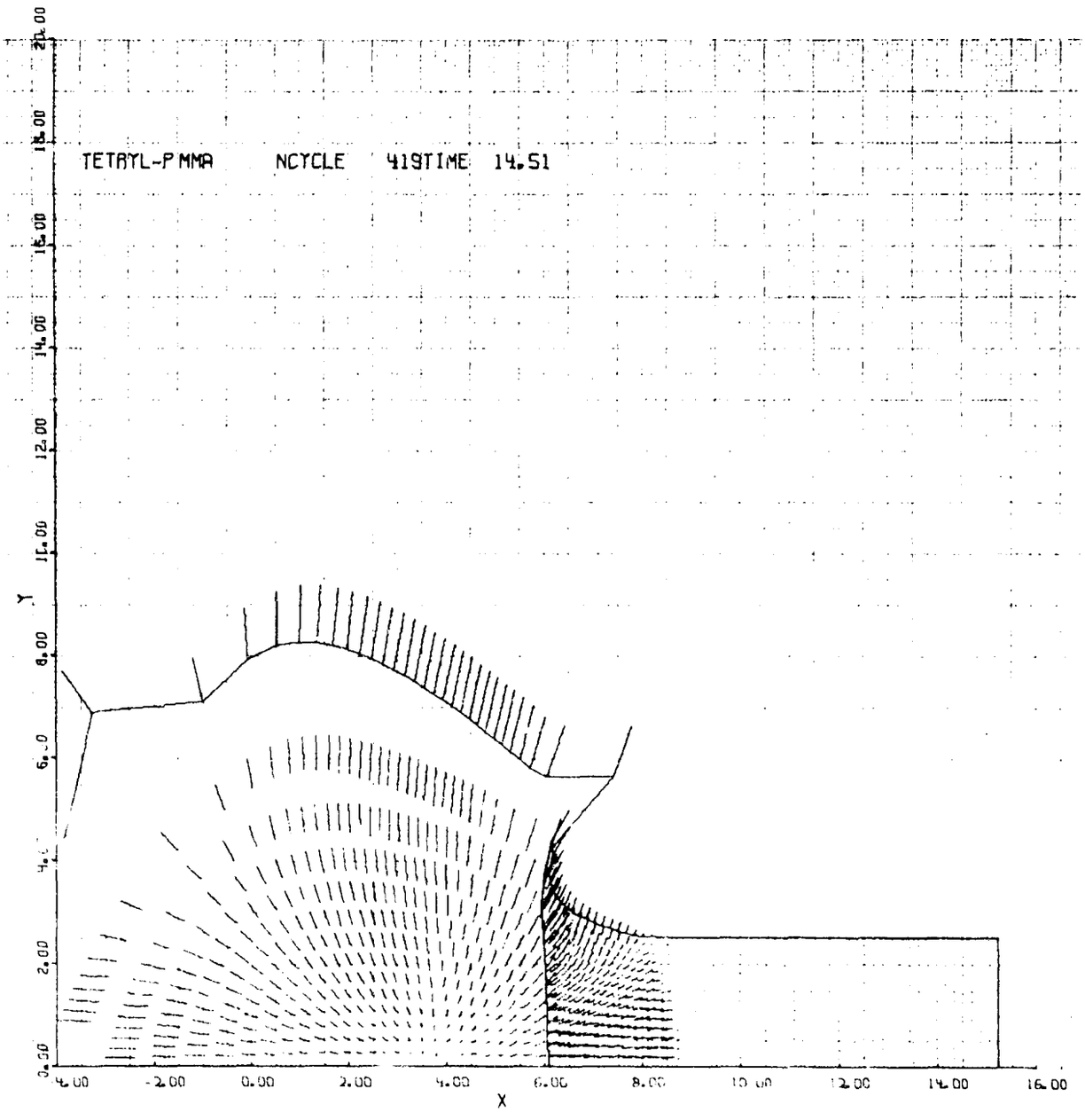
TETRYL-PMMA NCYCLE 419TIME 14.51
Y
X
-4.00
-2.00
0.00
2.00
4.00
6.00
8.00
10.00
12.00
14.00
16.00
2.00
8.00
12.00
14.00
16.00

Figure A11(b)

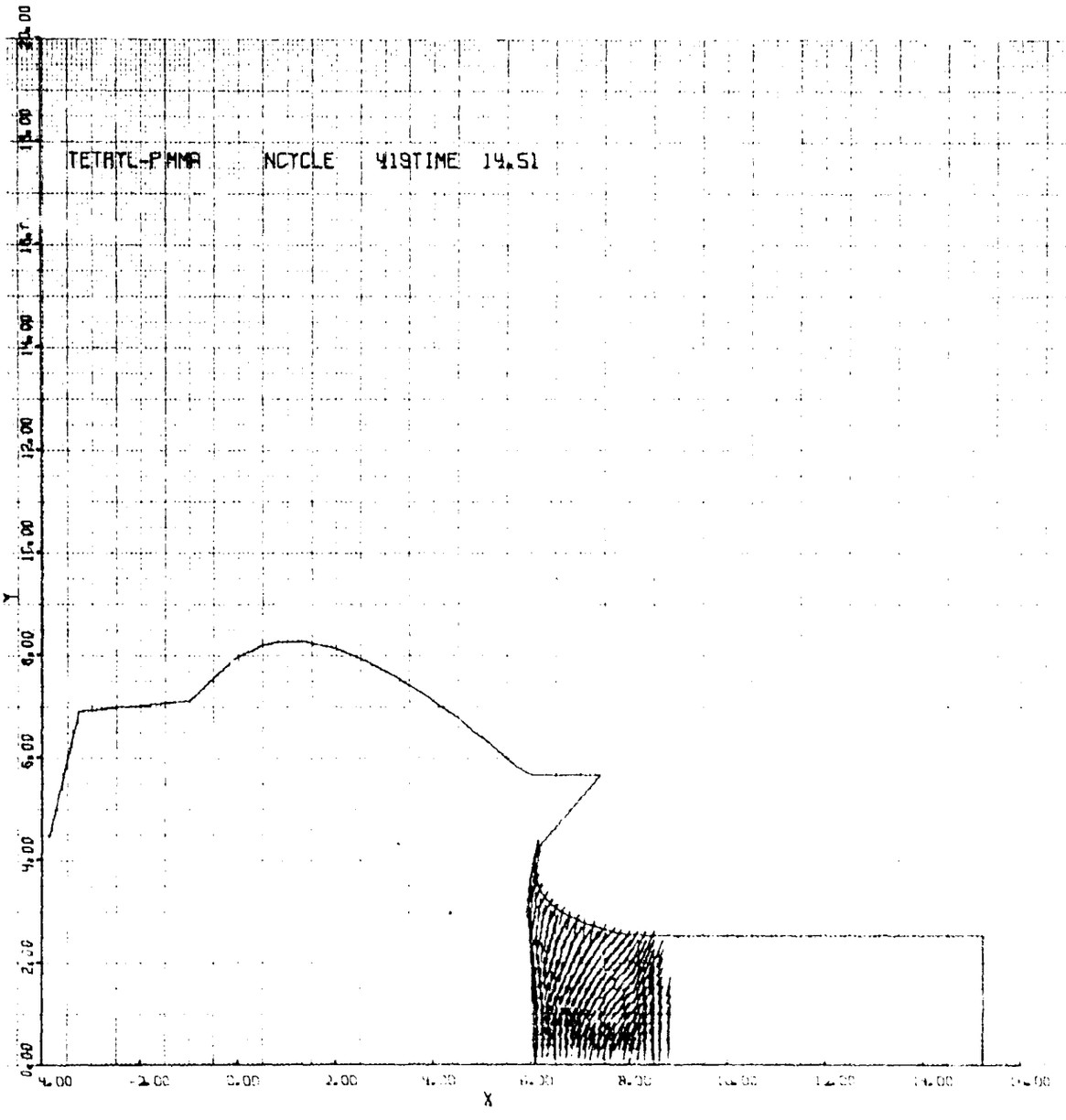
TETRYL-PMMA NCYCLE 419TIME 14.51
Y
X
4.00
-2.00
0.00
2.00
4.00
6.00
8.00
12.00
14.00
0.00
2.00
4.00
6.00
12.00
14.00
16.00
18.00
20.00

Figure A11(e)

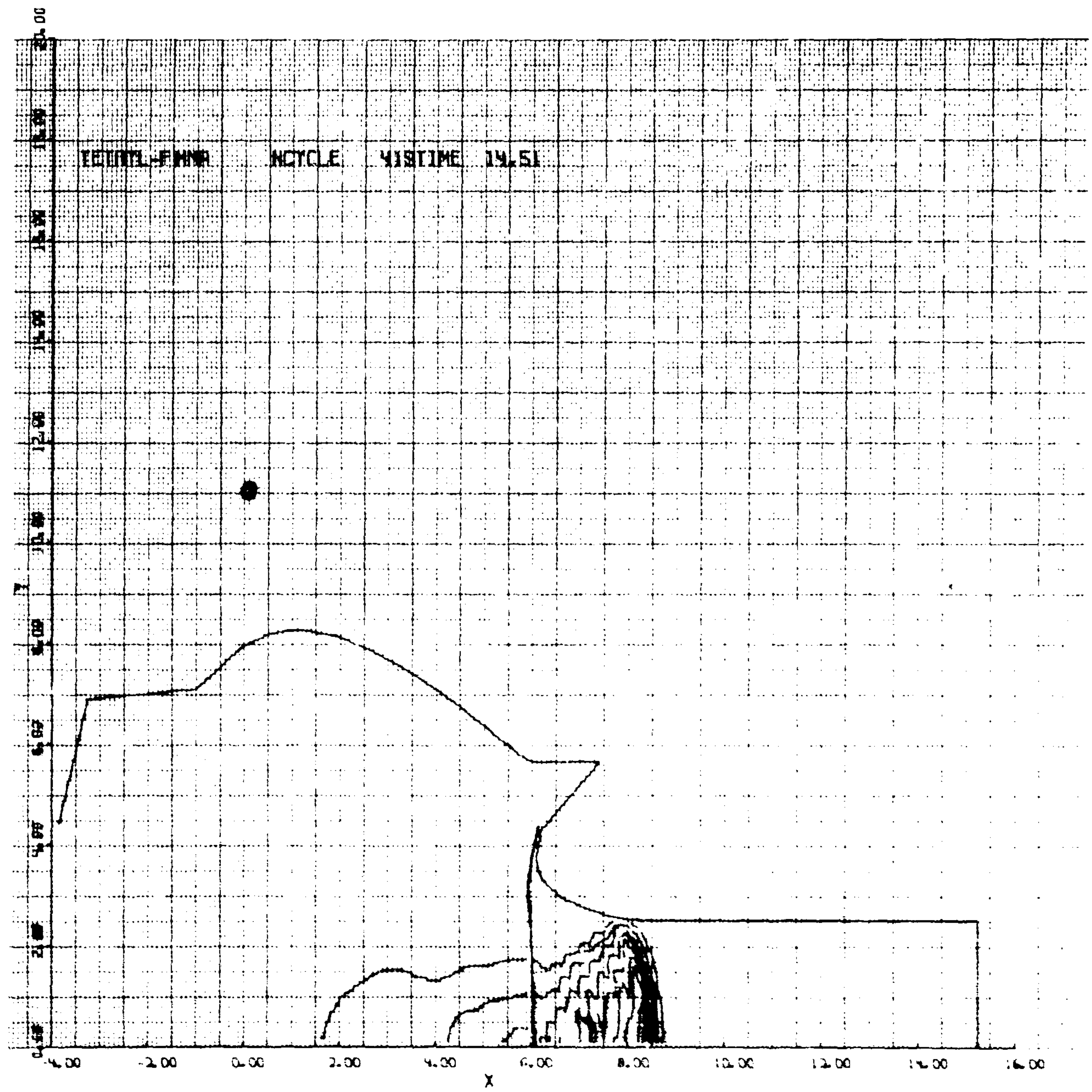
TETRYL-FHMA NCYCLE 41 STIME 14.51
X
Y
-4.00
-2.00
0.00
2.00
4.00
6.00
8.00
10.00
12.00
14.00
16.00

Figure A11(d)

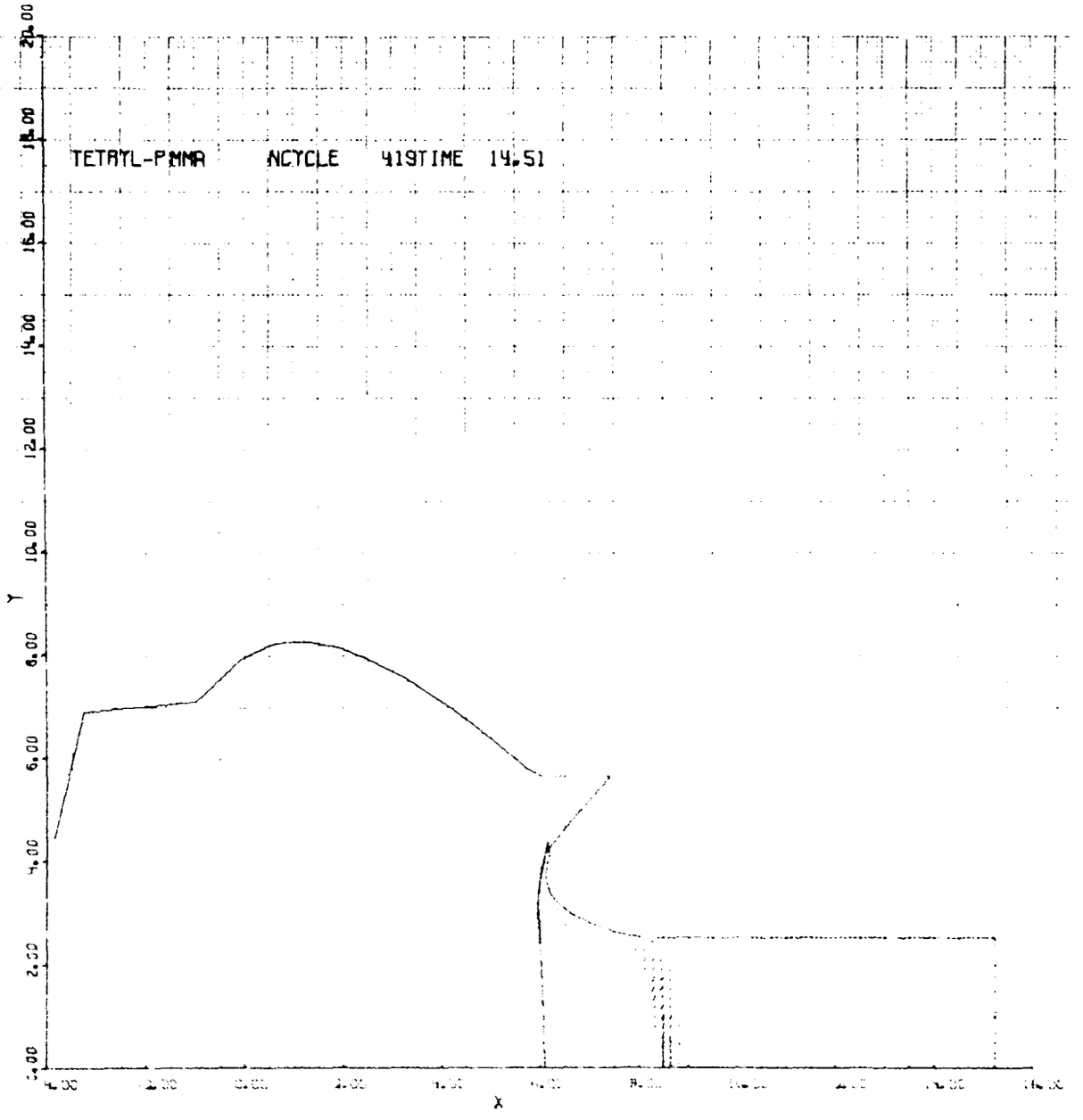

Figure A11(e)

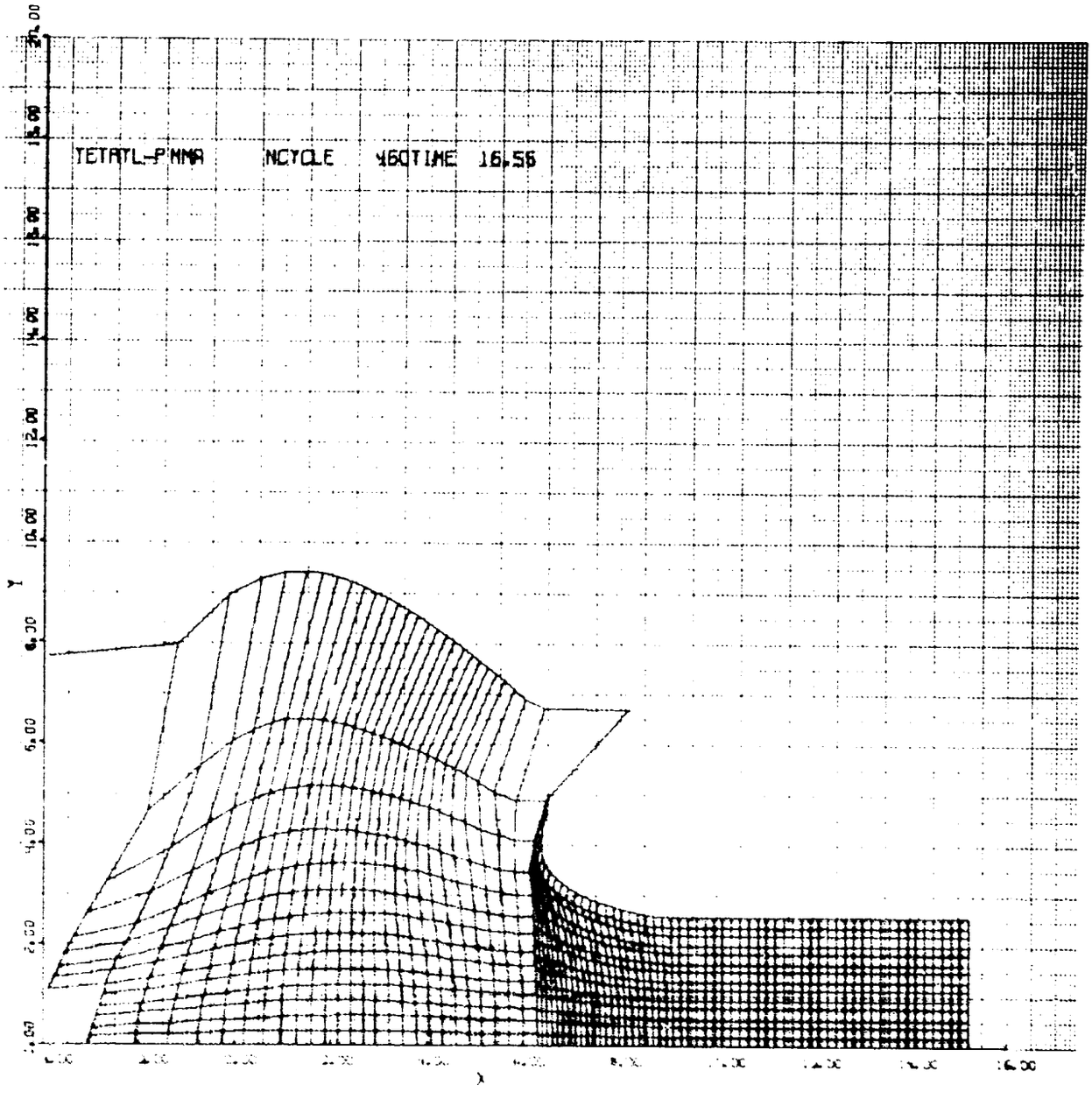

Figure A-20(c)

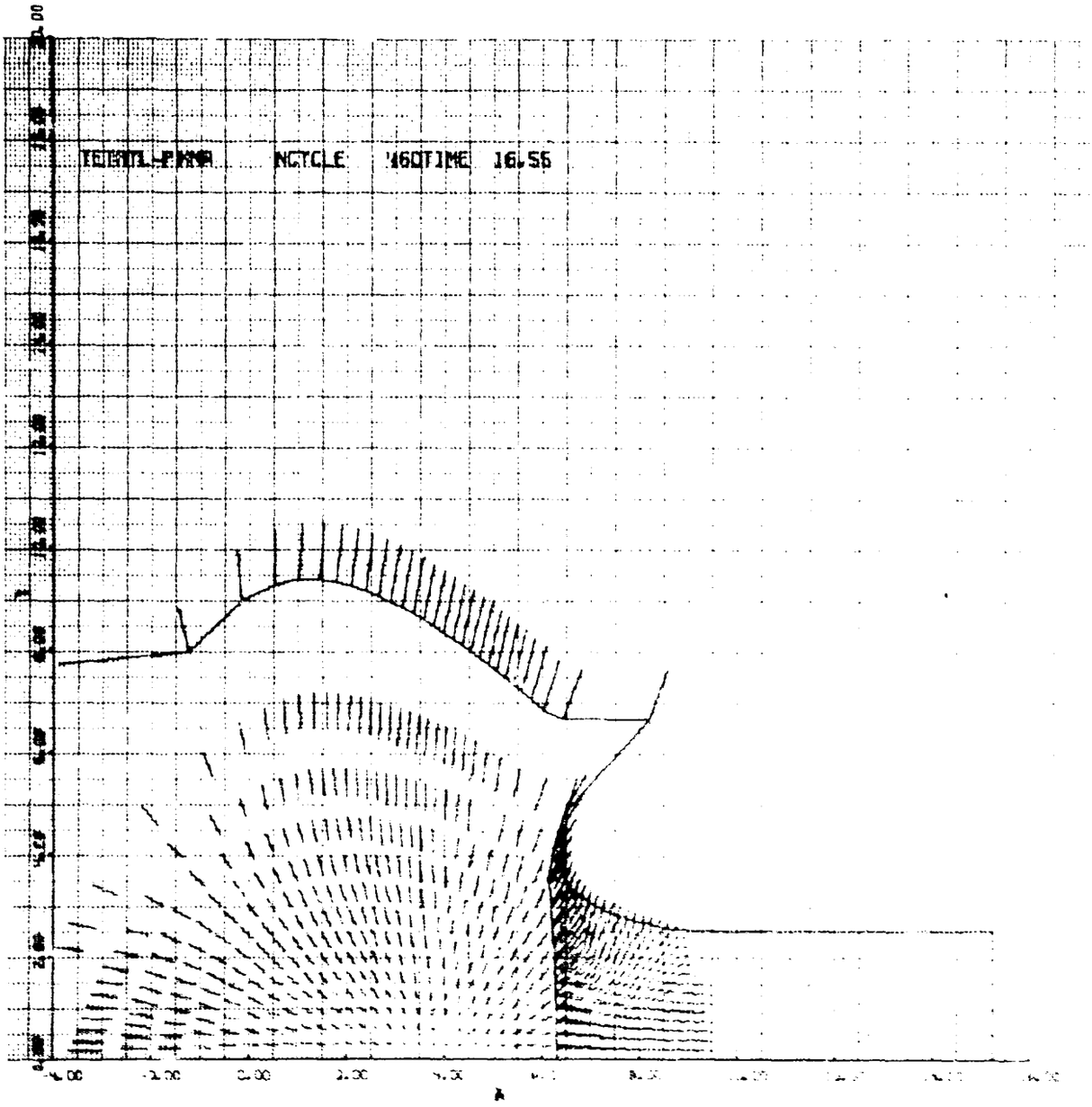

Figure A-26

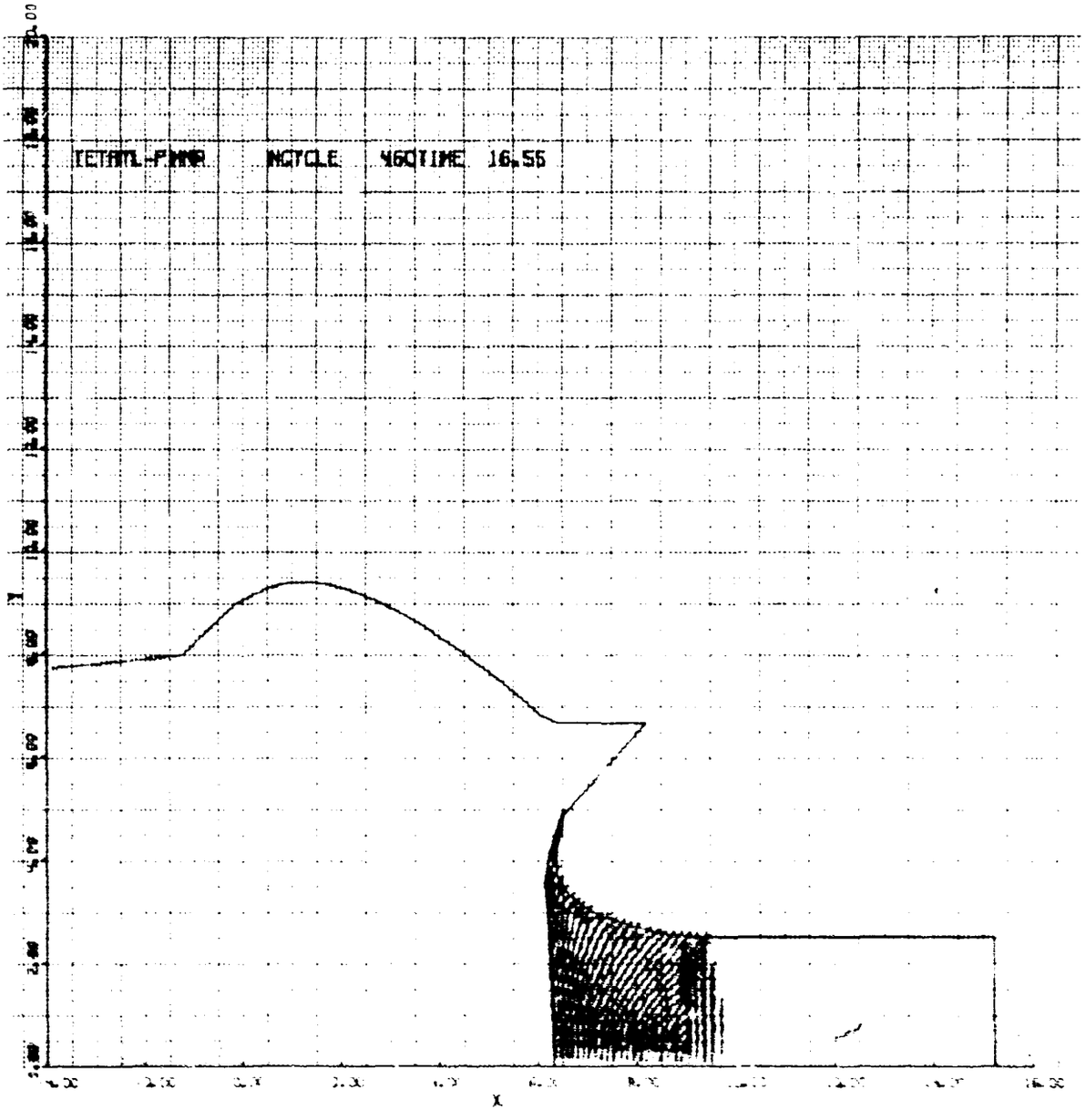
METAL-FLOW
NCYCLE 460TIME 16.56
Y
X

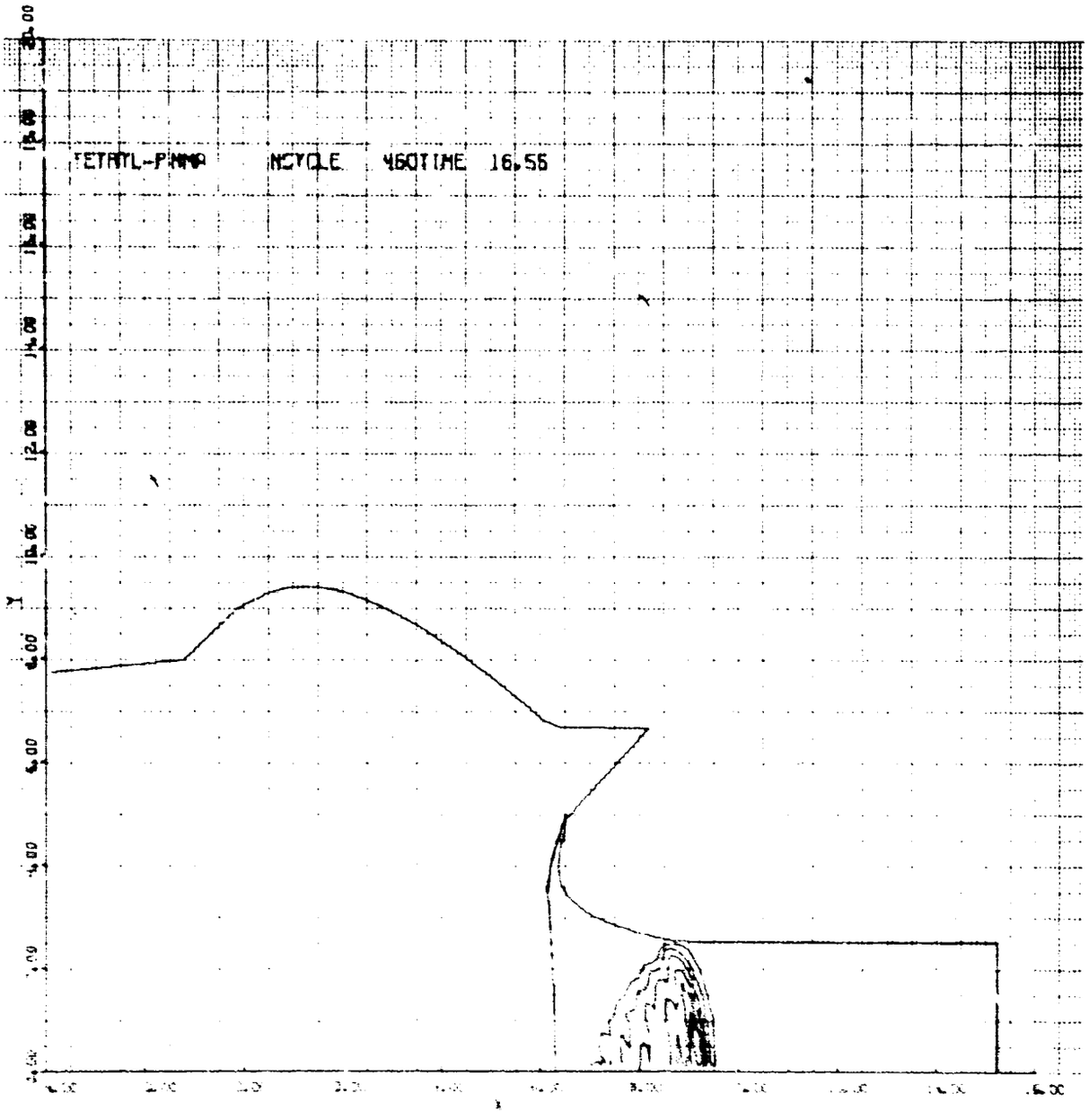
TETRTL-P
NCYCLE 460TIME 16.56

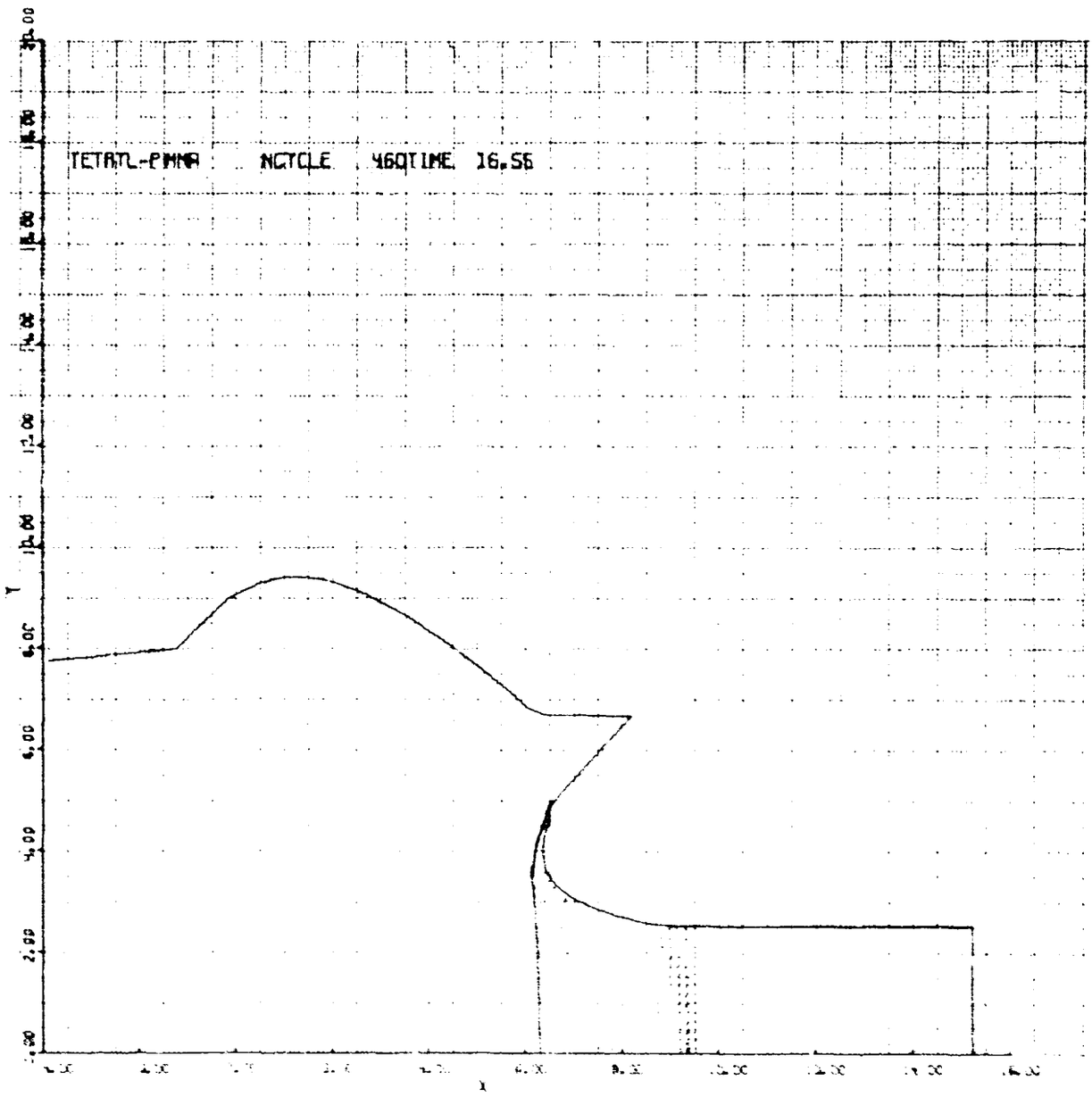

Figure [illegible]

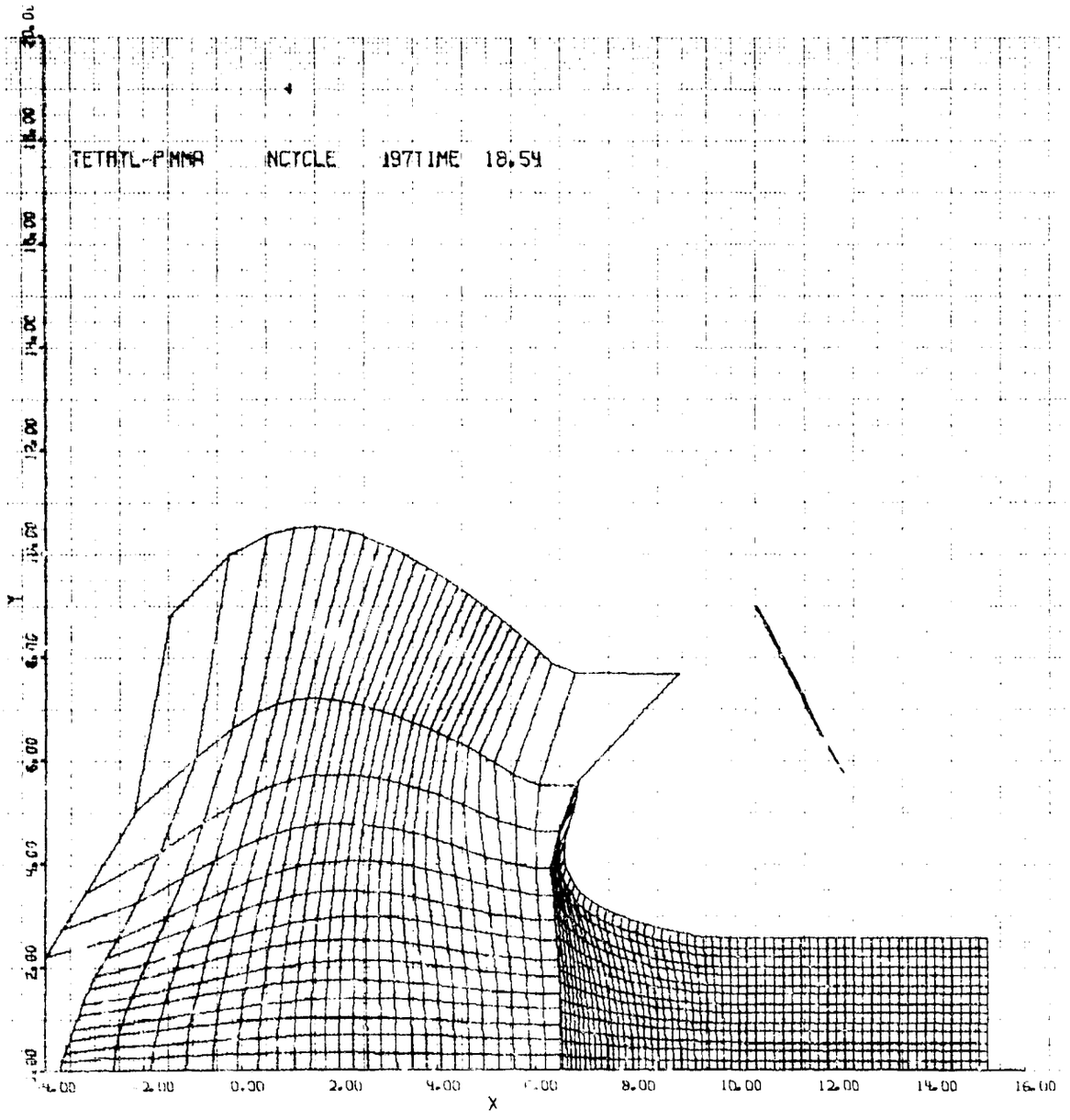
TETRTL-PMMA NCYCLE 197TIME 18.54
Y
X
2.00
0.00
2.00
4.00
8.00
10.00
12.00
14.00
16.00

Figure A13(a)

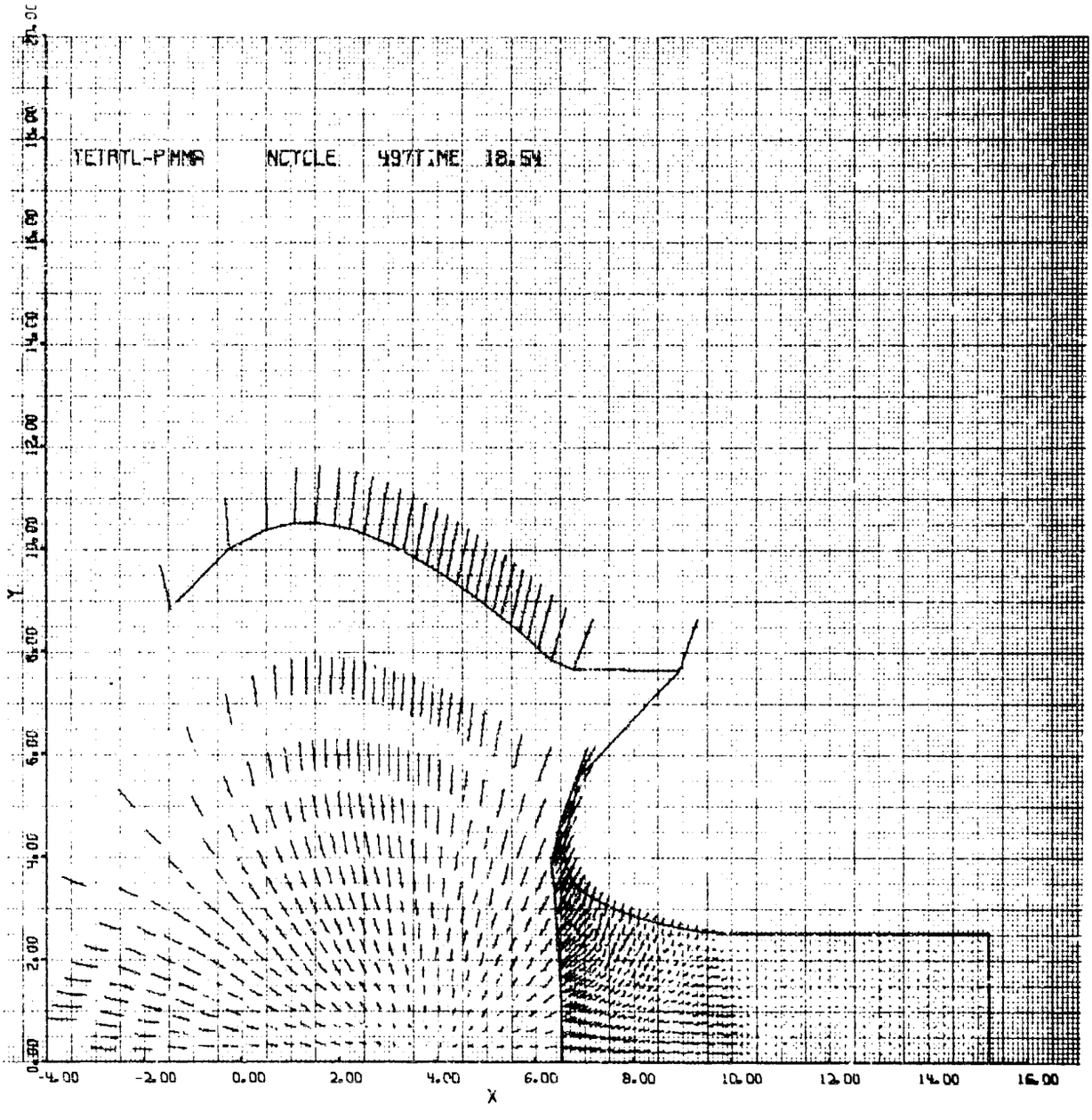
TETRTL-PMMA NCYCLE 497TIME 18.54
Y
X
-4.00
-2.00
0.00
2.00
4.00
6.00
8.00
10.00
12.00
14.00
16.00

Figure A13(b)

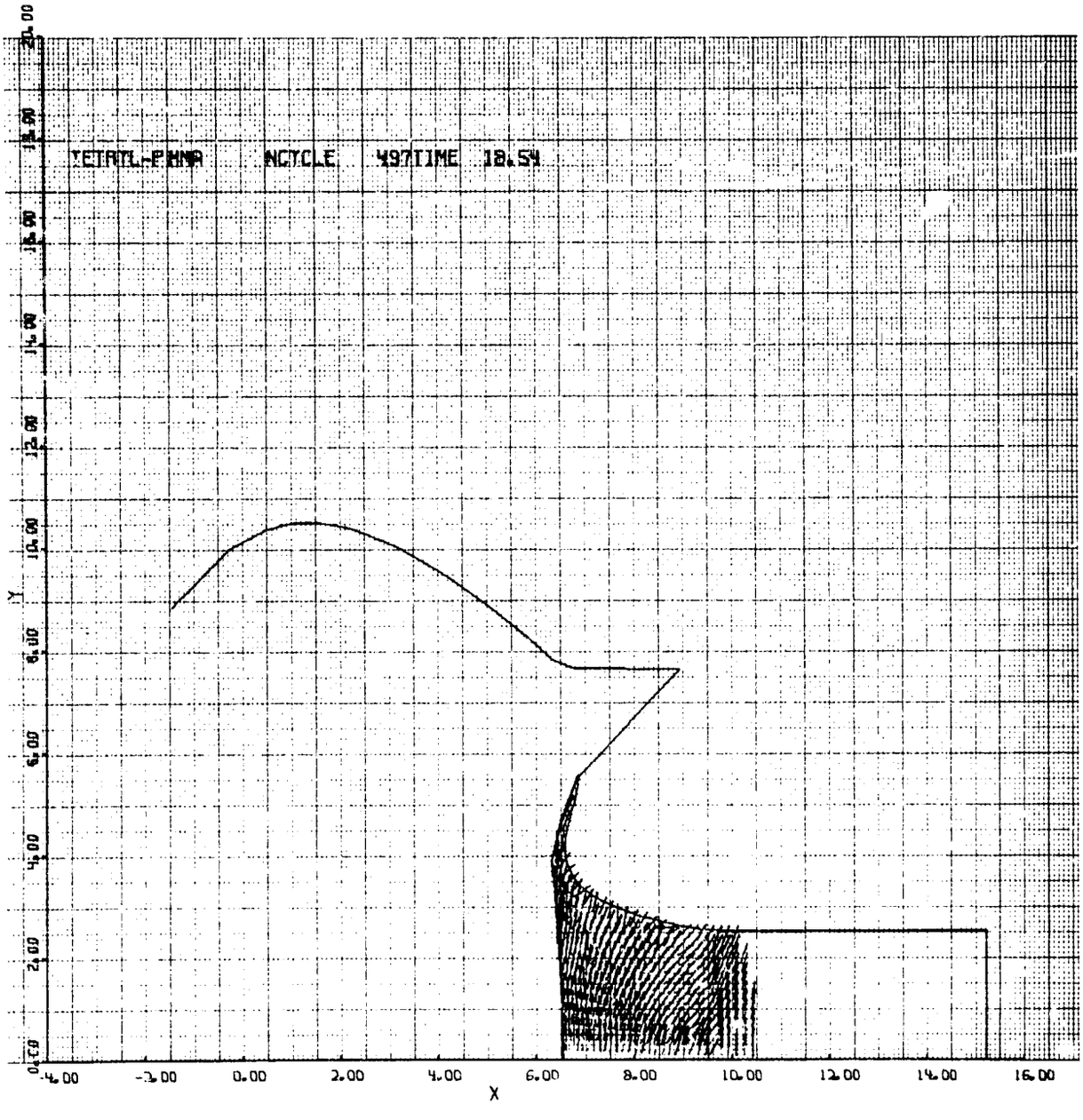
TETRTL-P HMA NCYCLE 497TIME 18.54
Y
X
-4.00
-2.00
0.00
2.00
4.00
6.00
8.00
10.00
12.00
14.00
16.00
2.00
4.00
6.00
8.00
10.00
12.00
14.00
16.00
18.00
20.00

Figure A15(c)

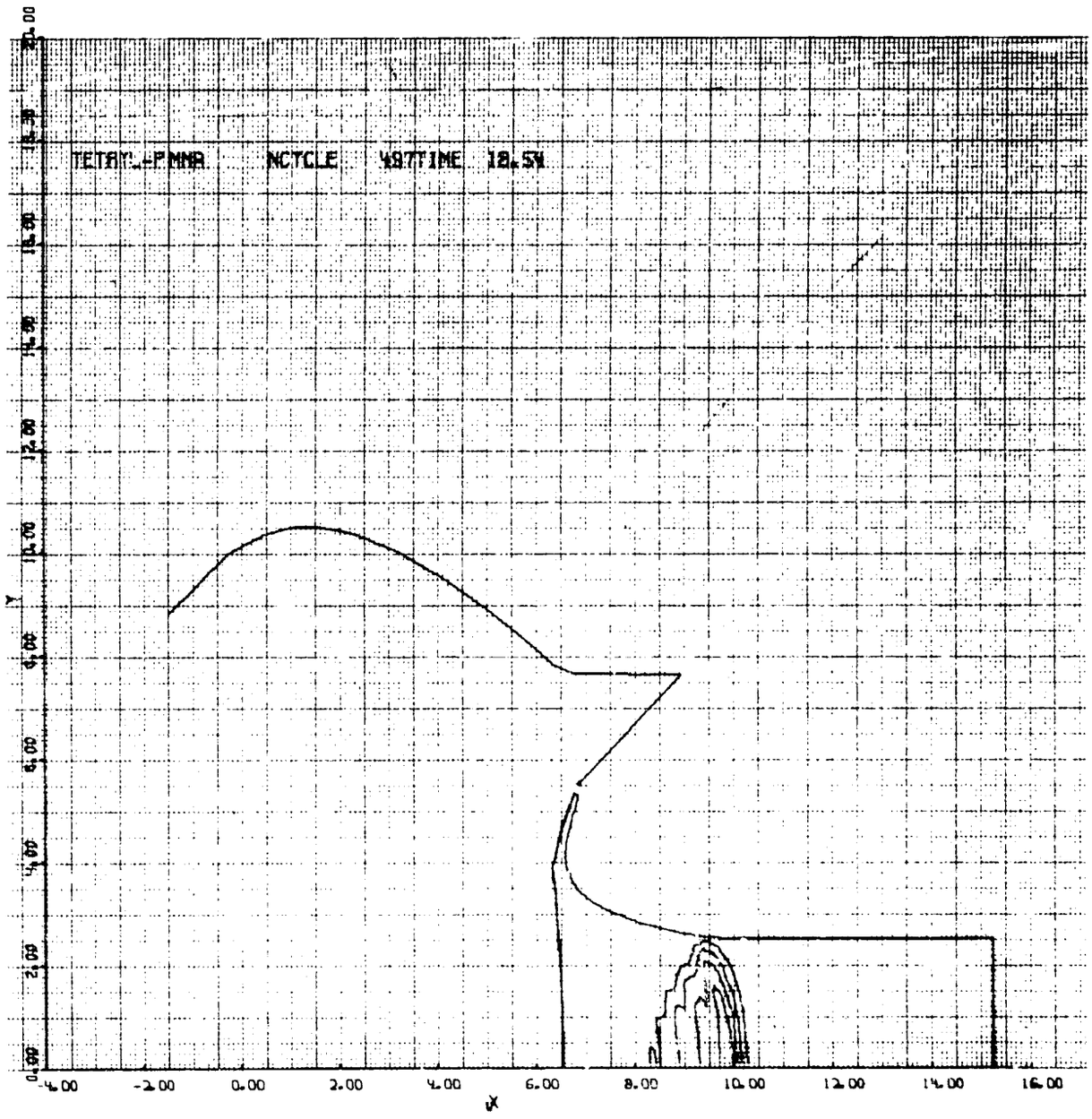
TETRA-PMNR
NCYCLE 497TIME 18.54
-6.00
-2.00
0.00
2.00
4.00
6.00
8.00
10.00
12.00
14.00
16.00
X

Figure A13(d)

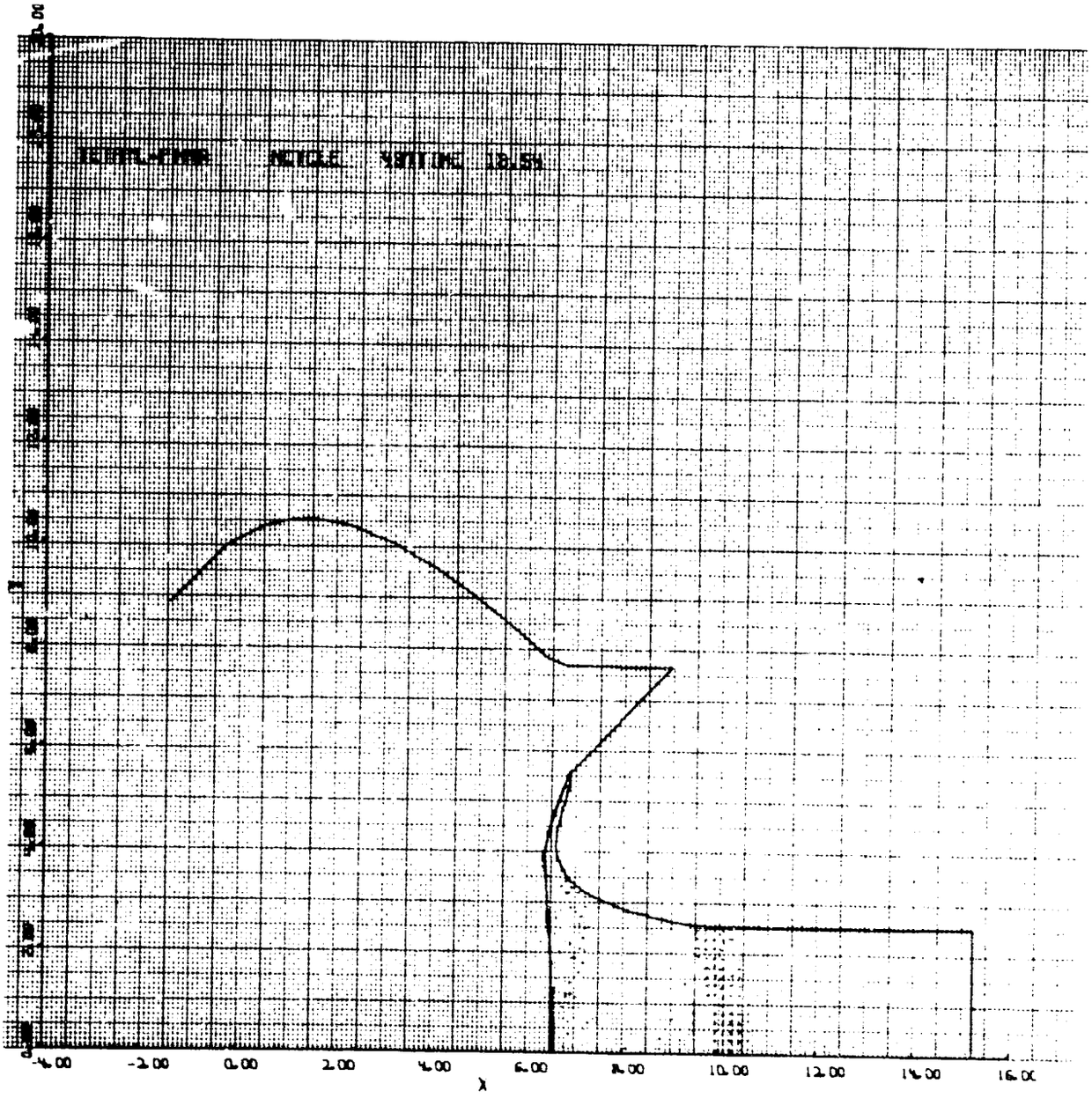

Figure A13(c)

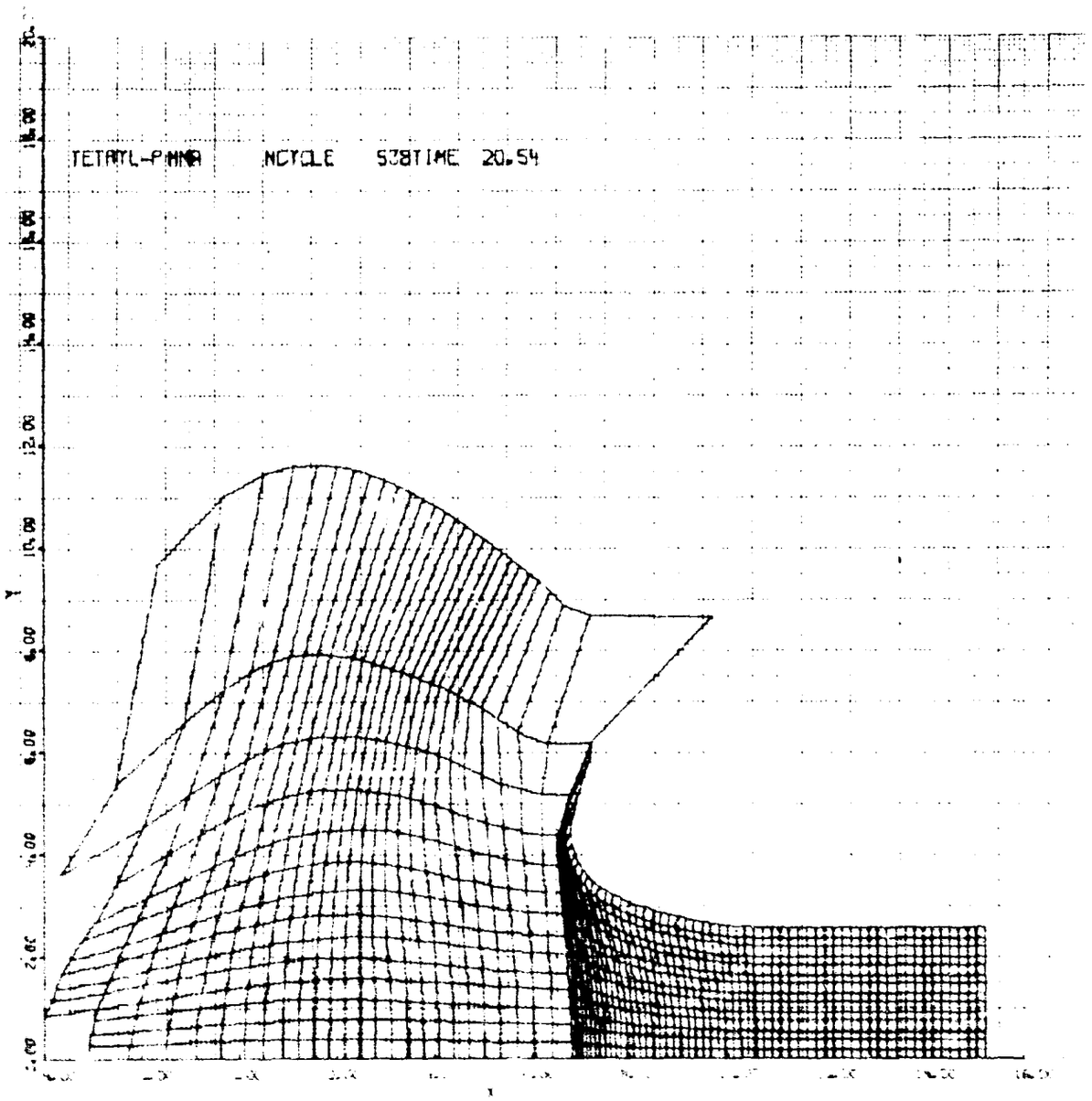
TETRYL-PMMA
NCYCLE 538TIME 20.54
Y
X

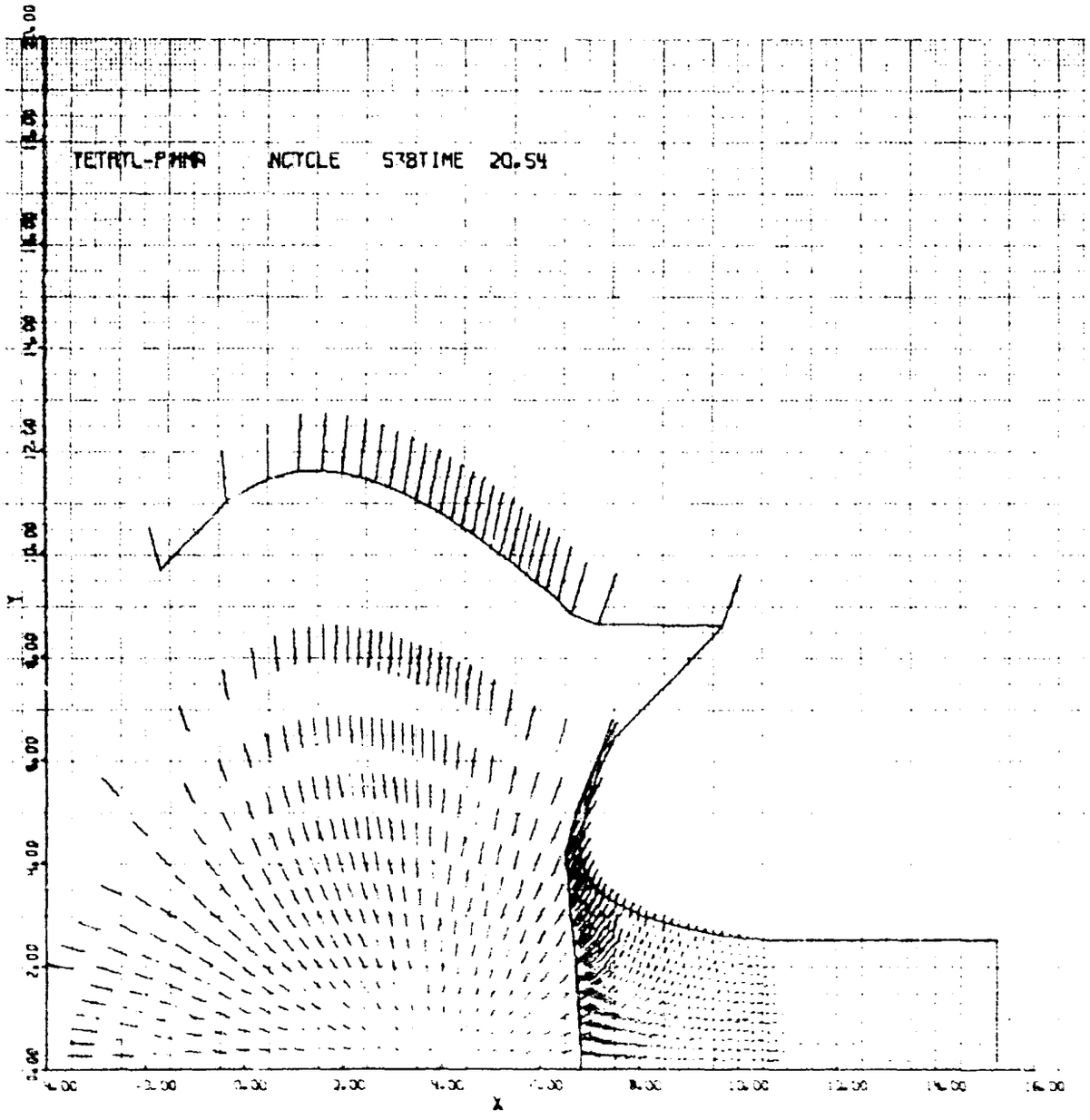

Figure A14(b)

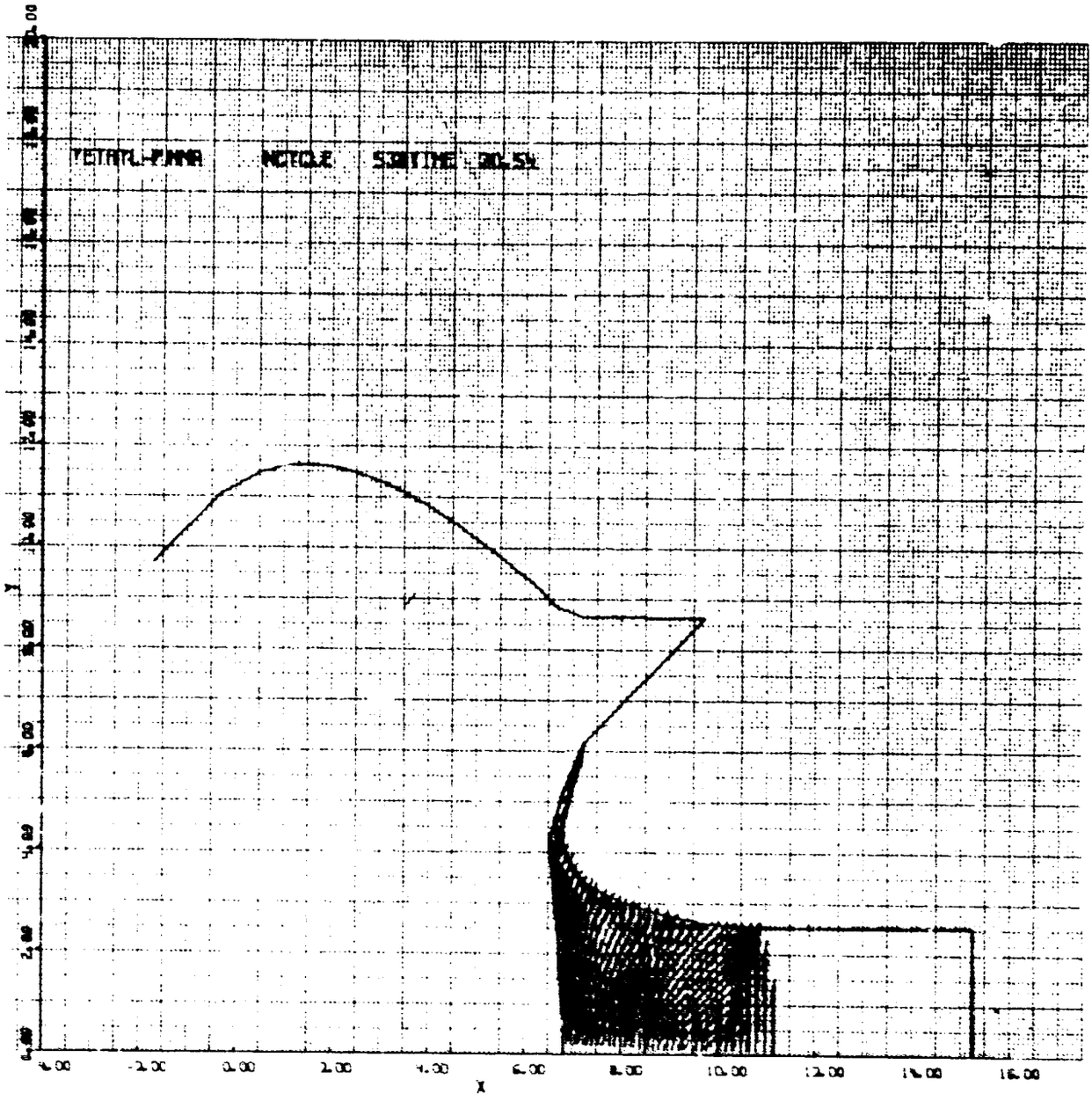
TETRYL-PMMA
NITROLE
-4.00
-2.00
0.00
2.00
4.00
6.00
8.00
10.00
12.00
14.00
16.00
X

Figure A14(c)

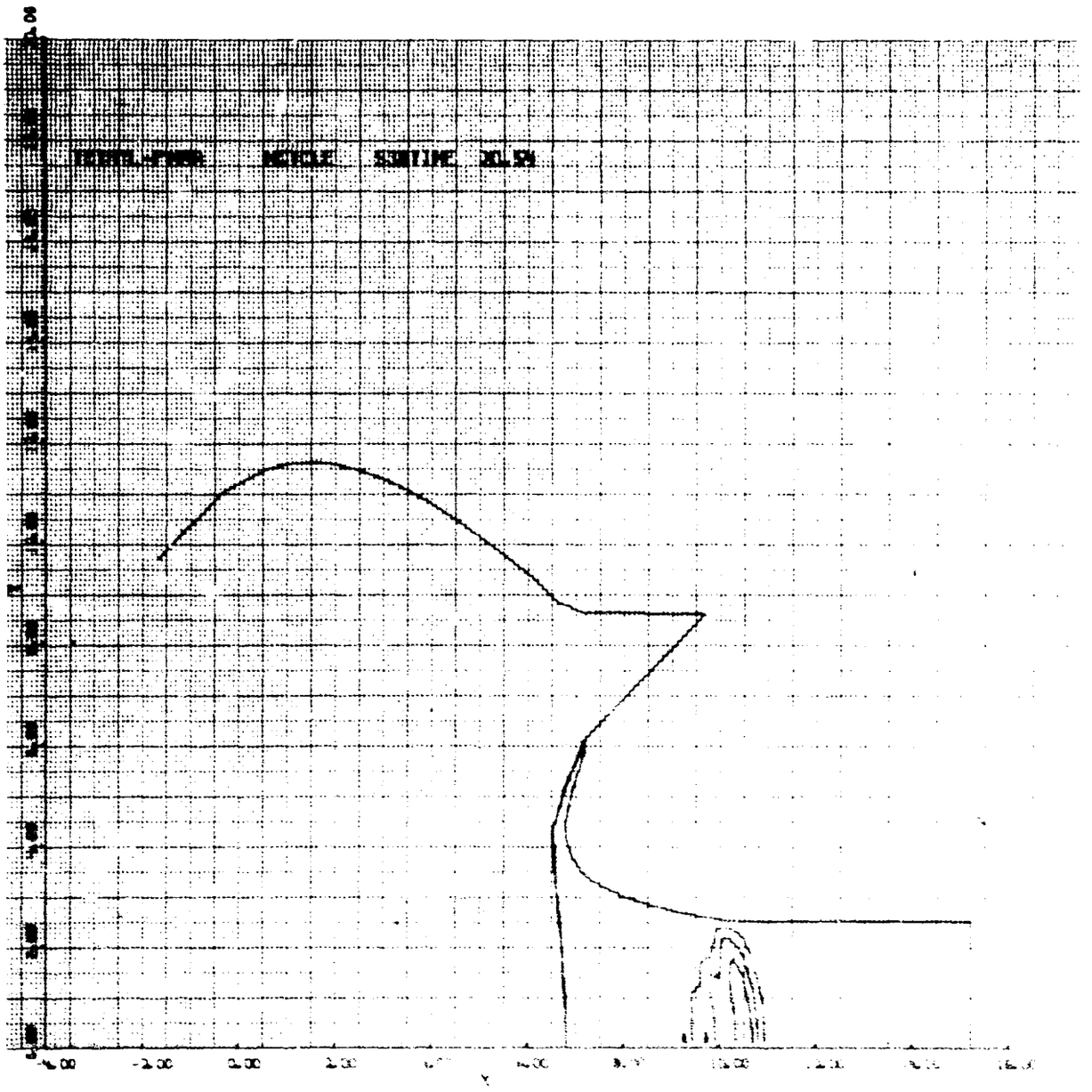

Figure A14(c)

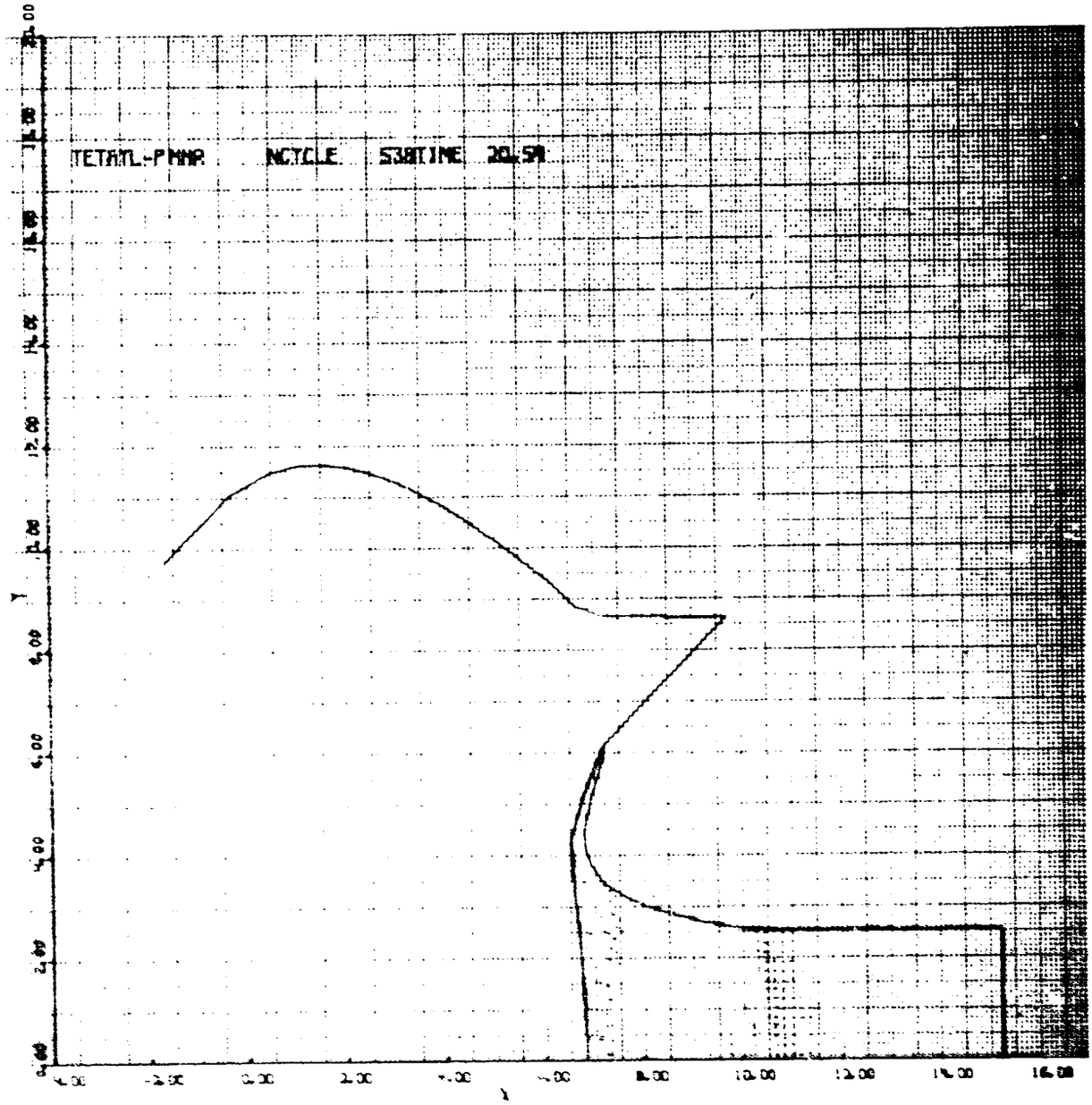

Figure A14(e)

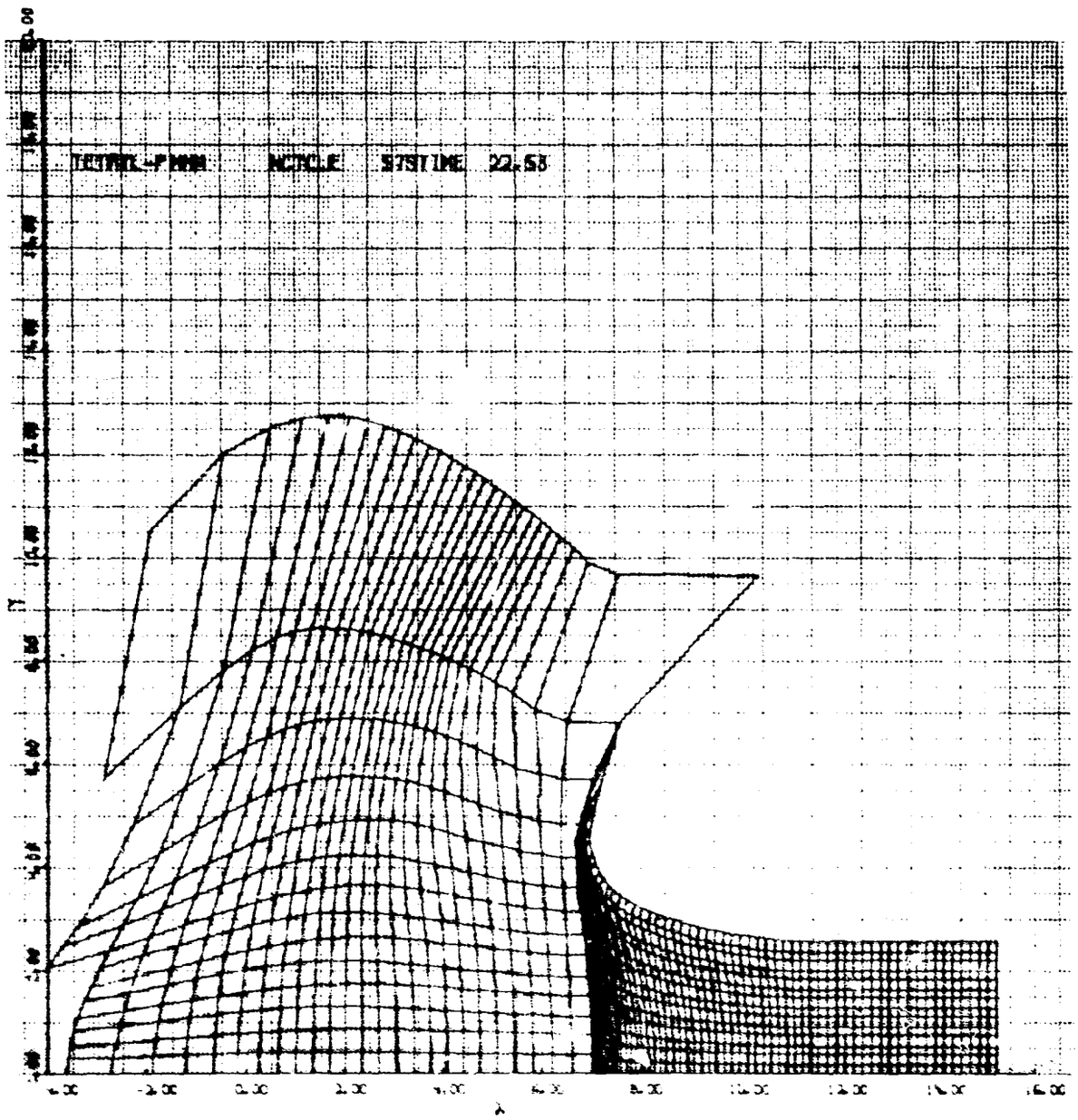

Figure A16

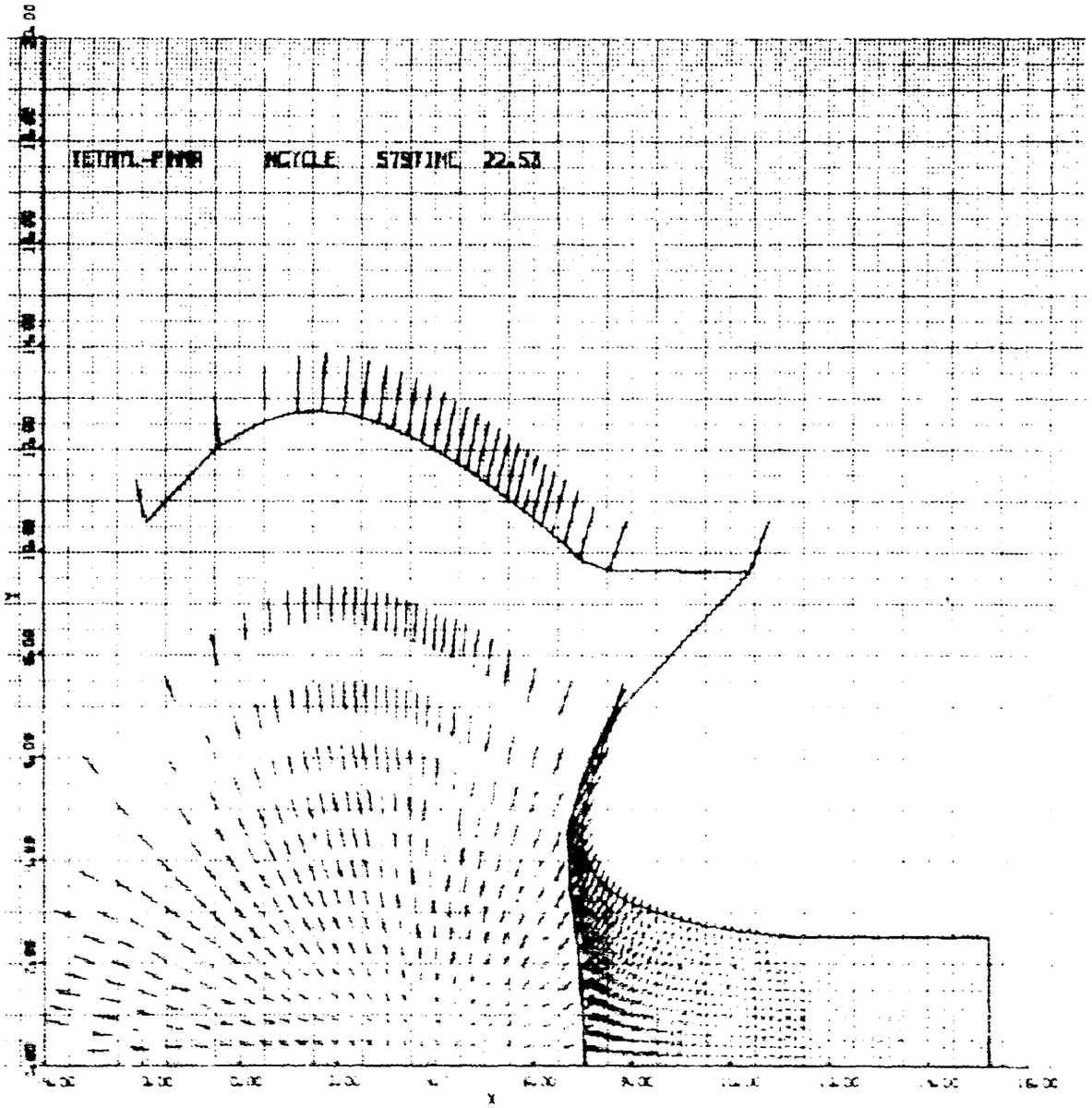
NCYCLE
Y
X

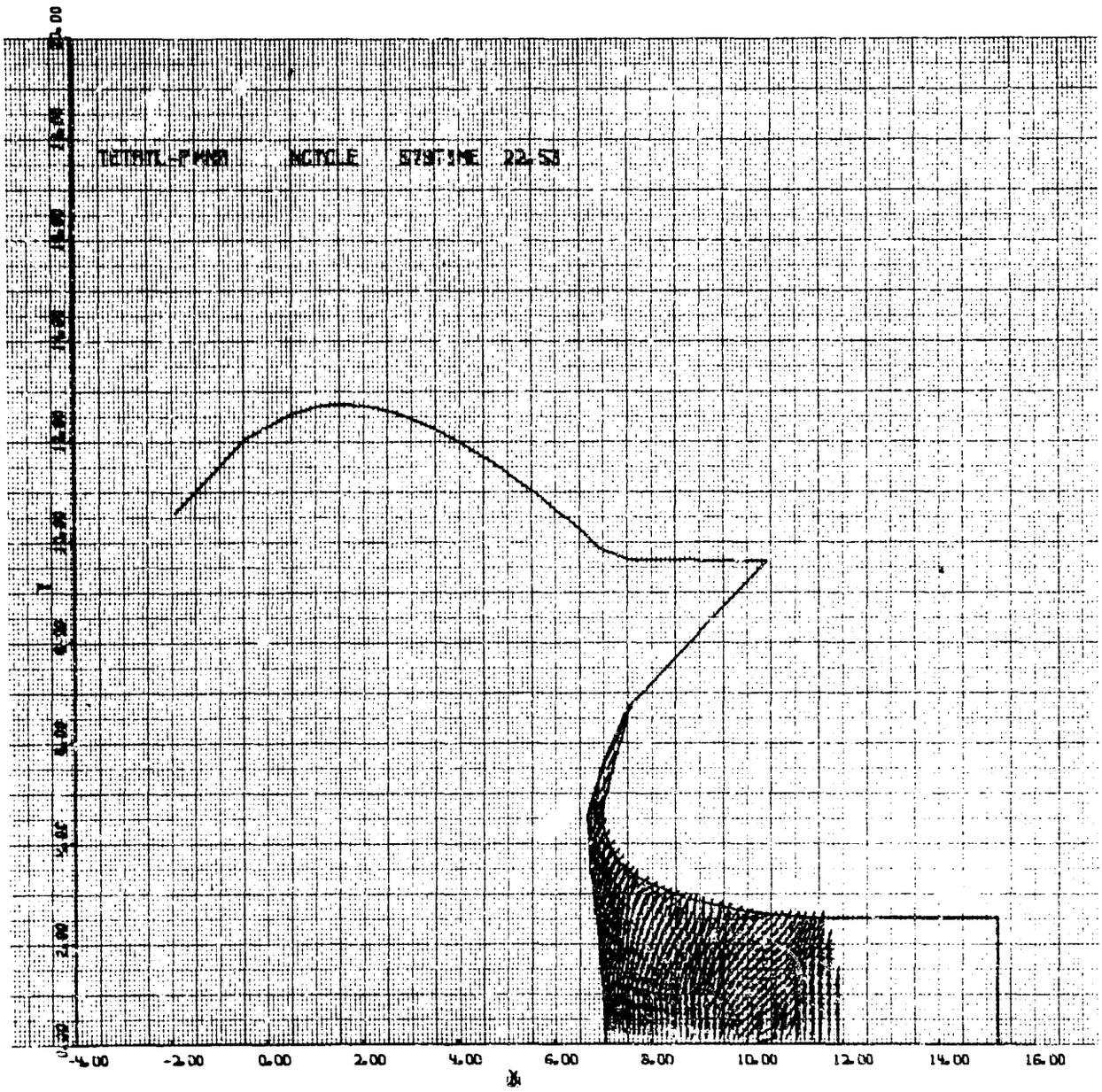
DETAIL-PWR
NCTCLE
STATIME 22.53
-4.00
-2.00
0.00
2.00
4.00
6.00
8.00
10.00
12.00
14.00
16.00

Figure A15(c)

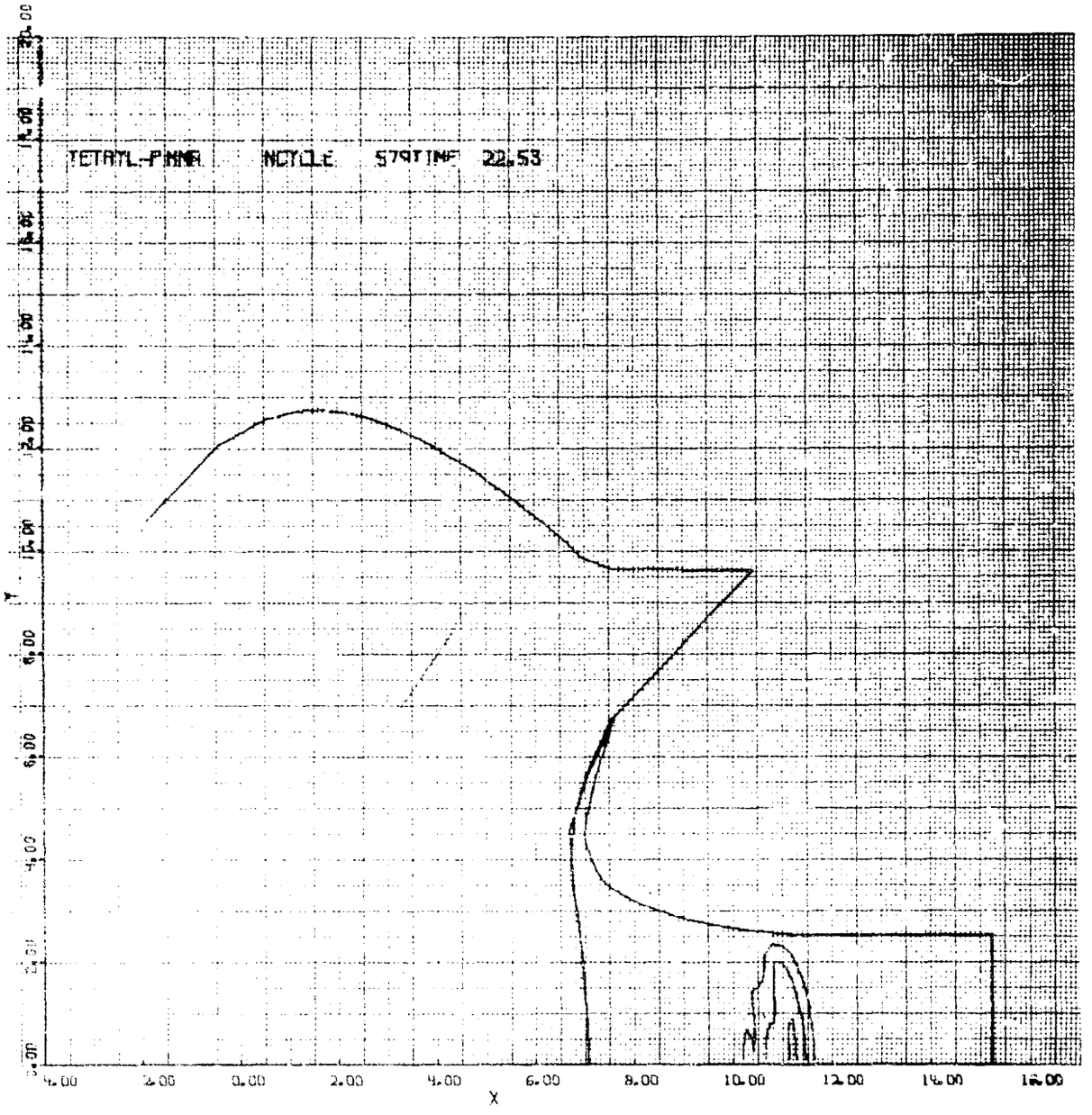
TETRTL-PNMR NOZZLE STRTING 22.53
Y
X
-4.00
-2.00
0.00
2.00
4.00
6.00
8.00
10.00
12.00
14.00
16.00

Figure A15(d)

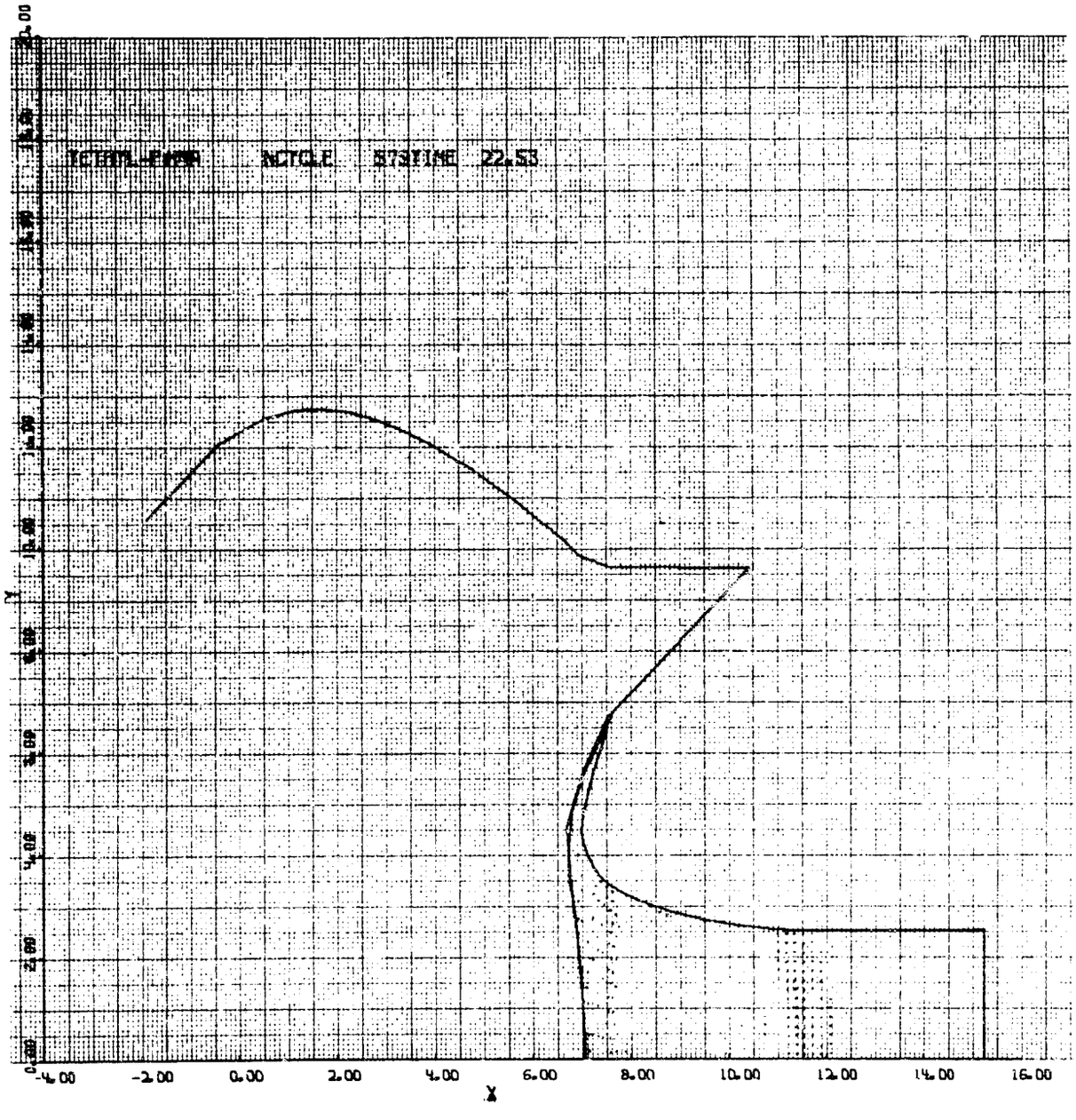
NCTCLE
573TIME 22.53
-4.00
-2.00
0.00
2.00
4.00
6.00
8.00
10.00
12.00
14.00
16.00
Y
X

Figure A15(e)

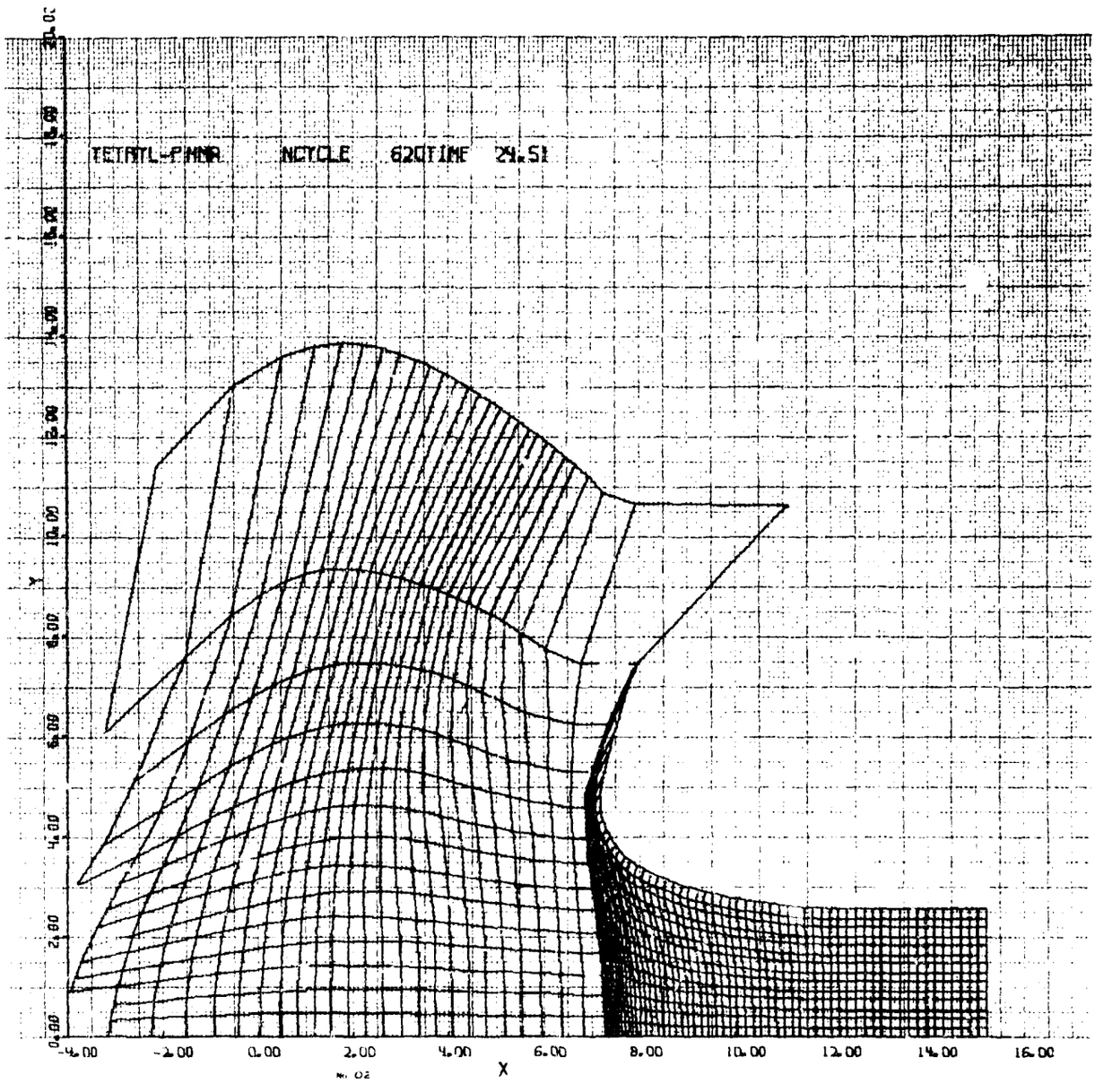
TETNTL-PMAR NCYCLE 620TIME 24.51
-4.00
-2.00
0.00
2.00
4.00
6.00
8.00
10.00
12.00
14.00
16.00
X
Y

Figure A16(a)

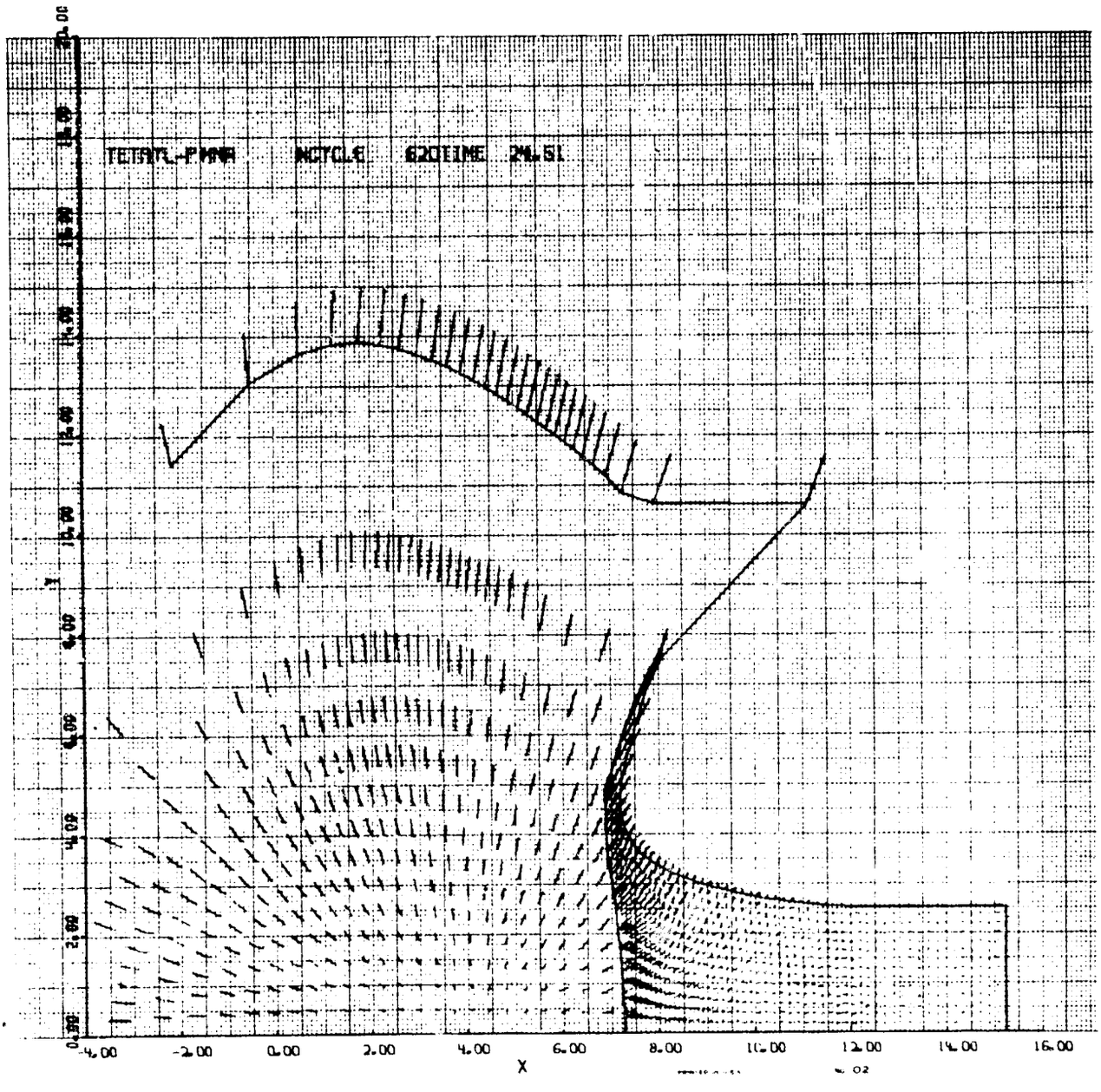
TETRA1_P MACH NCYCLE 620TIME 24.61
-4.00
-2.00
0.00
2.00
4.00
6.00
8.00
10.00
12.00
14.00
16.00
X

Figure A16(b)

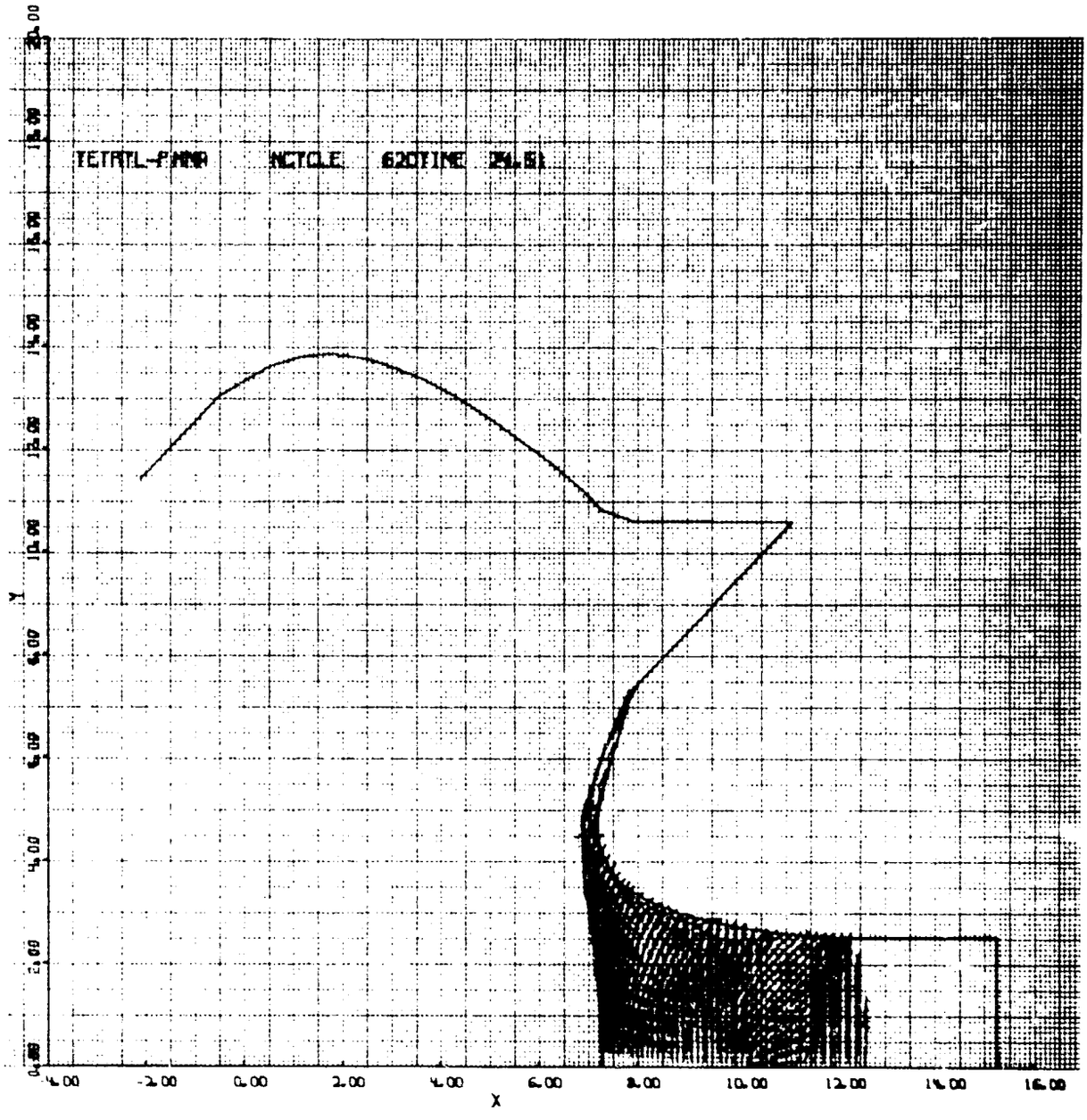
TETRTL-PMMP
NCTCLE
620TIME
Y
X
-4.00
-2.00
0.00
2.00
4.00
6.00
8.00
10.00
12.00
14.00
16.00

Figure A16(c)

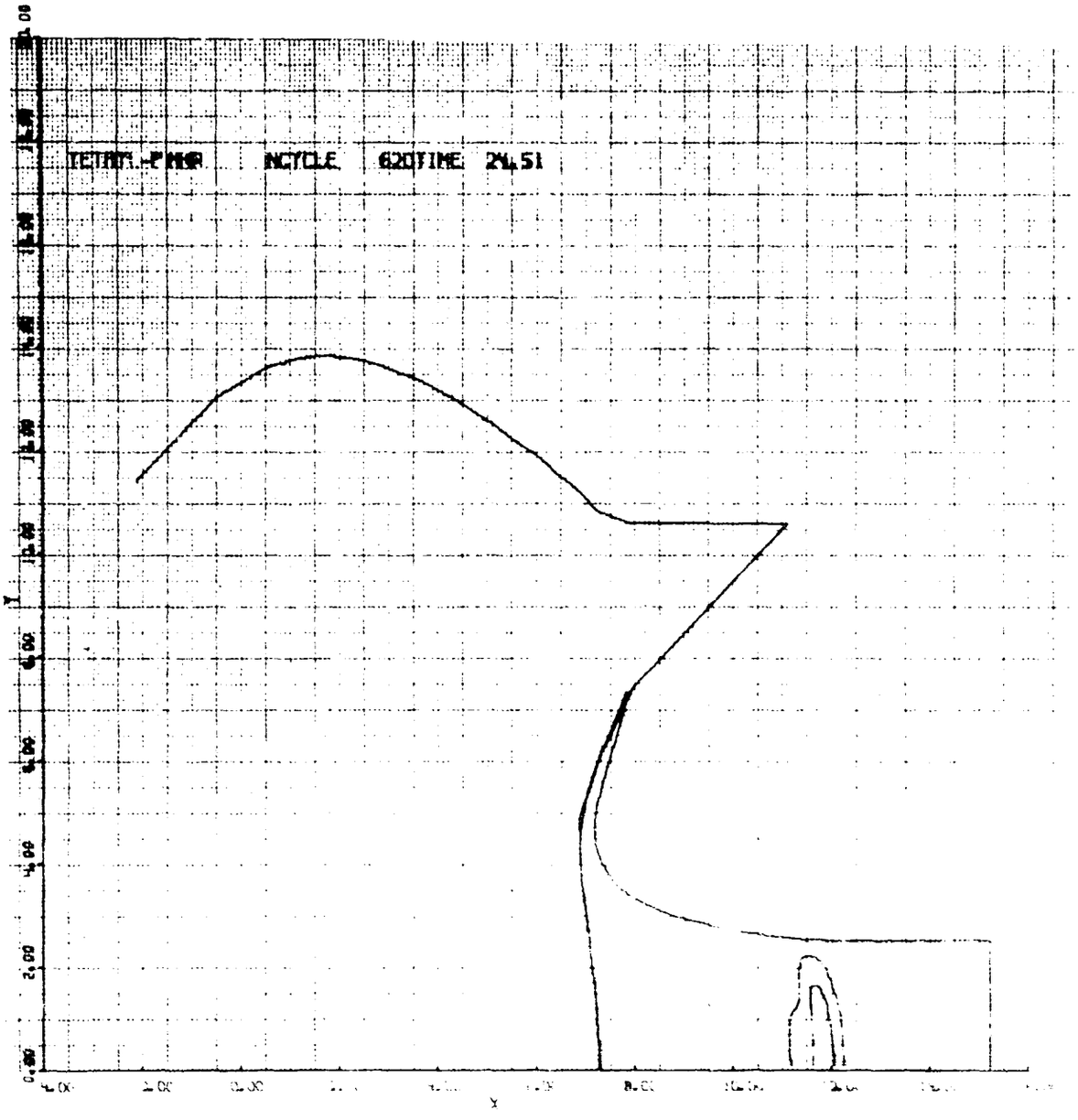

Figure A16(a)

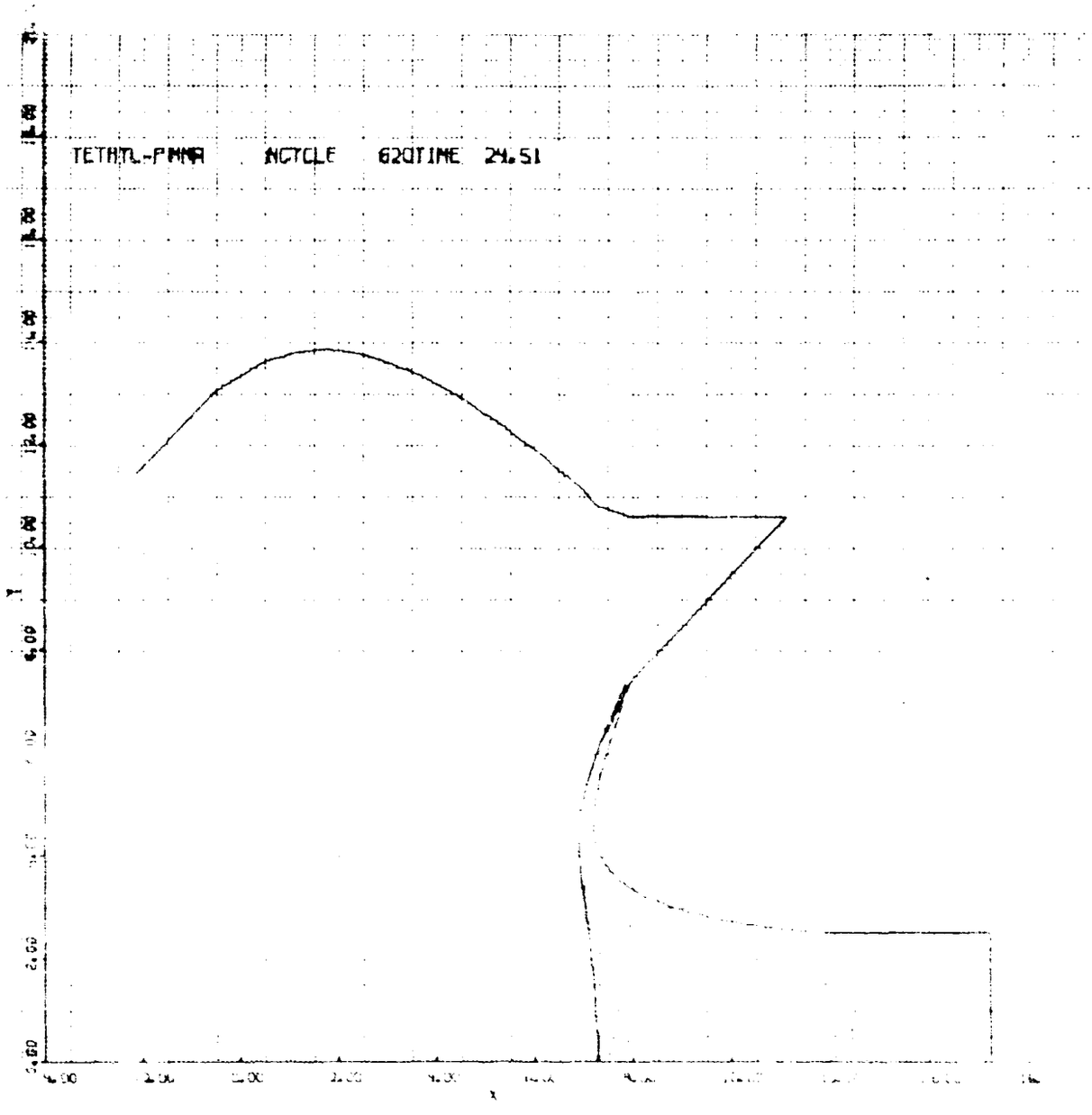

Figure VI-6(c)

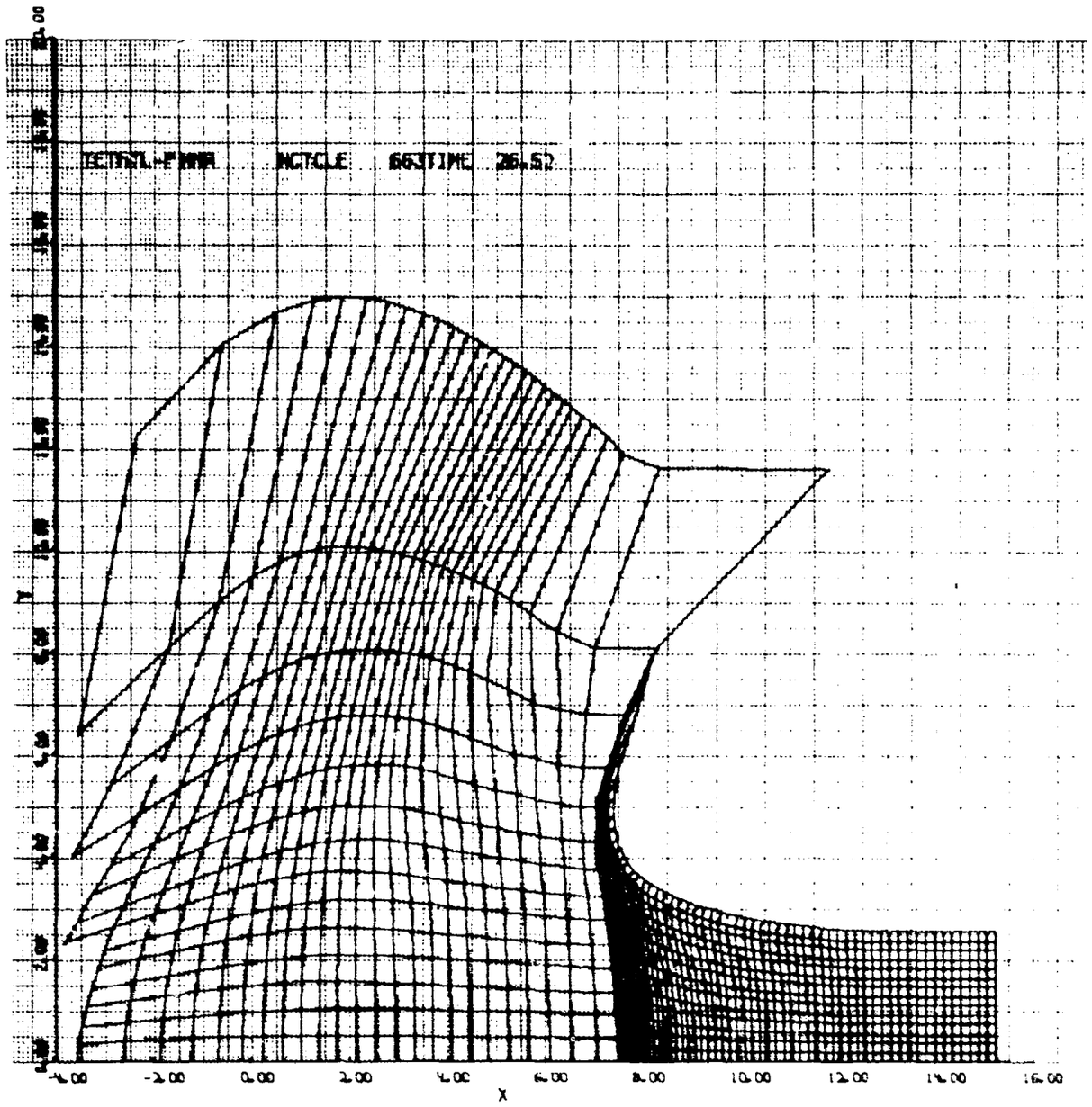

Figure A17(a)

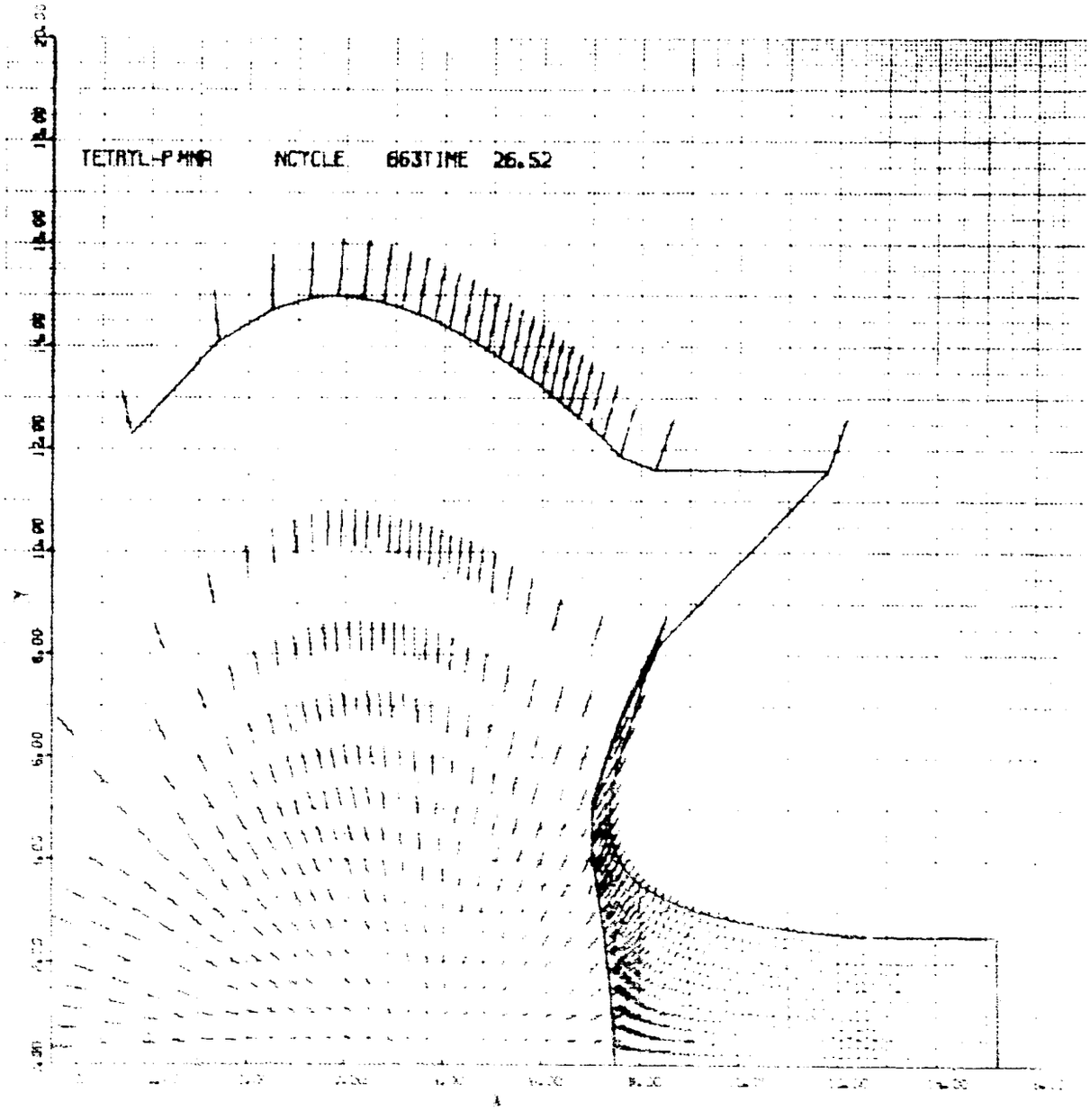
TETRYL-PMMA
NCYCLE
863TIME 26.52
Y
X

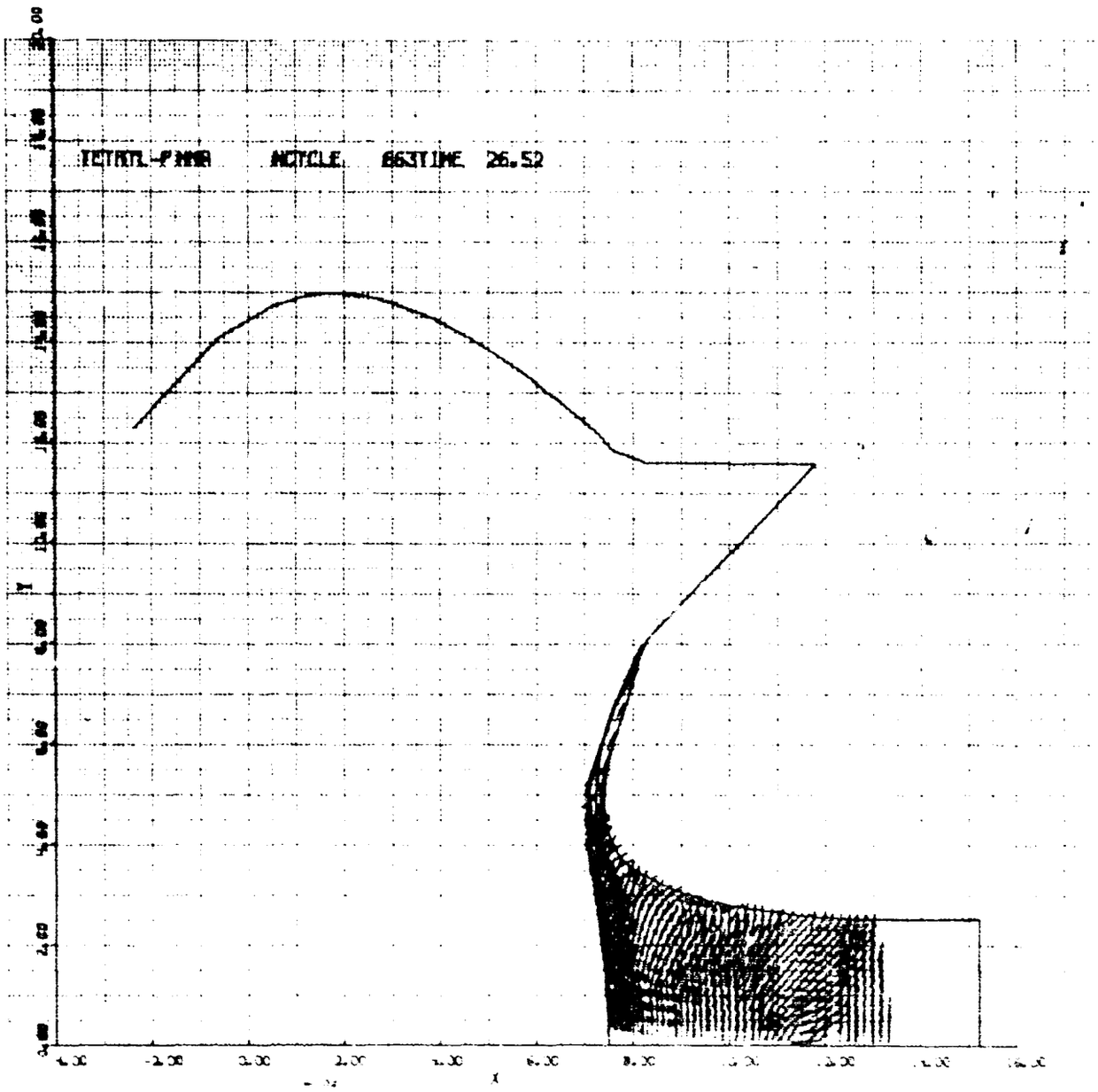
CYCLE
TIME 26.52

[illegible]

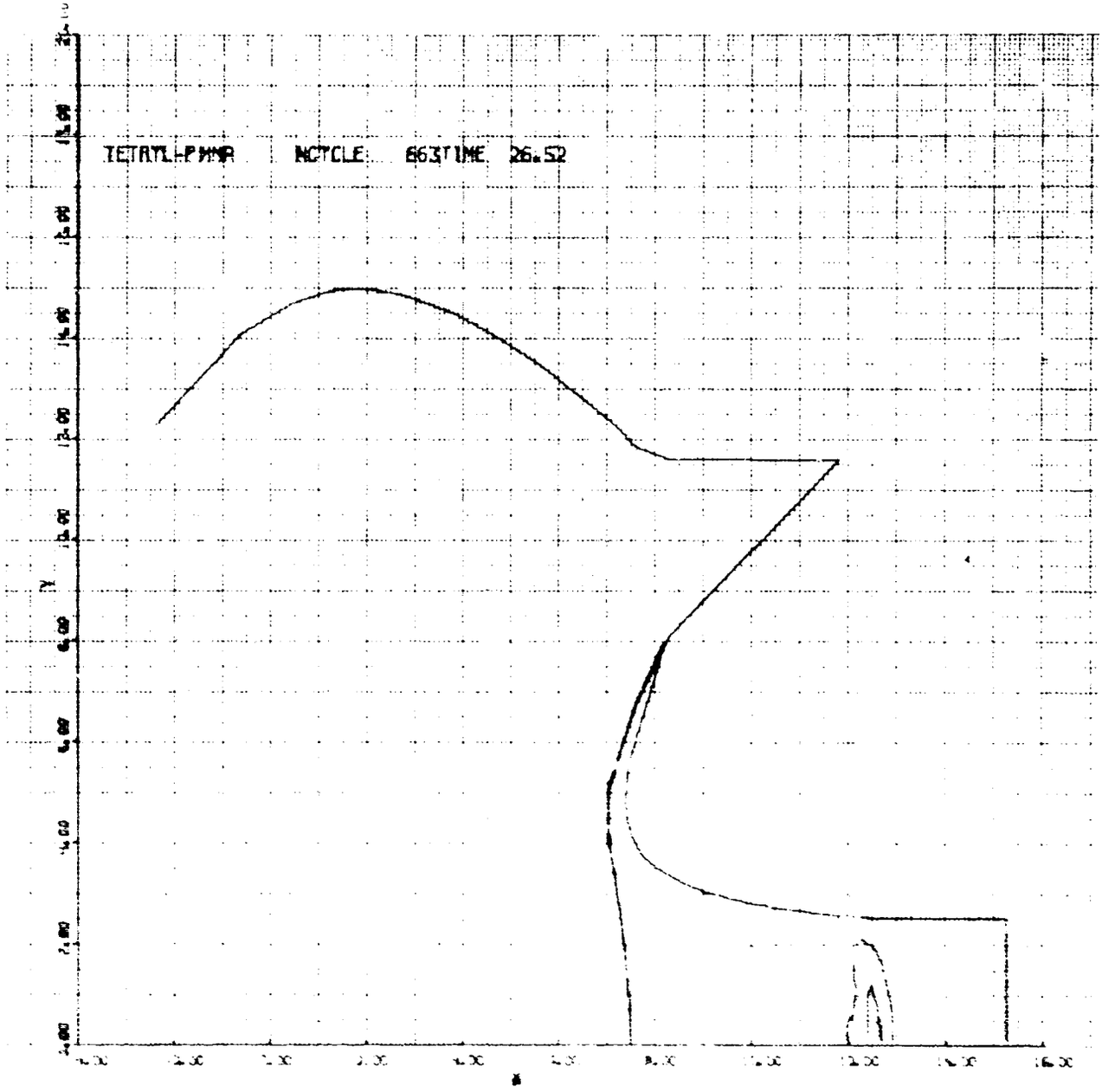
TETATL-PWR
NCTCLE 663TIME 26.52

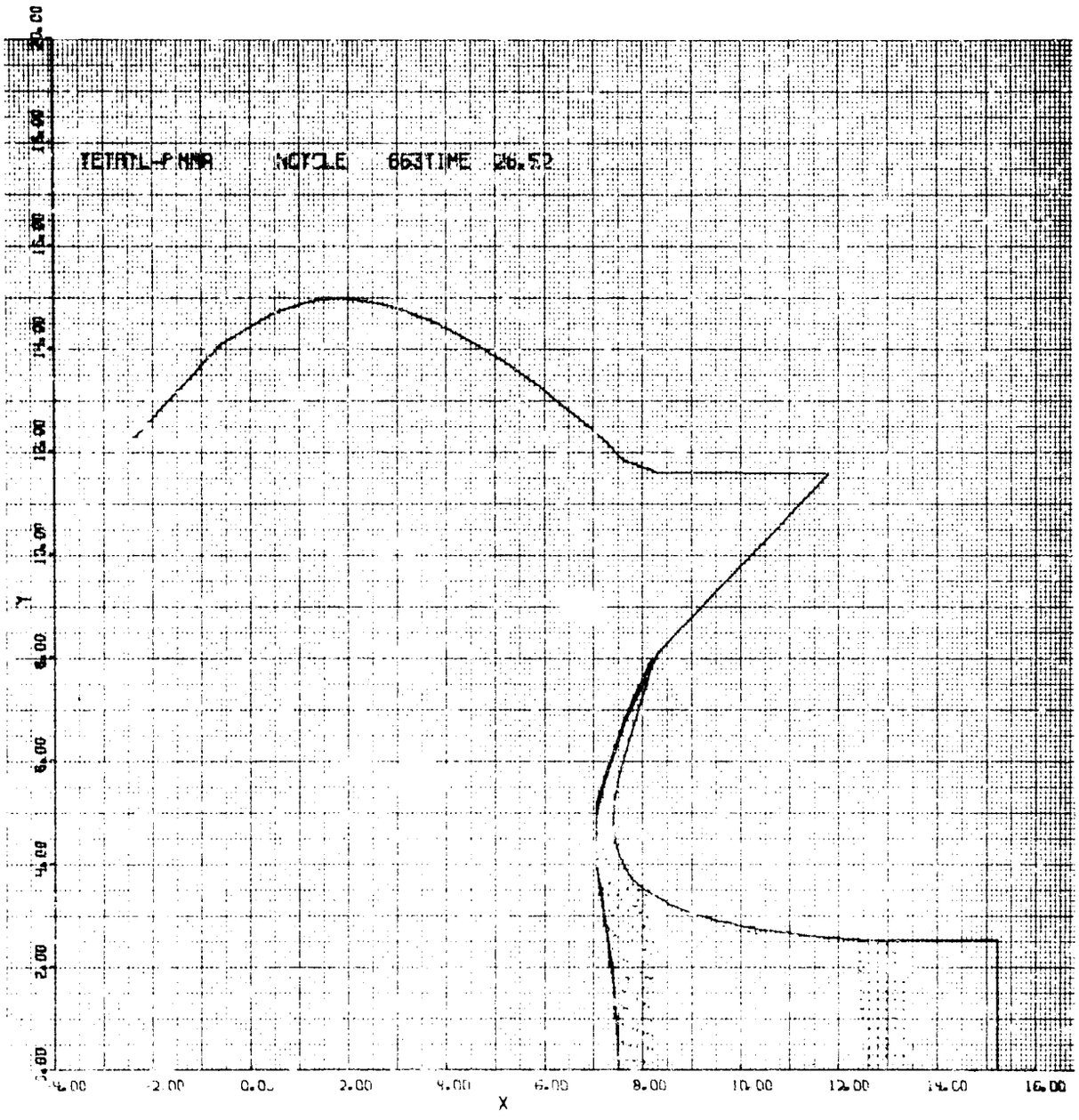
METAL-PMMA NOZZLE 663TIME 26.52
Y
X
-4.00
-2.00
0.00
2.00
4.00
6.00
8.00
10.00
12.00
14.00
16.00

Figure A.17(c)

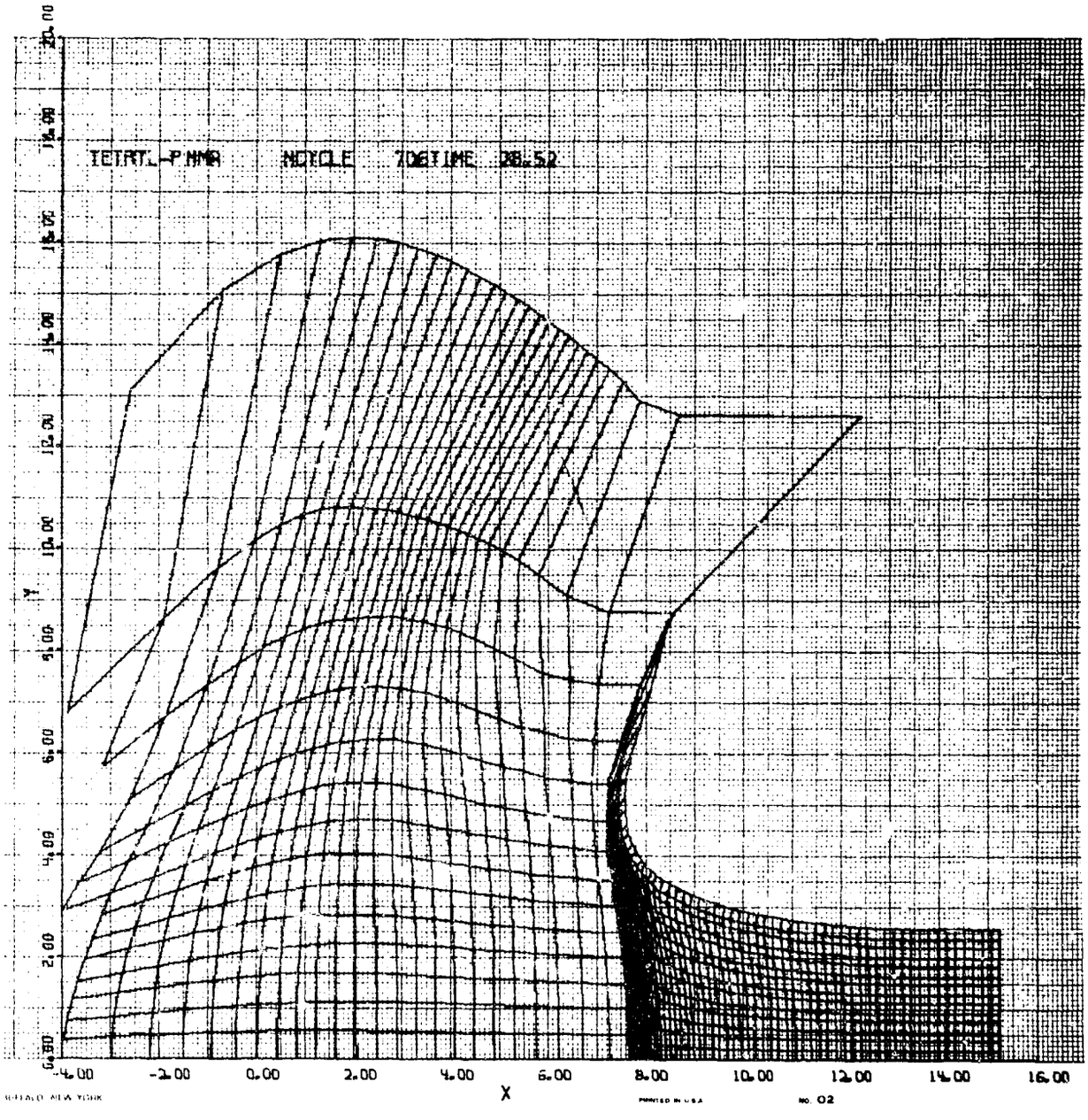
TETRT.-P NMR NOZZLE TOSTIME 38.52
Y
X
-4.00
-2.00
0.00
2.00
4.00
6.00
8.00
10.00
12.00
14.00
16.00

Figure A18(a)

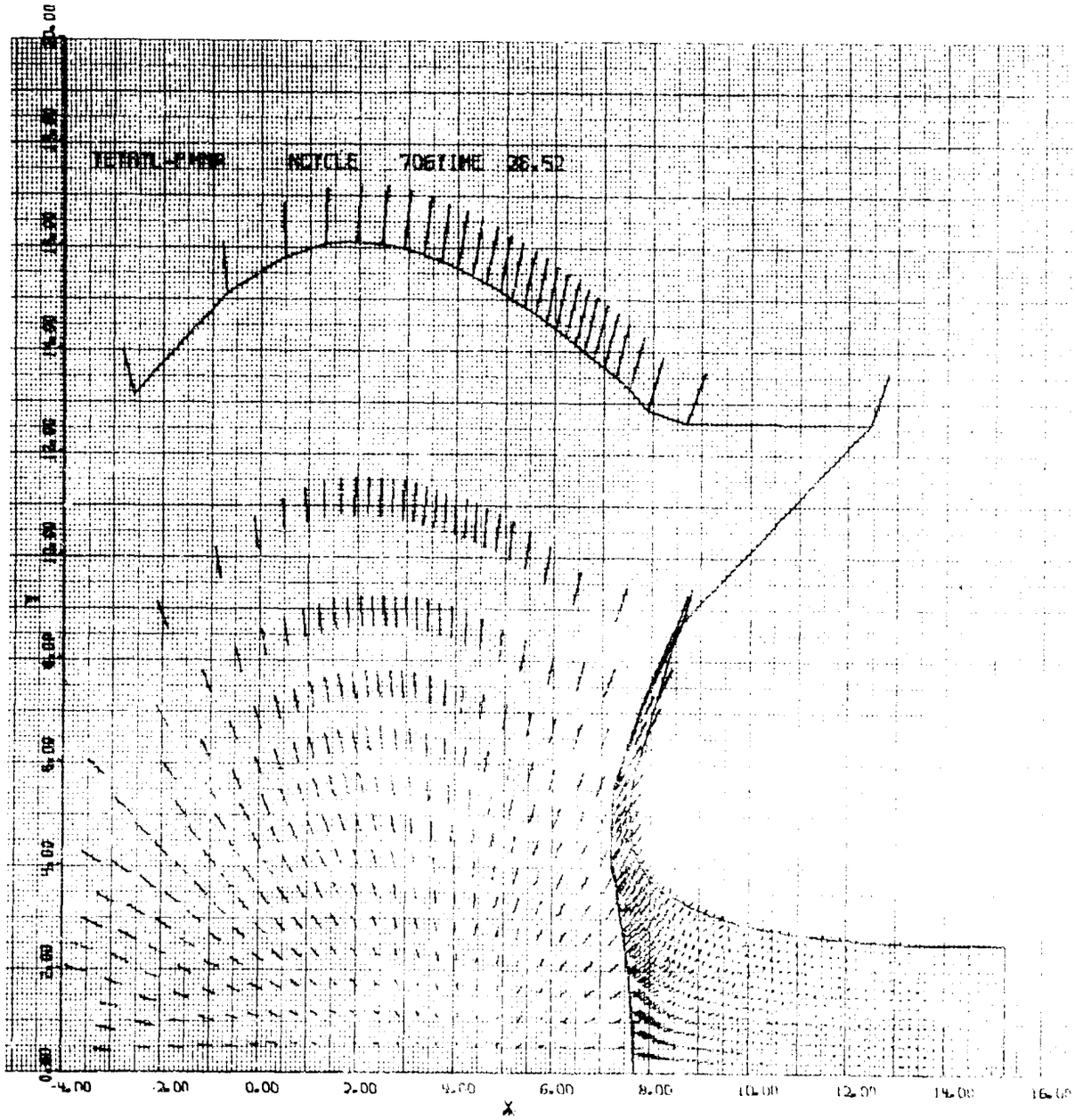
NOTCLE
706TIME 26.52
-4.00
-2.00
0.00
2.00
4.00
6.00
8.00
10.00
12.00
14.00
16.00
X

Figure A18(b)

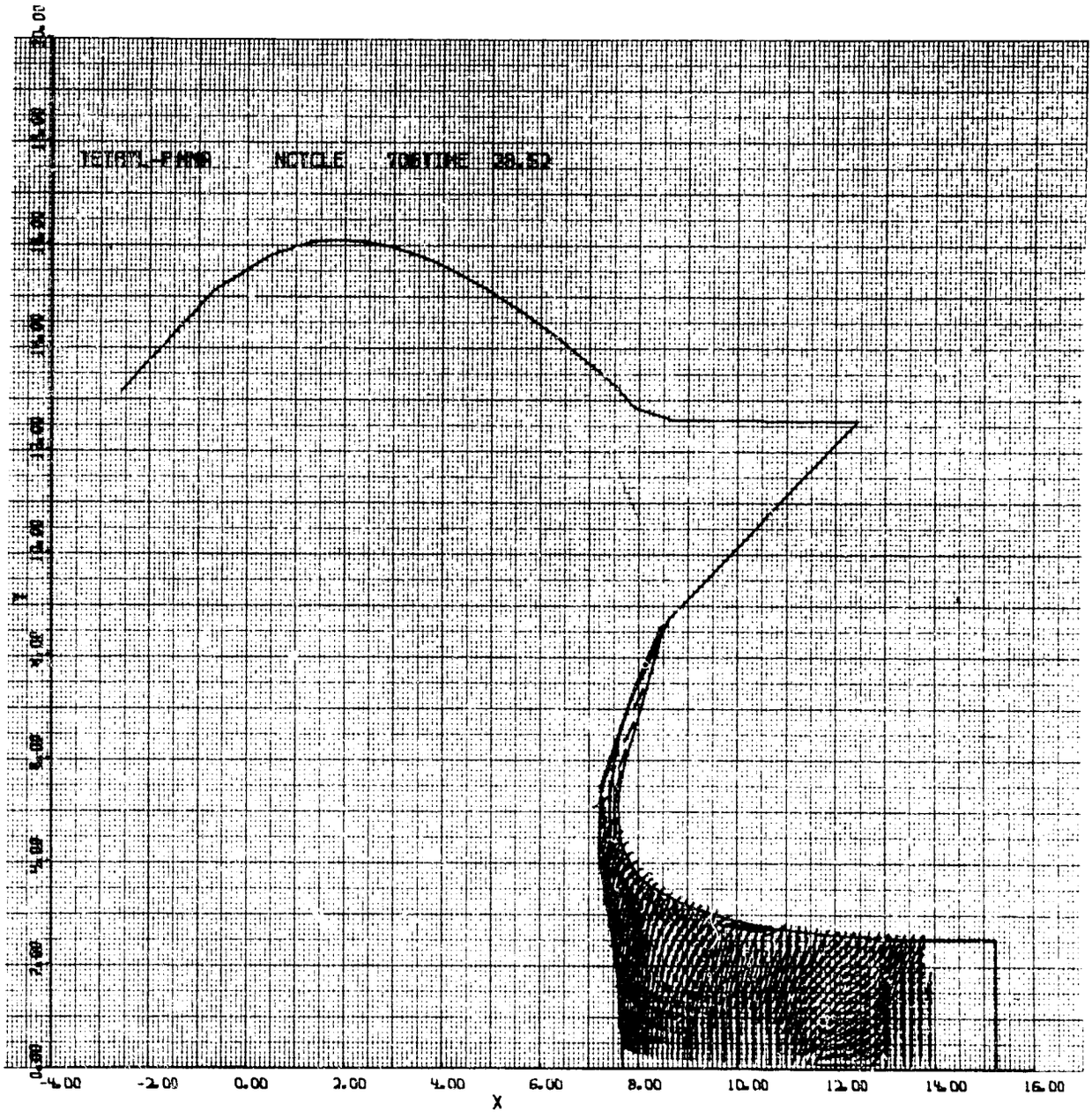

Figure A18(c)

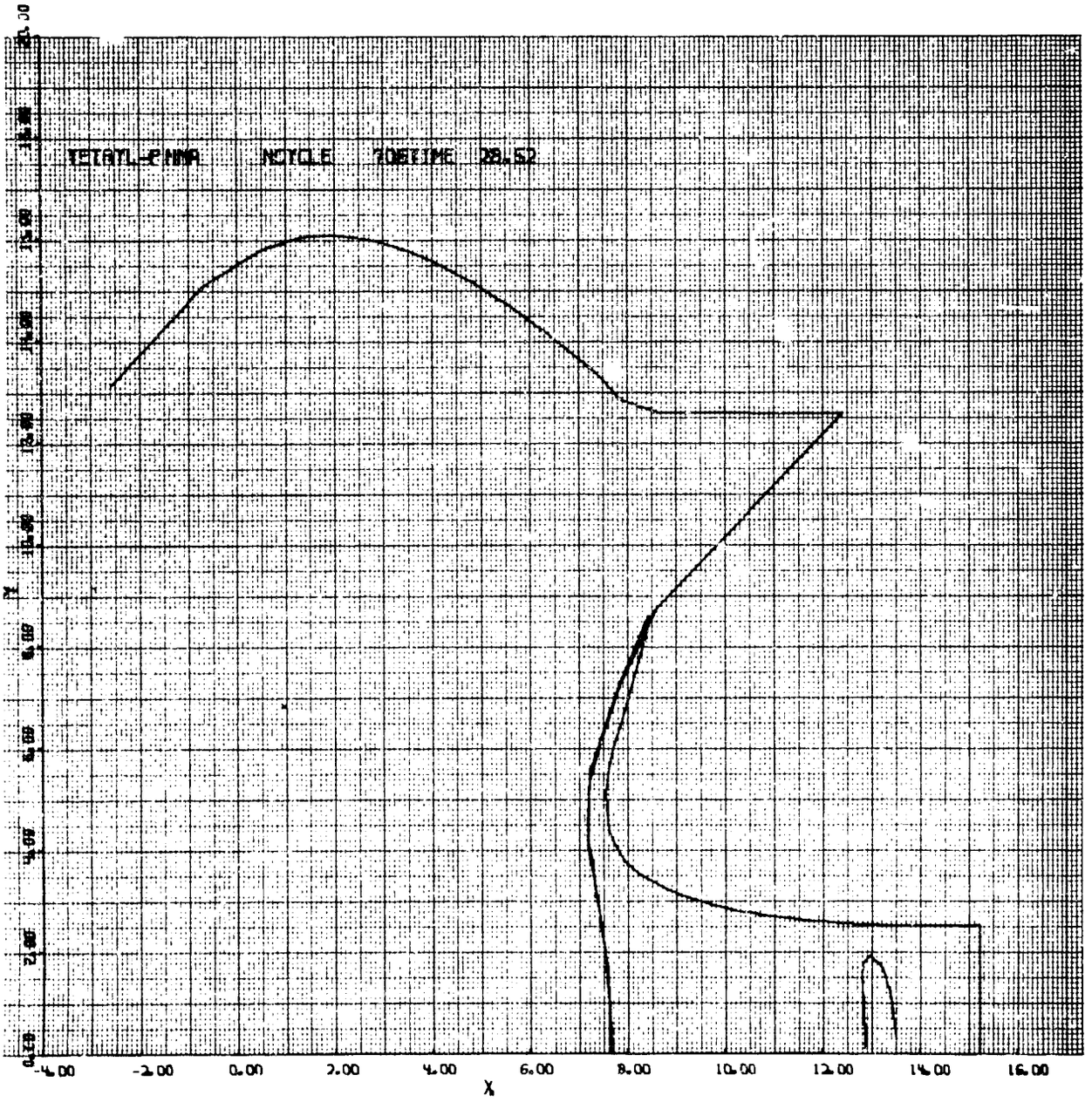
TOTAL-PMM
NCYCLE
TIMETIME 28.52
-4.00
-2.00
0.00
2.00
4.00
6.00
8.00
10.00
12.00
14.00
16.00
X

Figure A18(d)

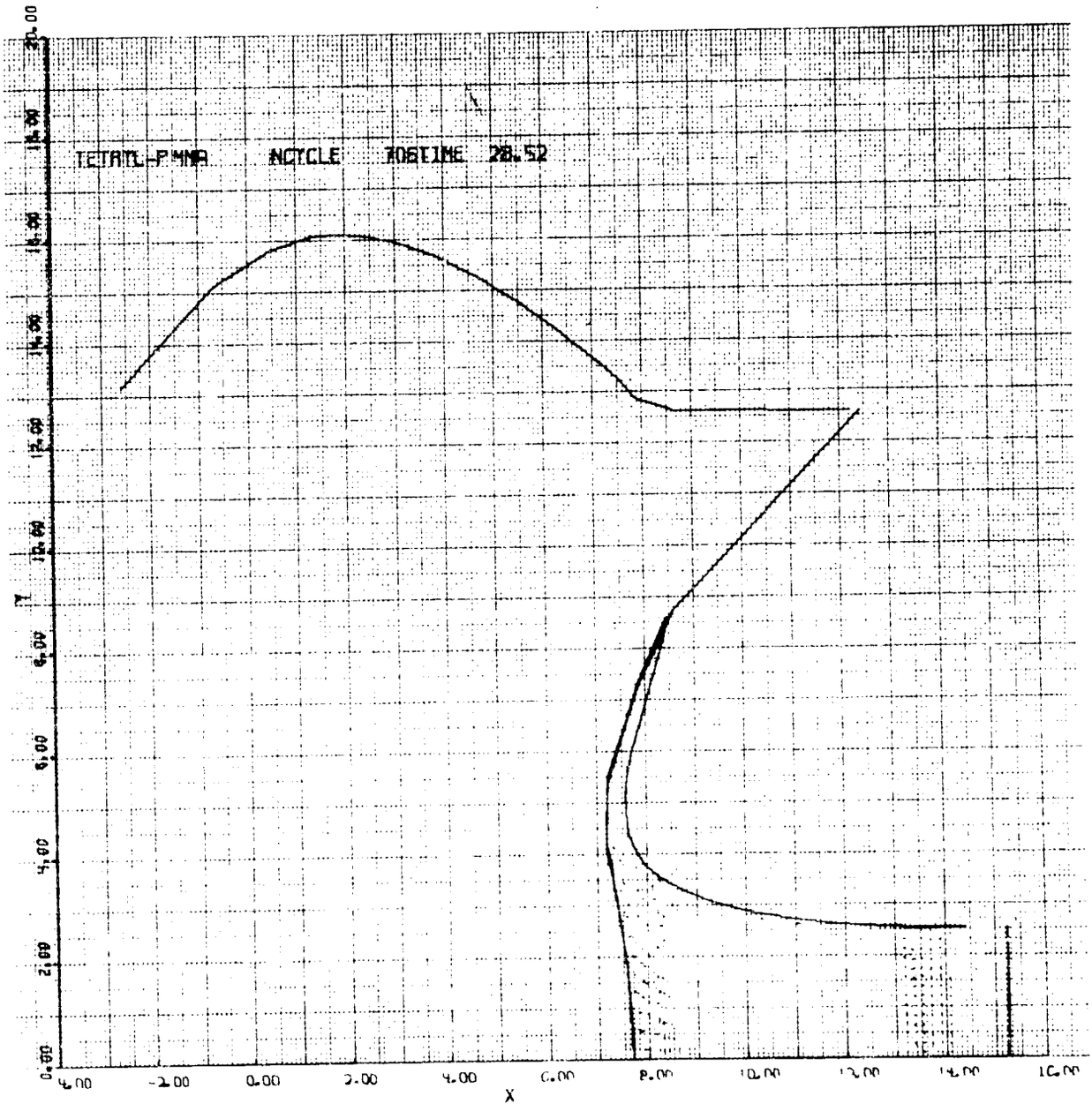
TETRAL-PMMA NOZCLE ROBTIME 28.52
Z
X
-4.00
-2.00
0.00
2.00
4.00
6.00
8.00
10.00
12.00
14.00
16.00
0.00
2.00
4.00
6.00
8.00
10.00
12.00
14.00
16.00
18.00
20.00

Figure A 18(e)

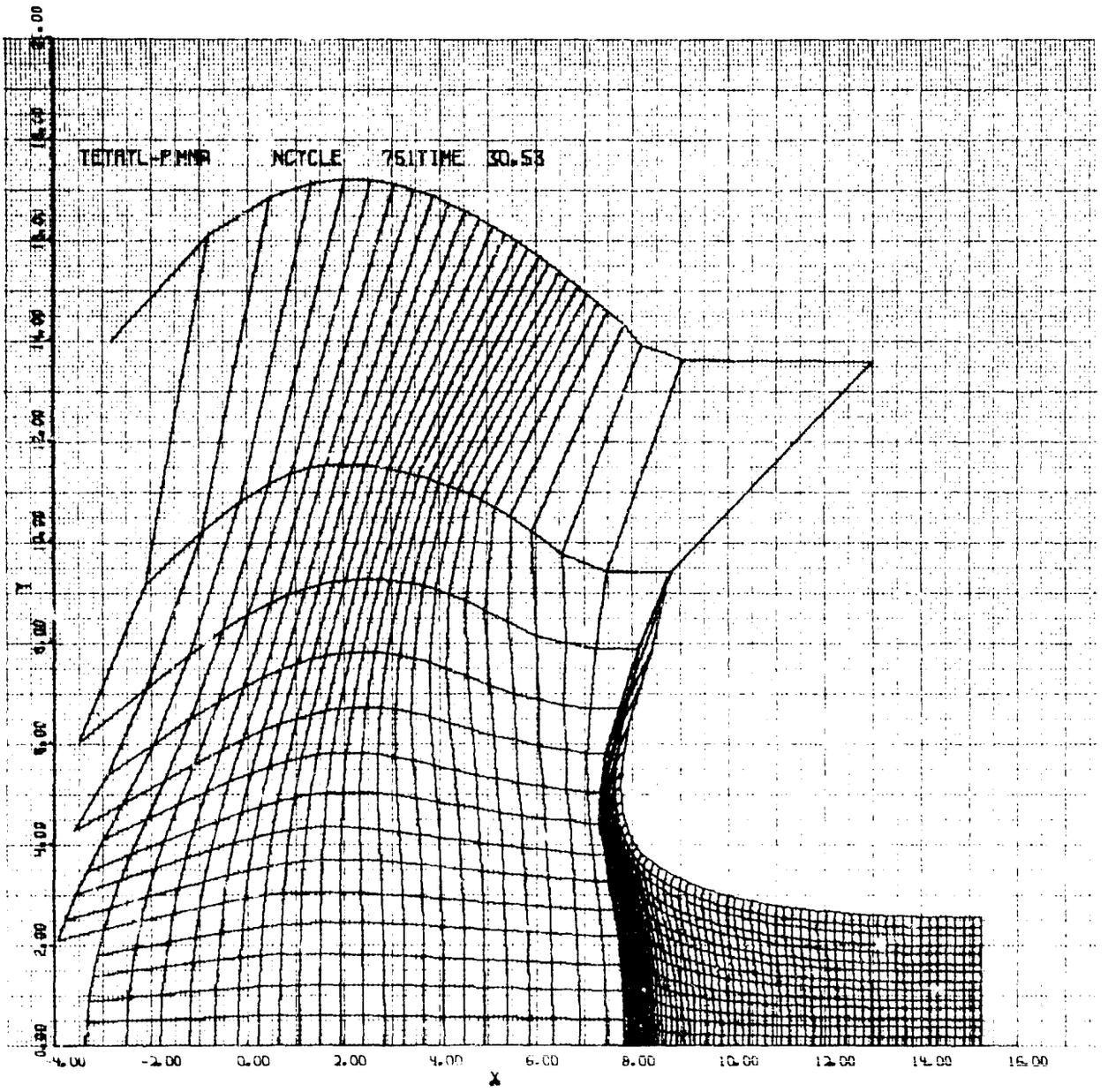
TETRTL-P MNR
NCYCLE 761TIME 30.53
Y
X
-4.00
-2.00
0.00
2.00
4.00
6.00
8.00
10.00
12.00
14.00
16.00

Figure A19(c)

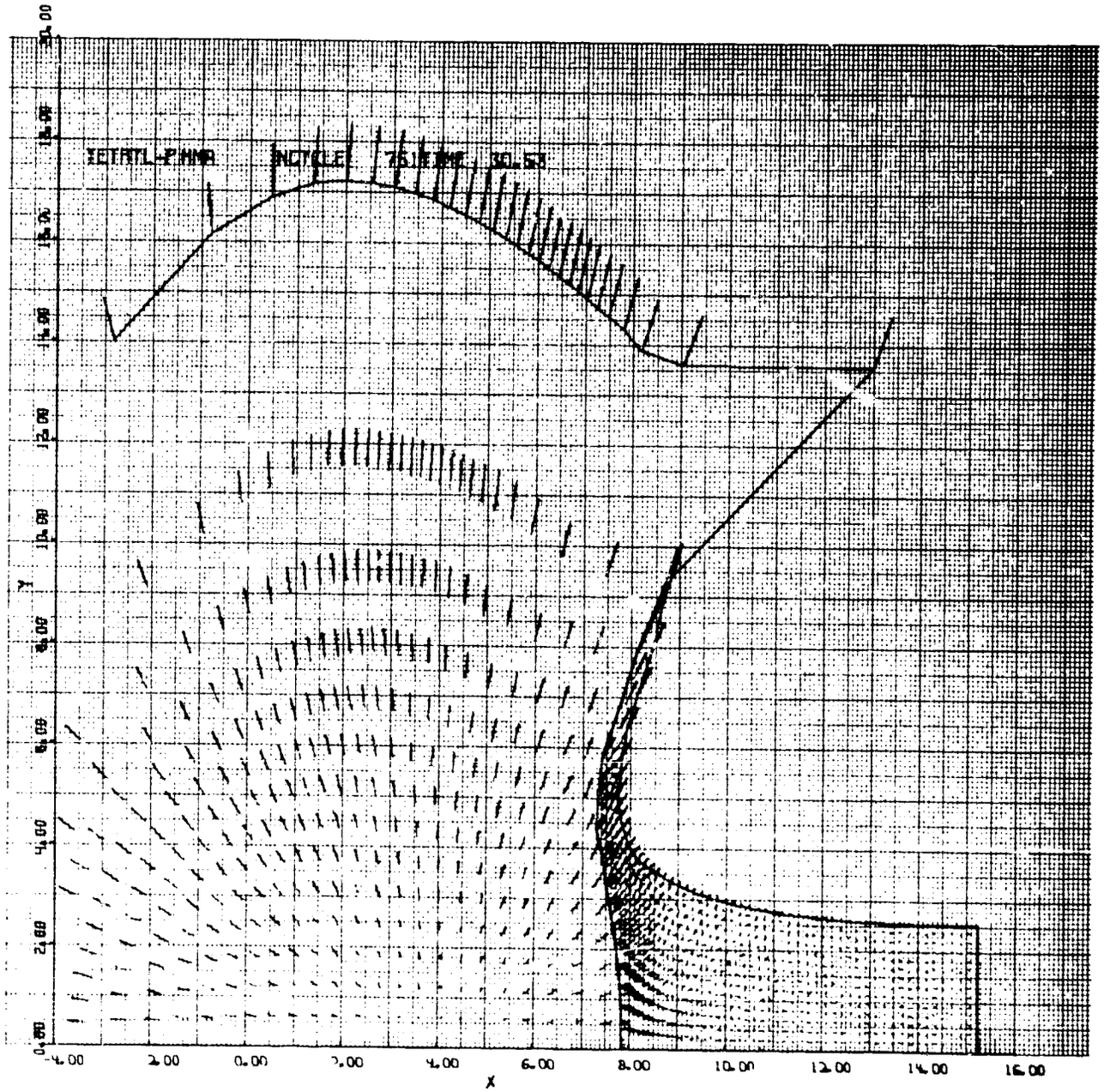

Figure A19(b)

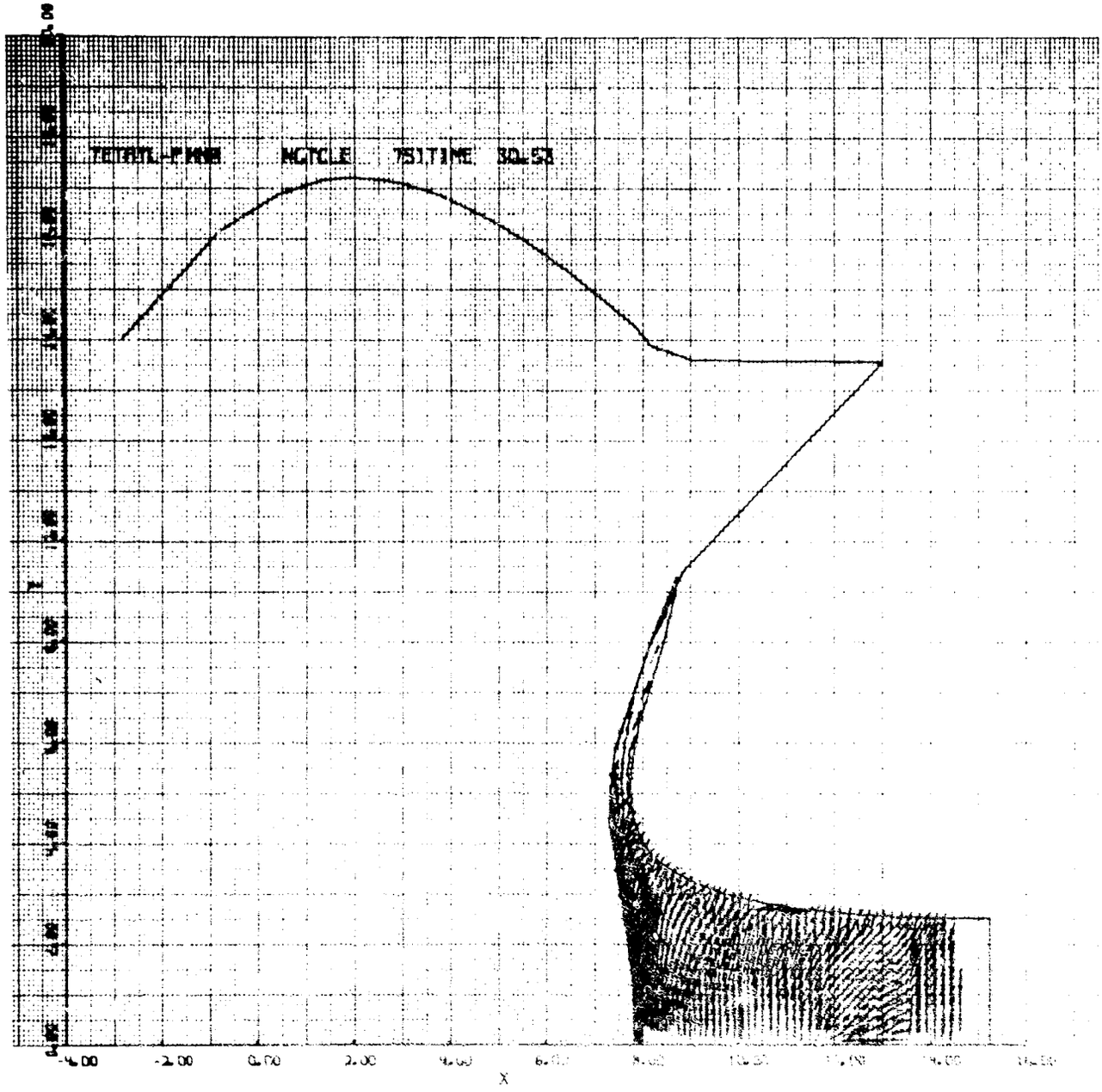

Figure A18(c)

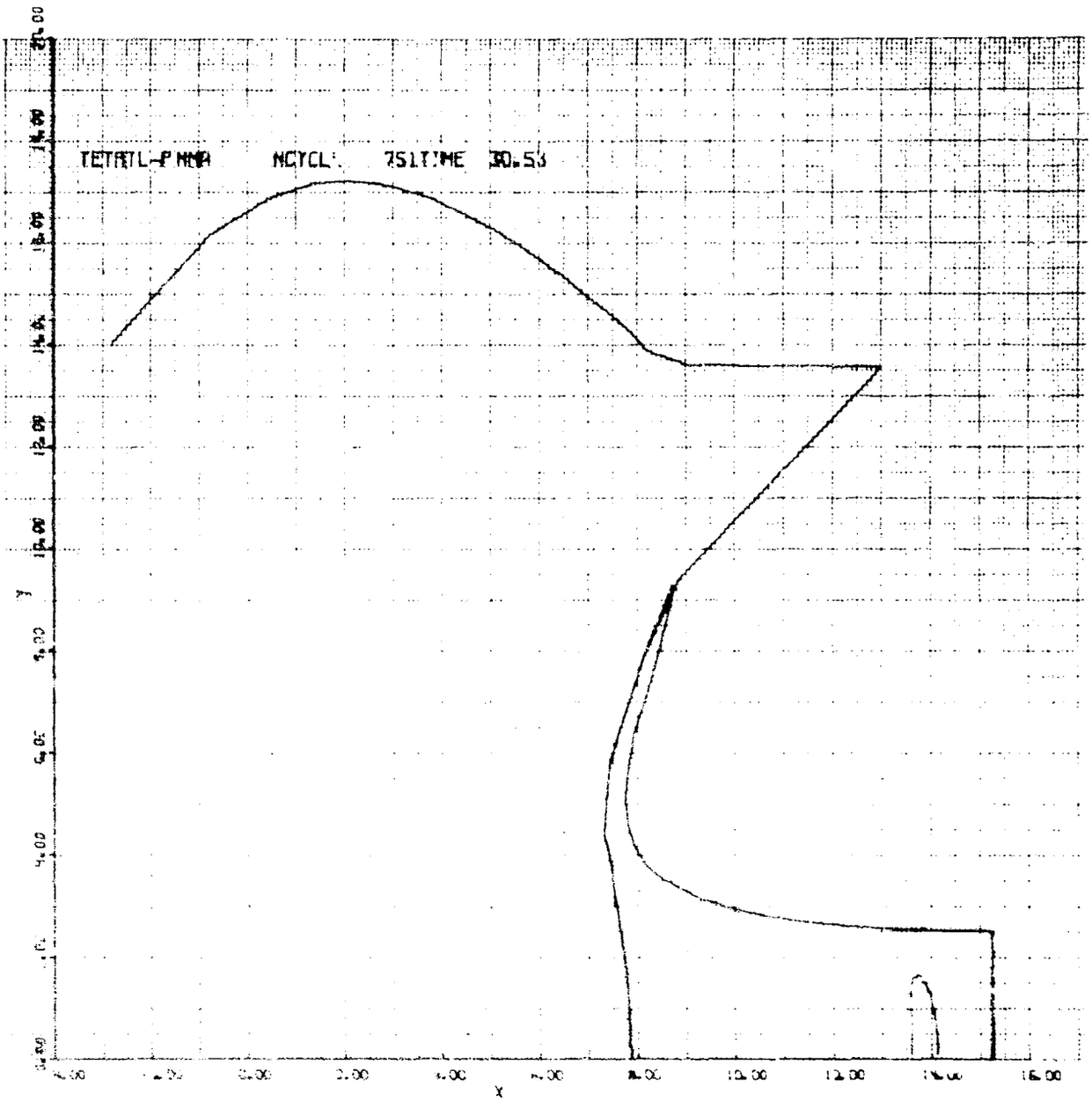

Figure A12(d)

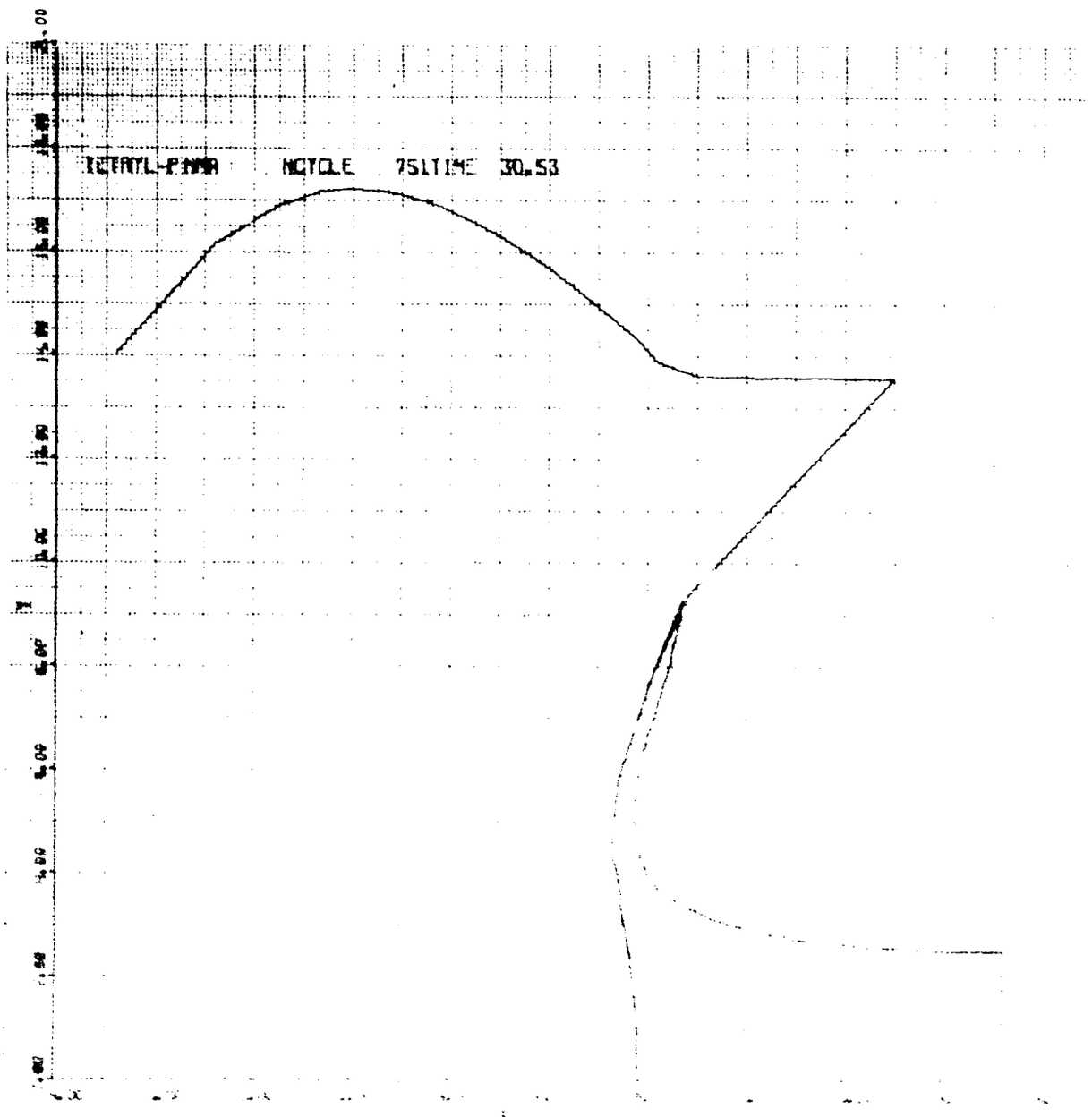
NCYCLE 751TIME 30.53

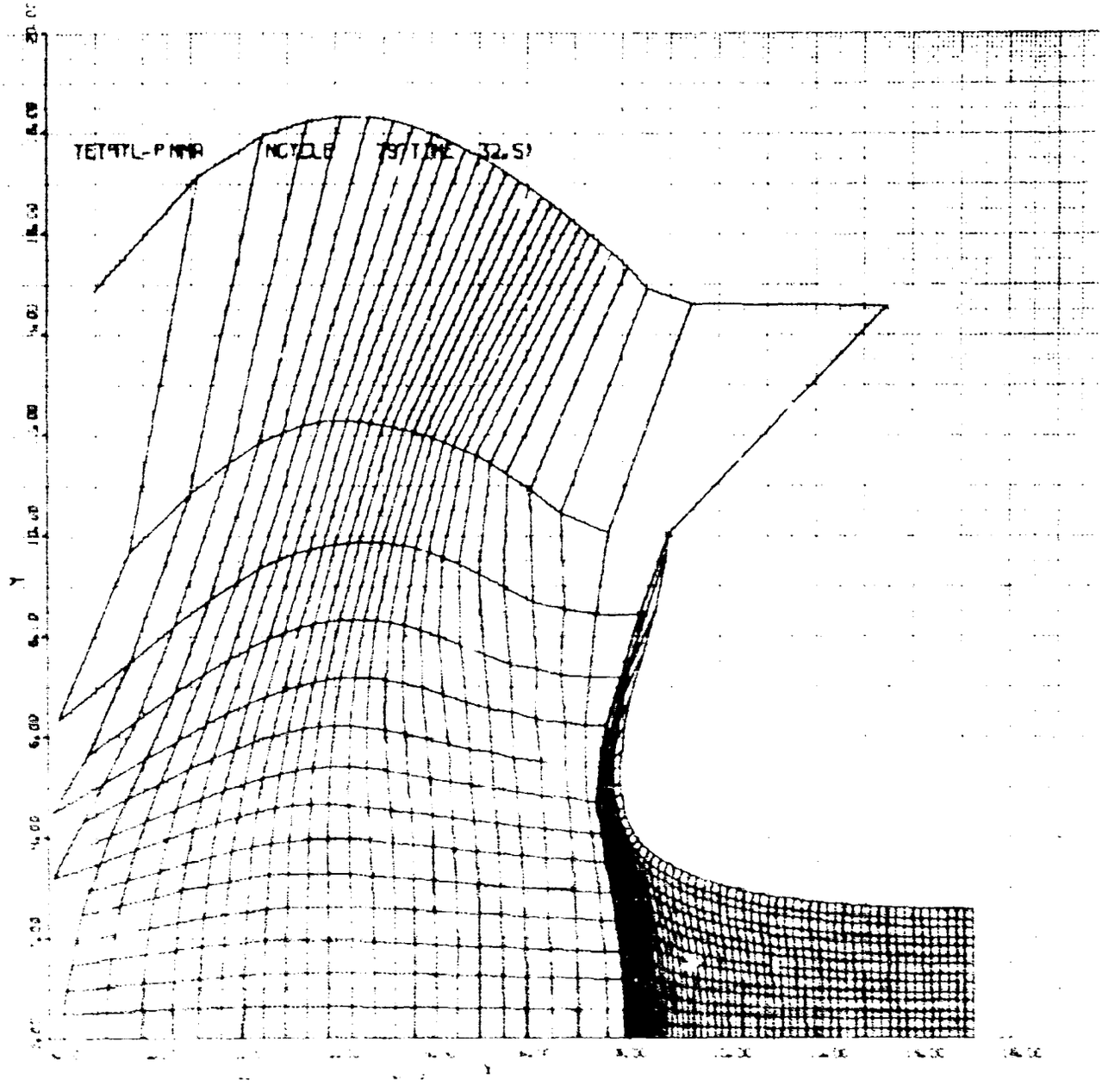

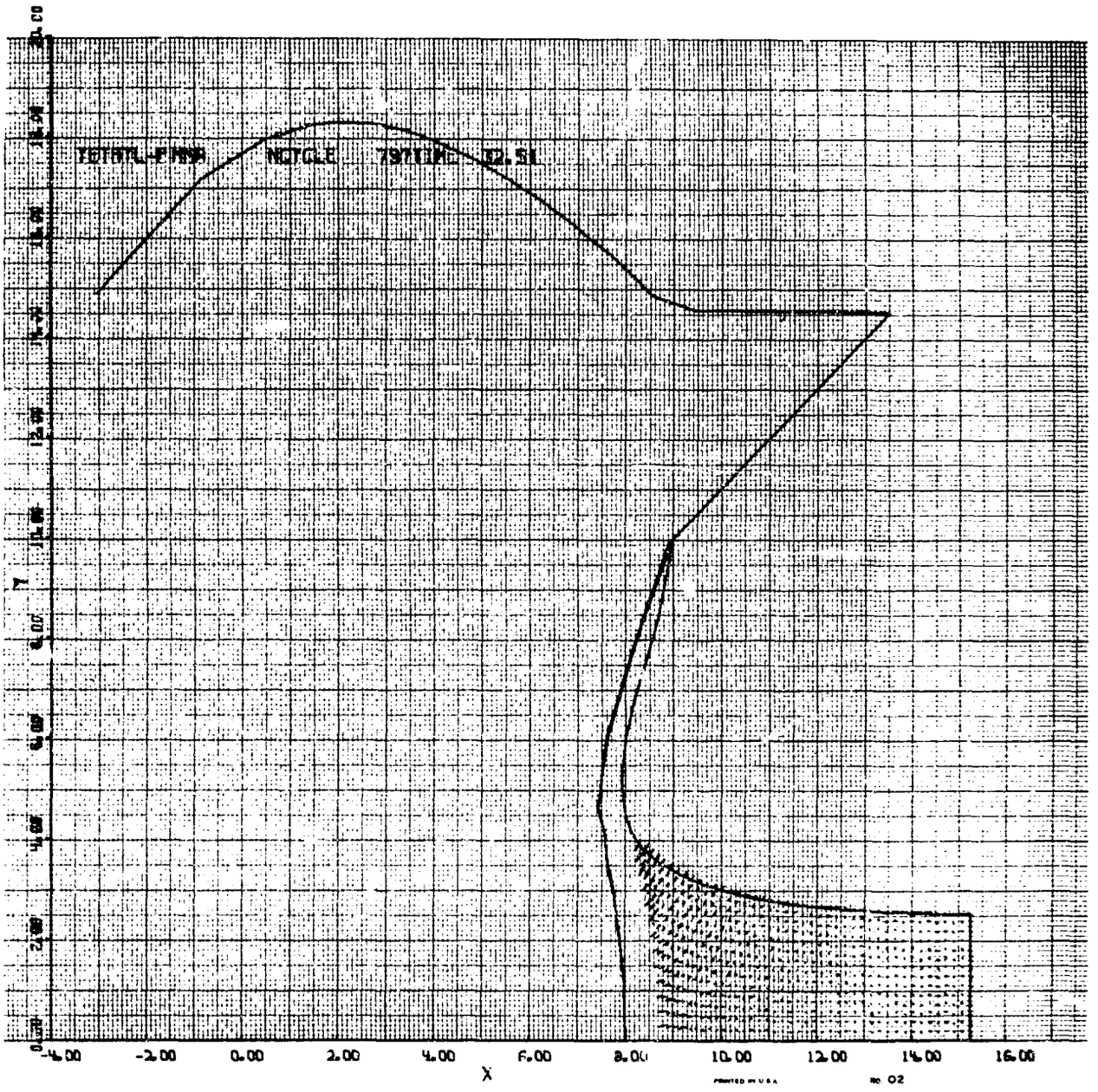

Figure A 20(e)

UNCLASSIFIED

Security Classification

DOCUMENT CONTROL DATA - R&D

(Security classification of title, body of abstract and indexing annotation must be entered when the overall report is classified)

1. ORIGINATING ACTIVITY (Corporate author)
U. S. Naval Ordnance Laboratory
White Oak, Silver Spring, Md

2a. REPORT SECURITY CLASSIFICATION
UNCLASSIFIED

2b. GROUP

3. REPORT TITLE
Simulation of the Dynamical Loading of PMMA in the NOL Regular Card Gap Test

4. DESCRIPTIVE NOTES (Type of report and inclusive dates)

5. AUTHOR(S) (Last name, first name, initial)
Fisher, E.E., Johnson, R. G., Paulsen, R.F., Honeywell Inc., Systems & Research Div, Research Dept, St. Paul, Minn.

6. REPORT DATE	7a. TOTAL NO. OF PAGES	7b. NO. OF REFS
2 April 1970	133	9

8a. CONTRACT OR GRANT NO.
N60921-69-M-2003

b. PROJECT NO.
ORD 331-0021/092-1/UF 19-332-302

c.

d.

9a. ORIGINATOR'S REPORT NUMBER(S)
12135-FRI
NOLTR 69-219

9b. OTHER REPORT NO(S) (Any other numbers that may be assigned this report)

10. AVAILABILITY/LIMITATION NOTICES
This document has been approved for public release and sale, its distribution is unlimited.

11. SUPPLEMENTARY NOTES

12. SPONSORING MILITARY ACTIVITY
Naval Ordnance Systems Command

13. ABSTRACT

Results are presented of a computer simulation of the flow induced in a Plexiglass (PMMA) rod by a charge of tetryl. The charge and the rod are the standard donor and attenuator of the Naval Ordnance Laboratory Large Scale Gap Test (LSGT). The computations provide a better understanding of the flow and hence of phenomena which have been observed in PMMA rods during calibration studies of the LSGT. They also give data on the shape and duration of the pressure pulse (in the PMMA) which is transmitted into the acceptor explosive in the LSGT. Such data are needed in the study of shock sensitivity of explosives.

DD FORM 1 JAN 64 1473

UNCLASSIFIED

Security Classification

14. KEY WORDS	LINK A		LINK B		LINK C	
	ROLE	WT	ROLE	WT	ROLE	WT
explosives						
sensitivity						
computer simulation						
high pressure flow						
gap tests						

INSTRUCTIONS

1. ORIGINATING ACTIVITY: Enter the name and address of the contractor, subcontractor, grantee, Department of Defense activity or other organization *(corporate author)* issuing the report.

2a. REPORT SECURITY CLASSIFICATION: Enter the overall security classification of the report. Indicate whether "Restricted Data" is included. Marking is to be in accordance with appropriate security regulations.

2b. GROUP: Automatic downgrading is specified in DoD Directive 5200.10 and Armed Forces Industrial Manual. Enter the group number. Also, when applicable, show that optional markings have been used for Group 3 and Group 4 as authorized.

3. REPORT TITLE: Enter the complete report title in all capital letters. Titles in all cases should be unclassified. If a meaningful title cannot be selected without classification, show title classification in all capitals in parenthesis immediately following the title.

4. DESCRIPTIVE NOTES: If appropriate, enter the type of report, e.g., interim, progress, summary, annual, or final. Give the inclusive dates when a specific reporting period is covered.

5. AUTHOR(S): Enter the name(s) of author(s) as shown on or in the report. Enter last name, first name, middle initial. If military, show rank and branch of service. The name of the principal author is an absolute minimum requirement.

6. REPORT DATE: Enter the date of the report as day, month, year; or month, year. If more than one date appears on the report, use date of publication.

7a. TOTAL NUMBER OF PAGES: The total page count should follow normal pagination procedures, i.e., enter the number of pages containing information.

7b. NUMBER OF REFERENCES: Enter the total number of references cited in the report.

8a. CONTRACT OR GRANT NUMBER: If appropriate, enter the applicable number of the contract or grant under which the report was written.

8b, 8c, & 8d. PROJECT NUMBER: Enter the appropriate military department identification, such as project number, subproject number, system numbers, task number, etc.

9a. ORIGINATOR'S REPORT NUMBER(S): Enter the official report number by which the document will be identified and controlled by the originating activity. This number must be unique to this report.

9b. OTHER REPORT NUMBER(S): If the report has been assigned any other report numbers *(either by the originator or by the sponsor)*, also enter this number(s).

10. AVAILABILITY/LIMITATION NOTICES: Enter any limitations on further dissemination of the report, other than those imposed by security classification, using standard statements such as:

(1) "Qualified requesters may obtain copies of this report from DDC."

(2) "Foreign announcement and dissemination of this report by DDC is not authorized."

(3) "U. S. Government agencies may obtain copies of this report directly from DDC. Other qualified DDC users shall request through _____."

(4) "U. S. military agencies may obtain copies of this report directly from DDC. Other qualified users shall request through _____."

(5) "All distribution of this report is controlled. Qualified DDC users shall request through _____."

If the report has been furnished to the Office of Technical Services, Department of Commerce, for sale to the public, indicate this fact and enter the price, if known.

11. SUPPLEMENTARY NOTES: Use for additional explanatory notes.

12. SPONSORING MILITARY ACTIVITY: Enter the name of the departmental project office or laboratory sponsoring *(paying for)* the research and development. Include address.

13. ABSTRACT: Enter an abstract giving a brief and factual summary of the document indicative of the report, even though it may also appear elsewhere in the body of the technical report. If additional space is required, a continuation sheet shall be attached.

It is highly desirable that the abstract of classified reports be unclassified. Each paragraph of the abstract shall end with an indication of the military security classification of the information in the paragraph, represented as *(TS), (S), (C), or (U)*

There is no limitation on the length of the abstract. However, the suggested length is from 150 to 225 words.

14. KEY WORDS: Key words are technically meaningful terms or short phrases that characterize a report and may be used as index entries for cataloging the report. Key words must be selected so that no security classification is required. Identifiers, such as equipment model designation, trade name, military project code name, geographic location, may be used as key words but will be followed by an indication of technical context. The assignment of links, roles, and weights is optional.